Technical Report Documentation Page

1. Report No.	2. Government Accession No.	3. Recipient's Catalog No.
FHWA/TX-07/0-5123-2		

4. Title and Subtitle	5. Report Date
GUIDELINES FOR EVALUATION OF EXISTING PAVEMENTS FOR HMA OVERLAY	November 2006 Resub: Feb. 2007 Pub: May 2007
	6. Performing Organization Code

7. Author(s)	8. Performing Organization Report No.
Fujie Zhou and Tom Scullion	Report 0-5123-2

9. Performing Organization Name and Address	10. Work Unit No. (TRAIS)
Texas Transportation Institute The Texas A&M University System College Station, Texas 77843-3135	11. Contract or Grant No. Project 0-5123

12. Sponsoring Agency Name and Address	13. Type of Report and Period Covered
Texas Department of Transportation Research and Technology Implementation Office P. O. Box 5080 Austin, Texas 78763-5080	Technical Report: September 2005-August 2006
	14. Sponsoring Agency Code

15. Supplementary Notes

Project performed in cooperation with the Texas Department of Transportation and the Federal Highway Administration.

Project Title: Development of an Advanced Overlay Design System Incorporating Both Rutting and Reflection Cracking Requirements

URL: http://tti.tamu.edu/documents/0-5123-2.pdf

16. Abstract

This report discusses the application of nondestructive test (NDT) tools for evaluating existing pavements for hot-mix asphalt (HMA) overlays. The NDT tools covered in this report include ground penetrating radar (GPR), falling weight deflectometer (FWD), and rolling dynamic deflectometer (RDD). The GPR is used to estimate the thickness of existing pavement layers, and identify section breaks and potential trapped moisture problems. The FWD is used to evaluate the structural capacity of the existing pavement, and the in-situ layer modulus can be backcalculated from FWD data. In addition, for existing concrete pavements, the FWD can be used to determine load transfer efficiency (LTE) at joints and/or cracks.

The application of the RDD to evaluate existing concrete pavements is also discussed. The major advantage the RDD has over other discrete NDT devices (e.g., FWD) is that it provides continuous deflection profiles of the pavement, which can be used to identify joints with poor LTE. However, no software is available to automatically interpret the RDD data. After reviewing RDD data collected on several different concrete pavements, the researchers developed some basic interpretation criteria for the RDD data. Based on the measured RDD deflection data and the monitored field reflective cracking performance on IH20, threshold values for RDD Sensor 1 deflection and the differential deflection between Sensors 1 and 3 are recommended. If either the Sensor 1 deflection or the differential deflection between Sensors 1 and 3 is larger than the proposed thresholds, the corresponding joint and/or cracks is recommended for pretreatment before placing a new HMA overlay. Finally, general guidelines for evaluating existing pavements for HMA overlays are proposed in this report.

17. Key Words	18. Distribution Statement
Nondestructive Testing, FWD, GPR, RDD, Reflective Cracking, Asphalt Overlay Thickness Design	No restrictions. This document is available to the public through NTIS: National Technical Information Service Springfield, Virginia 22161 http://www.ntis.gov

19. Security Classif.(of this report)	20. Security Classif.(of this page)	21. No. of Pages	22. Price
Unclassified	Unclassified	110	

GUIDELINES FOR EVALUATION OF EXISTING PAVEMENTS FOR HMA OVERLAY

by

Fujie Zhou, Ph.D., P.E.
Assistant Research Engineer
Texas Transportation Institute

and

Tom Scullion, P.E.
Senior Research Engineer
Texas Transportation Institute

Report 0-5123-2
Project 0-5123
Project Title: Development of an Advanced Overlay Design System Incorporating Both Rutting and Reflection Cracking Requirements

Performed in cooperation with the
Texas Department of Transportation
and the
Federal Highway Administration

November 2006
Resub: Feb. 2007 Pub.: May 2007

TEXAS TRANSPORTATION INSTITUTE
The Texas A&M University System
College Station, Texas 77843-3135

DISCLAIMER

The contents of this report reflect the views of the authors, who are responsible for the facts and the accuracy of the data presented herein. The contents do not necessarily reflect the official view or policies of the Texas Department of Transportation (TxDOT) or the Federal Highway Administration (FHWA). This report does not constitute a standard, specification, or regulation. The engineer in charge was Dr. Fujie Zhou, P.E. (Texas, # 95969).

There is no invention or discovery conceived or first actually reduced to practice in the course of or under this contract, including any art, method, process, machine, manufacture, design or composition of matter, or any new useful improvement thereof, or any variety of plant, which is or may be patentable under the patent laws of the United States of America or any foreign country.

ACKNOWLEDGMENTS

This project was made possible by the Texas Department of Transportation in cooperation with the Federal Highway Administration. The authors thank the many personnel who contributed to the coordination and accomplishment of the work presented herein. Special thanks are extended to Magdy Mikhail, P.E., and Elias Rmeili, P.E., for serving as the project director and project coordinator, respectively. Many people volunteered their time to serve as project advisors, including:

Joe Leidy, P. E.
Richard Williammee, P. E.
Zhiming Si, Ph.D., P. E.
Albert Pardo, P. E.
Hua Chen, P. E.
Tomas Saenz, P. E.

TABLE OF CONTENTS

TABLE OF CONTENTS (Continued)

LIST OF FIGURES

LIST OF FIGURES (Continued)

Figure **Page**

LIST OF TABLES

Table **Page**

CHAPTER 1
INTRODUCTION

1.1 BACKGROUND

The construction of a hot-mix asphalt (HMA) overlay is the most common method used by the Texas Department of Transportation (TxDOT) to rehabilitate existing asphalt and concrete pavements. It is well known that the existing pavement condition has a significant influence on selecting an HMA overlay strategy and on the eventual long-term performance of the HMA overlay.

Different techniques including both nondestructive testing (NDT) and destructive testing have been employed to evaluate the existing pavements before HMA overlay. There are two major purposes for this evaluation: firstly to identify problem locations where pretreatments will be required, and secondly to characterize the properties of the existing pavement layer (e.g., thickness and modulus) and load transfer efficiency (LTE) at joints or cracks for use in the HMA overlay thickness design. The commonly used NDT devices in Texas for evaluating existing pavements include ground penetrating radar (GPR), falling weight deflectometer (FWD), and rolling dynamic deflectometer (RDD). Therefore, in this report the research team has developed guidelines for collecting and interpreting NDT data for these three tools, with a focus on how this information can be used in the HMA overlay design process.

1.2 OBJECTIVES

The two primary objectives of Project 0-5123 were to 1) develop an HMA overlay mixture design balancing rutting and reflective cracking requirements, and 2) develop an HMA overlay thickness design methodology focusing on reflective cracking and rutting. The first objective has been reached and documented in the Year 1 report entitled "Integrated Asphalt (Overlay) Mixture Design, Balancing Rutting and Cracking Requirements." Starting from the second fiscal year, the research team focused on the second objective. Part of the second objective was to develop guidelines for evaluating existing pavements focusing on identifying repair locations and collecting information needed for the HMA overlay thickness design in which the primary concern is reflective cracking.

1.3 REPORT ORGANIZATION

This report is organized into six chapters. A brief introduction is presented in Chapter 1. Chapter 2 discusses the application of GPR to identify the layer thickness of existing pavement, section breaks, and potential trapped moisture problems. Chapter 3 focuses on FWD backcalculation and determining load transfer efficiency from FWD measurement. The use of RDD to continuously evaluate existing Portland cement concrete (PCC) is specifically described in Chapter 4. Chapter 5 provides general guidelines for evaluating existing pavements for HMA overlay thickness design. Finally, Chapter 6 presents a brief summary of this report.

CHAPTER 2
APPLICATION OF GROUND PENETRATING RADAR ON EVALUATION OF EXISTING PAVEMENTS

2.1 BACKGROUND

GPR is a well-established nondestructive method for investigating the internal composition of many naturally occurring materials such as rocks, earth and gravel, and man-made materials like concrete, brick, and asphalt. It can also be used to detect metallic and non-metallic pipes, sewers, cables, cable ducts, voids, foundations, reinforcing rods in concrete, and a whole host of other buried objects. GPR technology was implemented by TxDOT in the mid 1990s. Currently, TxDOT has a fleet of three units that are used routinely for forensic investigations and pavement rehabilitation studies.

2.1.1 Operational Principles of Ground Penetrating Radar

Figure 1 shows one of TxDOT's 1 GHz air-coupled GPR units. This system sends discrete pulses of radar energy into the pavement system and captures the reflections from each layer interface within the structure. Radar is an electro-magnetic (EM) wave and, therefore, obeys the laws governing reflection and transmission of EM waves in layered media. This particular GPR unit operates at highway speeds (70 mph), transmits and receives 50 pulses per second, and can effectively penetrate to a depth of 24 inches. A typical plot of captured reflected energy versus time for one pulse is shown in Figure 2 as a graph of amplitude in volts versus arrival time in nanoseconds. The reflection, A_1, is the energy reflected from the surface of the pavement, and A_2 and A_3 are reflections from the top of the base and subgrade, respectively. These are all illustrated as positive reflections, which indicate an interface with a transition from a low to a high dielectric material. As described later, these amplitudes of reflection and the time delays between reflections are used to calculate both layer dielectrics and thickness. The dielectric constant of a material is an electrical property that is most influenced by moisture content

Figure 1. TxDOT's Air-Coupled GPR Unit.

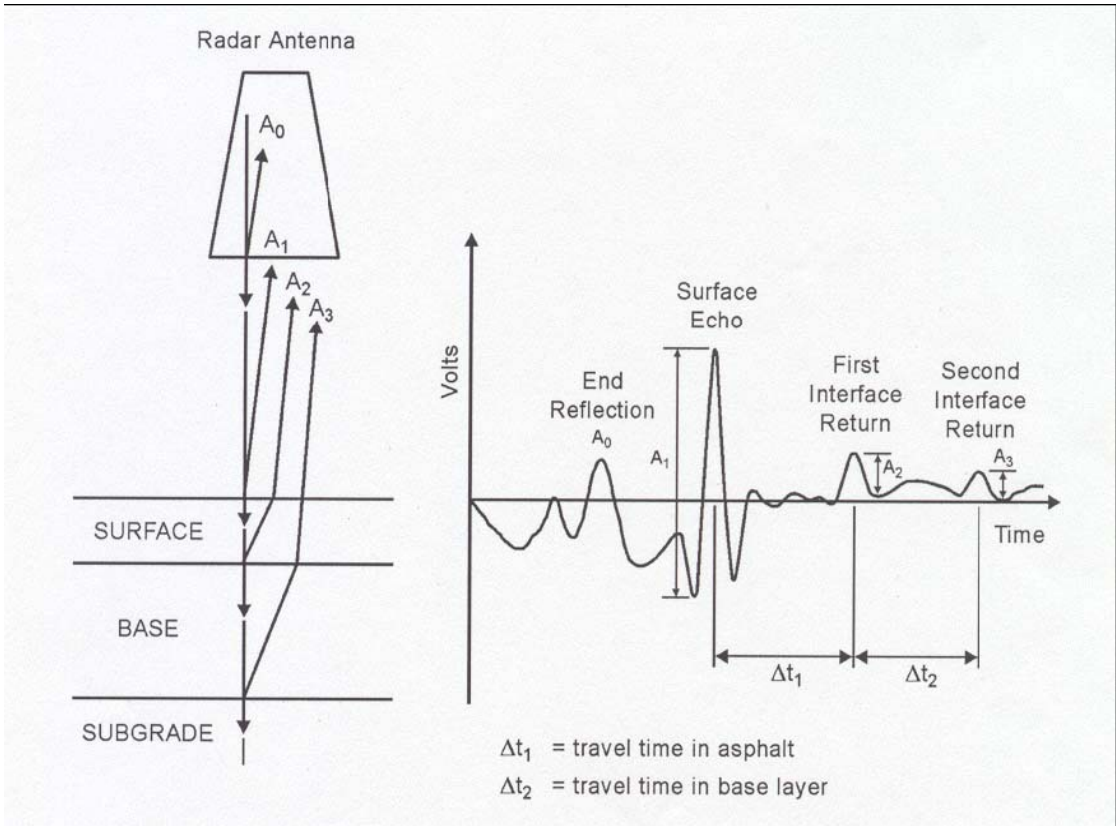

Figure 2. Principles of GPR *(1)*.

and density. An increase in moisture will cause an increase in layer dielectric. In contrast, an increase in air void content will cause a decrease in layer dielectric.

A range of typical dielectrics has been established for most paving materials. HMA layers normally have a dielectric value between 4.5 and 6.5, depending on the coarse aggregate type. Measured values significantly higher than this would indicate the presence of excessive moisture. Lower values could indicate a density problem or indicate that an unusual material, such as lightweight aggregate, has been used. The examples below illustrate how changes in the pavement's engineering properties would influence the typical GPR trace shown in Figure 2:

- If the thickness of the surface layer increases, then the time interval between A_1 and A_2 would increase.
- If the base layer becomes wetter, then the amplitude of reflection from the top of the base, A_2, would increase.
- If there is a significant defect within the surface layer, then an additional reflection will be observed between A_1 and A_2.
- Large changes in the surface reflection, A_1, would indicate changes in either the density or moisture content along the section.

2.1.2 Layer Thickness Calculation

Using the amplitudes (volts) and time delays (ns) from Figure 2, it is possible to calculate layer dielectrics and layer thickness. The equations used are summarized below:

$$\varepsilon_a = \left[\frac{1 + A_1 / A_m}{1 - A_1 / A_m}\right]^2 \quad (1)$$

where:

ε_a = the dielectric of the surfacing layer;

A_1 = the amplitude of surface reflection; and

A_m = the amplitude of reflection from a large metal plate in volts (this represents the 100 percent reflection case).

$$h_1 = \frac{c \times \Delta t_1}{\sqrt{\varepsilon_a}} \quad (2)$$

where:

h_1 = the thickness of the top layer;

c = speed of EM wave in air (150 mm/ns two-way travel); and

Δt_1 = the time delay between peaks, A_1 and A_2.

$$\sqrt{\varepsilon_b} = \sqrt{\varepsilon_a}\left[\frac{1-\left(\frac{A_1}{A_m}\right)^2+\left(\frac{A_2}{A_m}\right)}{1-\left(\frac{A_1}{A_2}\right)^2-\left(\frac{A_1}{A_m}\right)}\right] \quad (3)$$

where:

ε_b = the dielectric of base layer; and

A_2 = the amplitude of reflection from the top of the base layer.

$$h_{base} = \frac{c \times \Delta t_2}{\sqrt{\varepsilon_b}} \quad (4)$$

where:

h_{base} = thickness of base layer; and

Δt_2 = time delay between A_2 and A_3.

Using the above equations, one may calculate both layer thickness and dielectrics along the pavement. The use of the thickness information for either quality control of new construction or structural evaluation of existing structures is obvious to pavement engineers. However, the layer dielectric values and their variation along a highway are also of practical significance, as demonstrated by Saarenketo and Scullion (*2*) and by Saarenketo (*3*).

2.1.3 COLOR-Coded Images of Subsurface Conditions

In most GPR projects, several thousand GPR traces are collected. In order to conveniently display this information, color-coding schemes are used to convert the traces into line scans and stack them side-by-side so that a subsurface image of the pavement structure can be obtained (*4*). This approach is used extensively in Texas. A typical display from the Texas system for a thick HMA pavement is shown in Figure 3. This display is taken from a section of newly constructed thick asphalt pavement over a thin granular base. The labels on this figure are as follows:

- A: Files containing data;
- B: Main pull down menu;
- C: Button to define the color-coding scheme;
- D: Distance scale (miles and feet);
- E: End location;
- F: Depth scale; and
- G: Default dielectric value used to convert the measure time scale into a depth scale.

The important features of this figure are the lines marked H, I, and J; these are the reflection from the surface, top, and bottom of base, respectively. The pavement is homogeneous, and the layer interfaces are easy to detect. The variation in surface dielectric, computed using Equation 1, is shown at the bottom of the figure. When processing GPR data, the first step is to develop displays such as Figure 3. From these displays, it is possible to identify any clear breaks in pavement structure and to identify any significant anomalies. The intensity of the subsurface colors is related to the amplitude of reflection. Therefore, areas of wet base would be observed as bright red reflections.

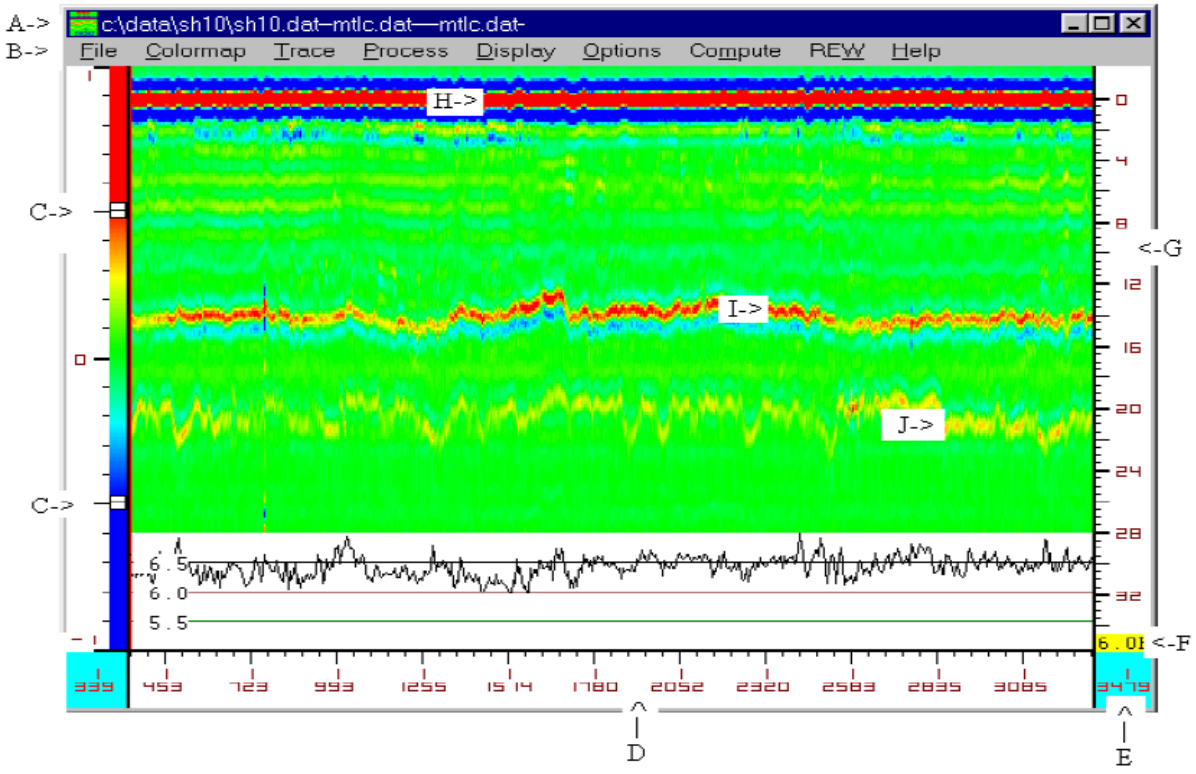

Figure 3. Color-Coded GPR Traces (*1*).

Based on the above background information, the rest of this chapter discusses the applications of GPR to determine layer thickness, potential moisture problem, and potential void under PCC slab in Texas, which are demonstrated by a series of case studies on existing asphalt pavement, PCC pavement, and composite pavement (asphalt overlay over PCC pavement).

2.2 APPLICATION OF GPR ON EXISTING ASPHALT PAVEMENTS

By far the biggest use of GPR within TxDOT has been in the area of evaluating existing asphalt pavements for pavement rehabilitation. GPR testing is often used to determine layer thickness, detect changes in the pavement structure, and identify subsurface defects, particularly moisture damage. This approach has proven to be highly effective in Texas with its mature highway network and its focus on pavement rehabilitation. When dealing with older road networks where numerous sections have been widened and/or received partial rehabilitation, it is extremely difficult to maintain reliable layer thickness information.

The data shown in Figure 4 is a short 2-mile section from a 14-mile project. The highway was exhibiting some localized failures, and only limited thickness information was available. The surface condition looked similar because the section had recently received a thin resurfacing. From the data shown in Figure 4, this short section had three distinctly different pavement structures. The interpreted structure information is at the bottom of the figure. The highway had been widened, and the old roadway had been buried beneath a flexible base overlay and a new thin surfacing. The widened sections consisted of a stabilized subgrade, flexible base, and thin HMA surfacing. The GPR rapidly identified the old pavement (section 3), the new pavement (section 1) as well as areas of localized full-depth rehabilitation (section 2). With this information plus necessary FWD data, the pavement engineer can make a clear decision on HMA overlay strategy.

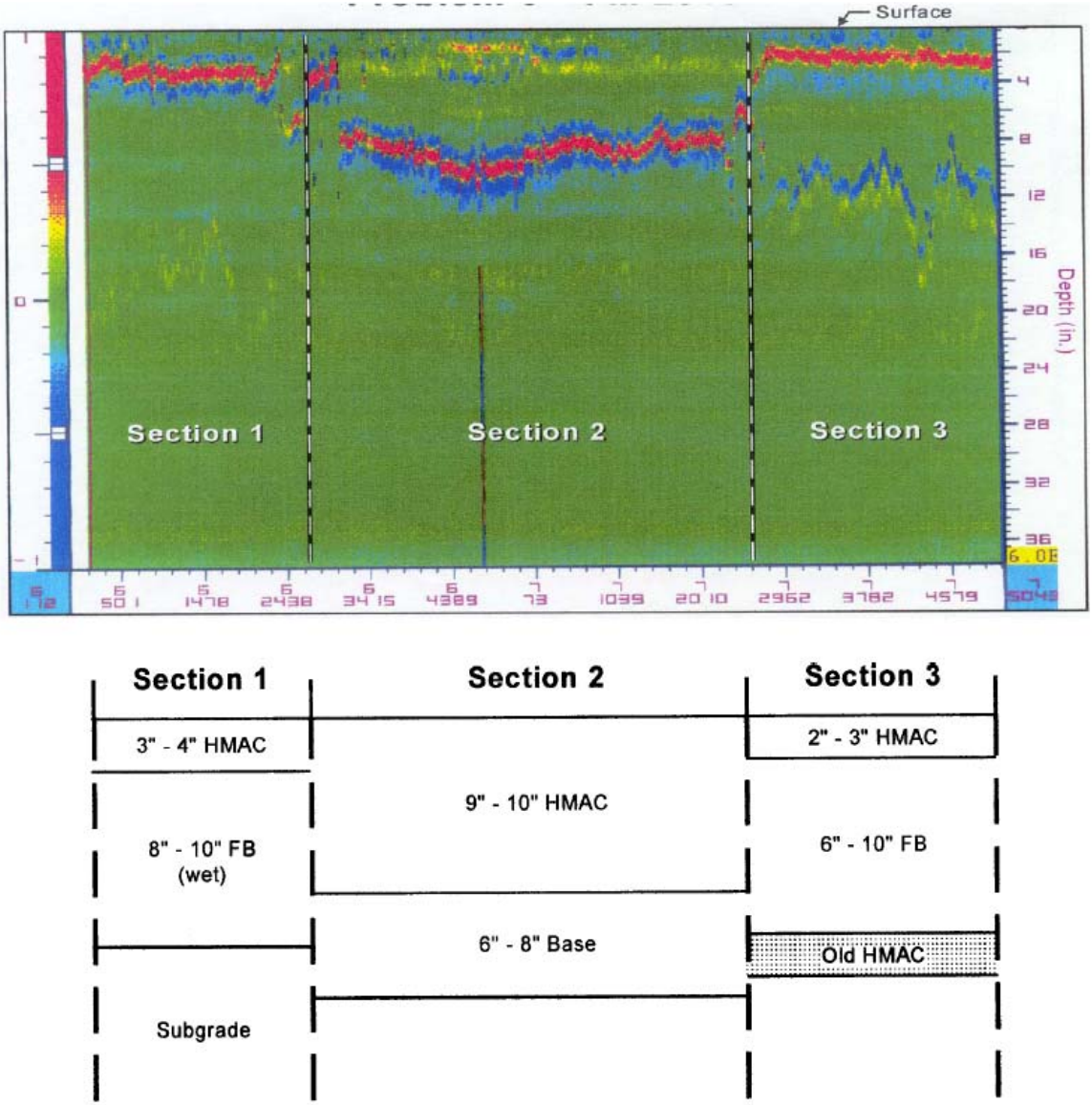

Figure 4. Raw GPR Data with Interpretation from FM 2818, near College Station, Texas *(1)*.

2.3 APPLICATION OF GPR ON EXISTING PCC PAVEMENTS

GPR data have also been collected on several jointed PCC pavements. On an investigation of the concrete pavements on IH45 in the Houston District, a wide variety of GPR signatures were obtained. Figures 5, 6, and 7 show the typical COLORMAP displays.

Figure 5 shows the ideal case. This figure is a GPR display of approximately 600 feet of IH45. The depth scale is on the right, and the distance scale in miles and feet is at

the bottom of the figure. The faint line at a depth of 4 inches below the surface is reflections from wire mesh reinforcing. The additional faint line at a depth of 12 inches is the reflection from the bottom of the concrete/top of the base. The intensity of reflection at this location indicates the presence of moisture or the presence of air-filled voids. Water will produce a strong reflection, and this would be shown as a strong red reflection at a depth of 12 inches. There are no strong reflections in Figure 5. An air-filled void would give a completely different reflection; with the color-coding scheme used in COLORMAP (*4*), an air-filled void would be represented as a blue line. Again, there are no indications of air-filled voids in Figure 5.

The graph at the bottom of the figure is a plot of surface dielectric from the joint concrete pavement (JCP). The periodic increases in the plot coincide with the joints in the pavement. The increase in surface dielectric is associated with increases in near surface moisture content. These patterns occur in some JCPs but not all; they are either associated with buildup in moisture in the joint itself or in the concrete immediately surrounding the joint.

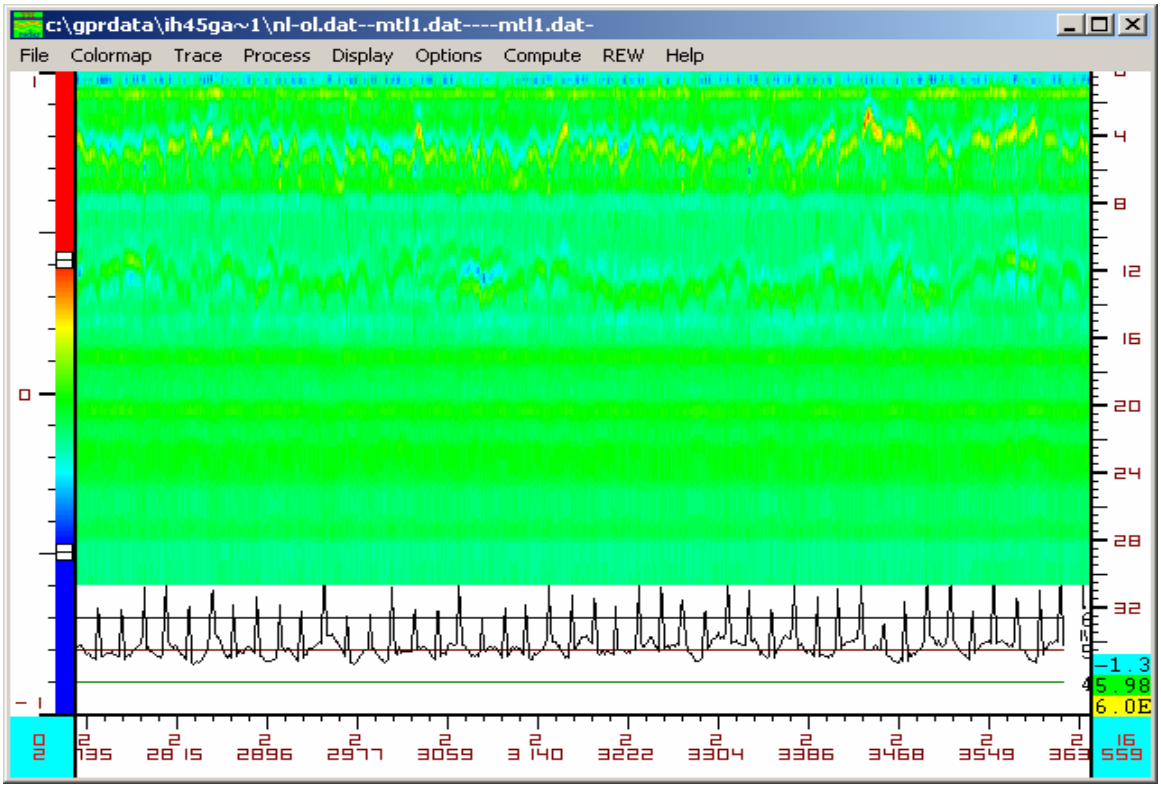

Figure 5. GPR Data from a JCP with No Obvious Sub-Slab Problems.

The COLORMAP display shown above (Figure 5) should be contrasted with that shown below in Figure 6. In this case, there are stronger periodic reflections both at the bottom of the slab and from within the slab itself at the depth of the reinforcing steel. The red reflections beneath the slab indicate the presence of additional moisture. The presence of free water beneath the slab could have a major impact on the selection of rehabilitation options. For overlays, if the overlay sealed the concrete surface, the concern would be that the trapped moisture may migrate up through the joints and cause layer debonding or stripping of the HMA layer.

As with all other investigations using GPR, it is critical to verify the interpretations. In this case, pilot holes were drilled through the concrete slab. The red areas at the bottom of the slab were found to be areas of wet clay rather than water-filled voids. The original base was sand material, which in these few locations now has become contaminated by clay. Coring indicated that the stronger reflections at mid depth were found to be associated with areas of corrosion of the reinforcing mesh used on this slab.

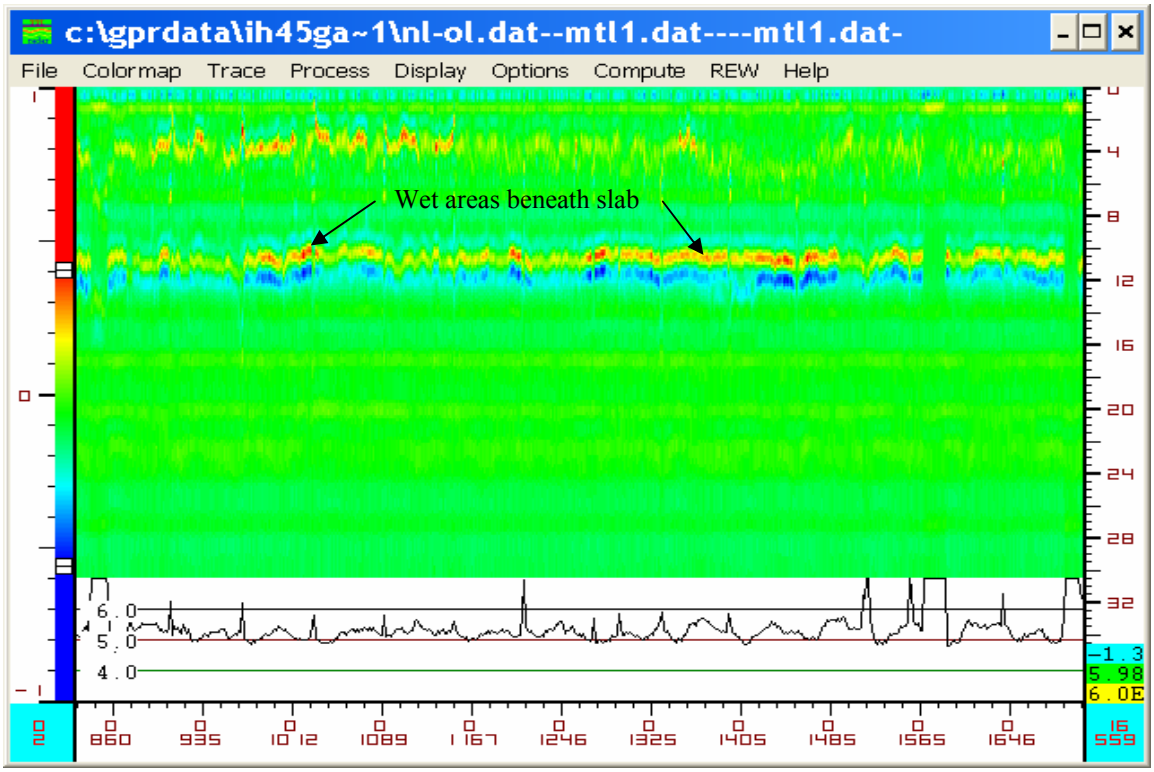

Figure 6. COLORMAP Display from a Section of JCP with Possible Problem Areas.

The third case shown in Figure 7 displays a different portion of the same highway. In this case, there is almost a continuous strong red reflection followed by a continuous blue reflection. The one gap in the middle of the plot is where a full depth patch has been placed. This location had already been undersealed; however, there was substantial staining along the shoulder of the pavement. This section was cored, and it was found that free water was present beneath the slab. In places, there was a localized 2 to 3 inch thick void beneath the slabs. Clearly, the rehabilitation options for this highway are limited because of the presence of the water.

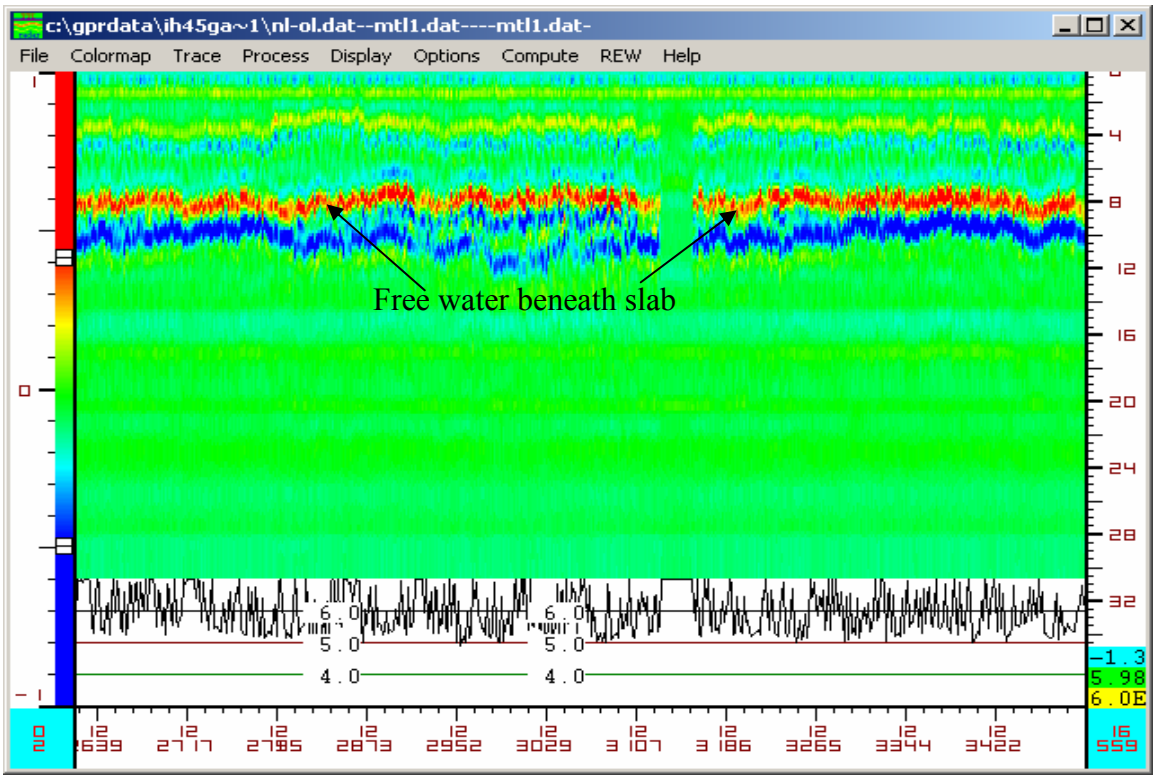

Figure 7. COLORMAP Display from an Area Where Free Water Exists beneath the Slab.

2.4 APPLICATION OF GPR ON COMPOSITE PAVEMENTS

On composite pavements where the jointed concrete is covered by an asphalt overlay, the GPR can also be used to identify any problems within the HMA layers in addition to identifying layer thickness and detecting water-filled voids. This is demonstrated in the following case.

Air-coupled GPR data were collected on the limits of the IH20 overlay project to document existing conditions and to provide information to personnel who were performing tests with RDD. GPR testing was performed first before the RDD test. The limits of the data collection were Texas reference markers (TRM) 610 to 614. Data were collected at 1-foot intervals in both inside and outside lanes in both directions. Figures 8 to 11 show examples of pre-construction GPR data. Color-coded representations of the GPR data on all lanes surveyed are given in Appendix A. Figures 8 to 11 show representative data taken on both directions. These cases are discussed in the following sections.

Eastbound Outside Lane – Outside Wheel Path

Figure 8 is a representative COLORMAP display from the eastbound lanes. Similar data were obtained for much of the eastbound direction. At this location, the surfacing consists of two 2-inch thick lifts of asphalt concrete. The dielectric of the upper layer is relatively low at around 4.2 and 4.5. A strong reflection is observed at the top of the second layer of asphalt concrete (AC). The dielectric of the lower asphalt layer appears normal, in the range of 5.5 to 6. In several locations, full depth AC patches have been placed on this lane. The dielectric values of these patches are close to 6, which is normal for AC. It is also possible to identify the bottom of the PCC slab in Figure 8. A faint reflection is observed from the middle of the PCC slab. The periodic, slightly brighter reflections could be from tie bars in the joints.

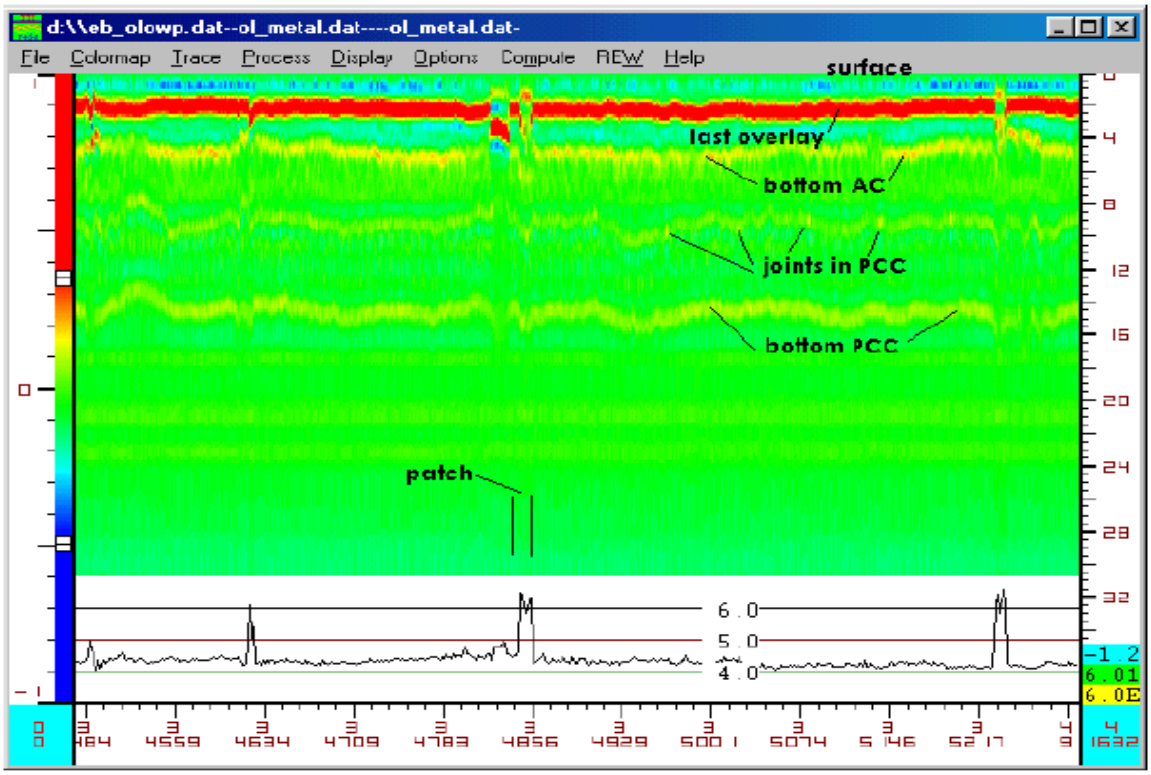

Figure 8. Typical COLORMAP Display from a Representative Area in the Eastbound Direction.

Westbound Outside Lane – Outside Wheel Path

The GPR images from the westbound direction were similar to those obtained in the eastbound direction. The total AC thickness is close to 4 inches. However, more patches have been placed on this lane, and the pavement structure is more variable. This observation is illustrated in Figure 9, which shows a section from TRM 611 – 0.3 to 611 – 0.6. In section 1, the original AC layers have been removed and replaced with a single homogeneous layer. Section 2 shows a different GPR display. In this section, periodic low-density areas are found in the lower AC layer, denoted by the blue areas in Figure 9. These could be areas of stripping in the lower AC layer, or they could be areas where the dense AC layer has been replaced with a drainable layer.

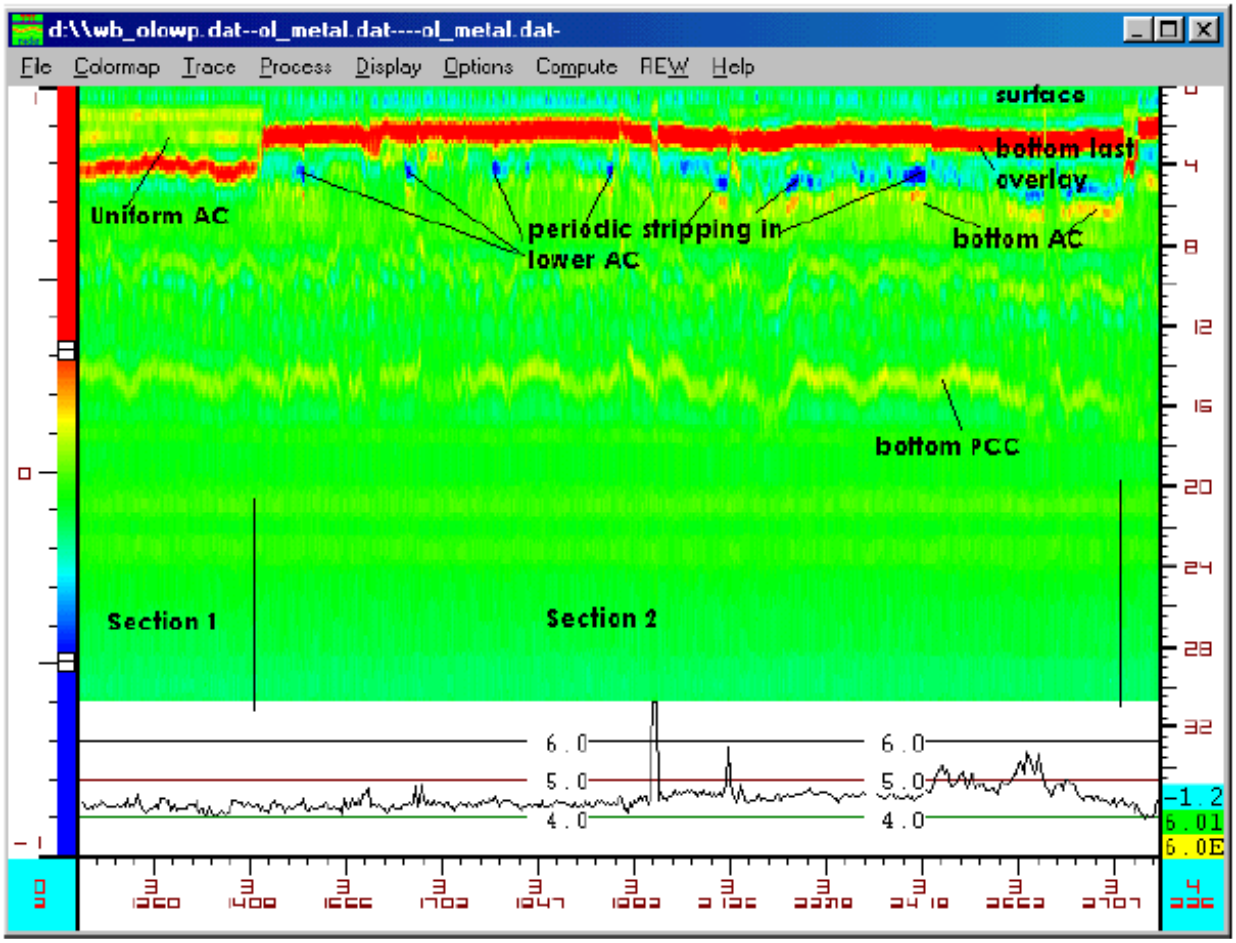

Figure 9. Potential Defect Areas on Westbound Outside Lane.

Individual Traces from IH20 (Westbound)

Figures 10 and 11 show two individual traces from locations 100 feet apart in the westbound outside lane of I20 (Figure 9). Figure 10 shows a strong negative reflection from the lower AC layer. The negative reflections are associated with the transition from a higher to a lower dielectric (density) area. In the past, this has been found to be associated with stripping in the lower AC layer. Figure 11 is a trace from a normal area in the westbound direction. No defects are apparent at this location. The reflection from the top and bottom of the PCC are faint, but still clear in the data.

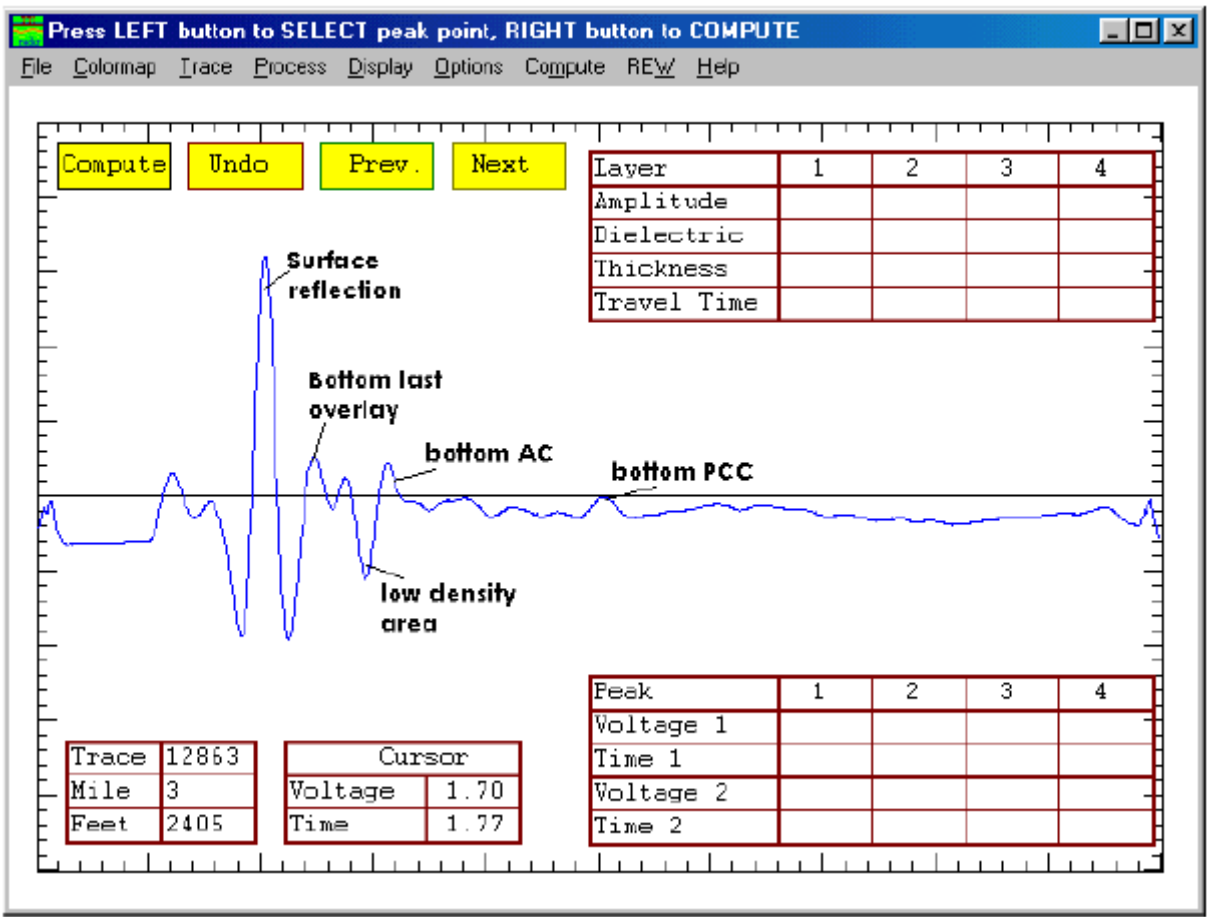

Figure 10. Individual Trace from an Area on the Westbound Outside Lane Where Lower AC Layer Gives a Strong Negative Reflection.

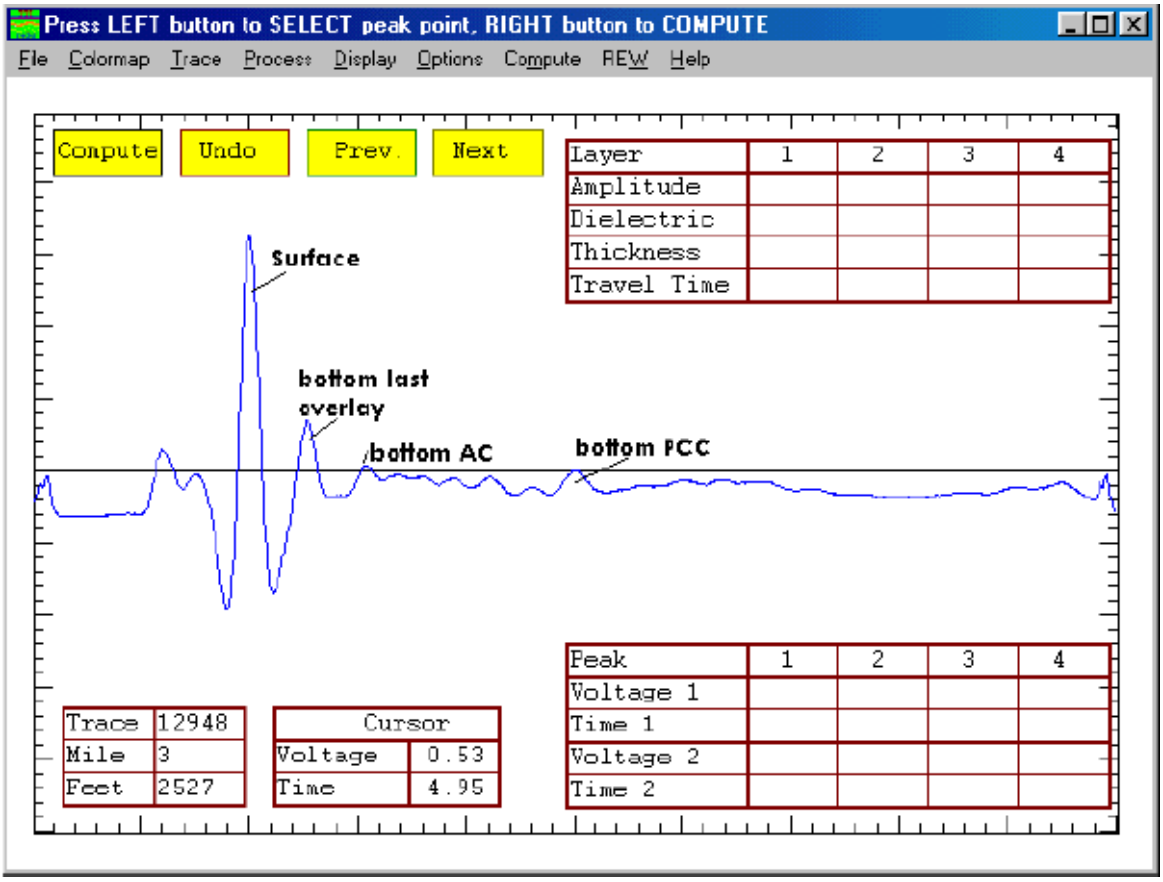

Figure 11. Individual Trace from a Normal Location on the Westbound Outside Lane.

In summary, the GPR data for the most part show that the AC thickness on the project is fairly uniform. It is possible to see all the major layer interfaces from the data. There are indications of potential buried defects such as stripping at various locations along the westbound outside lane.

2.5 GUIDELINES FOR GPR TESTING, DATA INTERPRETATION, AND REPORTING

Based on the information discussed above, some guidelines are briefly summarized for evaluating existing pavements using the GPR:

- GPR testing: GPR data should be collected for the whole HMA overlay project in the outside lane/outside wheel path with a data collection interval of

1 foot per trace, since the current 1 GHz air-coupled GPR unit can operate at highway speeds (20 mph).

- GPR data interpretation: The COLORMAP program can be used to interpret the collected GPR data. However, several important issues should be noted for interpreting GPR data:
  a. The GPR data certainly provide useful thickness information for the upper layers of flexible and composite pavements. However, it should be noted that applications of air-coupled GPR on concrete pavements have had limited success within TxDOT.
  b. GPR can be used to locate major defects in either the asphalt covering of JCPs or major defects such as water-filled voids beneath the slab. By combining GPR data with the deflection data from either FWD or RDD, the pavement engineer will have a comprehensive evaluation of pavement conditions.
  c. GPR will detect major defects, but it is doubtful if it will detect minor defects such as thin air-filled voids. The current 1 GHz GPR units also have restrictions on depth of penetration; little useful information will be obtained from deeper than 20 inches. This is not usually a restriction on old PCC; it could be a problem if the old concrete has a thick asphalt overlay, or if the slab is sitting on a thick base and the problem is in the subgrade layer.
  d. COLORMAP cannot provide quantitative values (layer dielectric) for the base layer beneath the slab. This is because concrete is a highly attenuative medium for GPR waves (whereas asphalt has little or no attenuation). The attenuation through a concrete slab is not adequately addressed in the current version of COLORMAP. Based on signal attenuation, if a strong positive reflection is observed beneath a concrete slab, then the base must have a very high dielectric indicating possible trapped moisture.
  e. All GPR interpretations require validation. As with the case on IH45, strong reflections beneath a slab do not automatically mean a water-filled

void. As found in this project, it could be areas of saturated base or wet clay, with no void. Note that GPR will never eliminate field coring, but it can certainly reduce the number of cores required.

- GPR data reporting: The expected data from GPR testing include 1) layer thickness, which is required by the HMA overlay thickness design system; and 2) major defects (such as stripping or water-filled voids beneath the slab), which should be treated before HMA overlay.

CHAPTER 3

APPLICATION OF FWD TESTING ON EVALUATING EXISTING PAVEMENTS

3.1 BACKGROUND

The FWD is a trailer-mounted device that delivers a transient force impulse to the pavement surface, as shown in Figure 12. By varying the mass or the drop height or both, the impulse load can be varied between 2500 lb to 27,000 lb for regular types of FWD. Generally, seven deflection sensors (Figure 12) measure the surface deflections caused by the impulse load. The first deflection sensor is always mounted in the center of the loading plate, while the rest are positioned at various spatial distances up to 6 feet from the load center. From all deflections recorded, peak values are stored and displayed. Load pulse base widths usually range from 20 to 60 ms for various equipment manufacturers. Note that for the Dynatest unit, the load pulse is approximately 28 ms.

The FWD is the most commonly used tool for evaluating existing pavements for asphalt overlay or rehabilitation in Texas. In most cases, the FWD is used to evaluate structural capacity and then to backcalculate pavement layer moduli. For JCP, the FWD has been used to determine load transfer across joints or cracks. Additionally, some efforts have been made to detect voids below the slab based on FWD testing. In 1995, the Texas Transportation Institute (TTI) conducted a comparative study on the effectiveness of existing void detection procedures that utilized FWD measurements. Based on the success rate of each

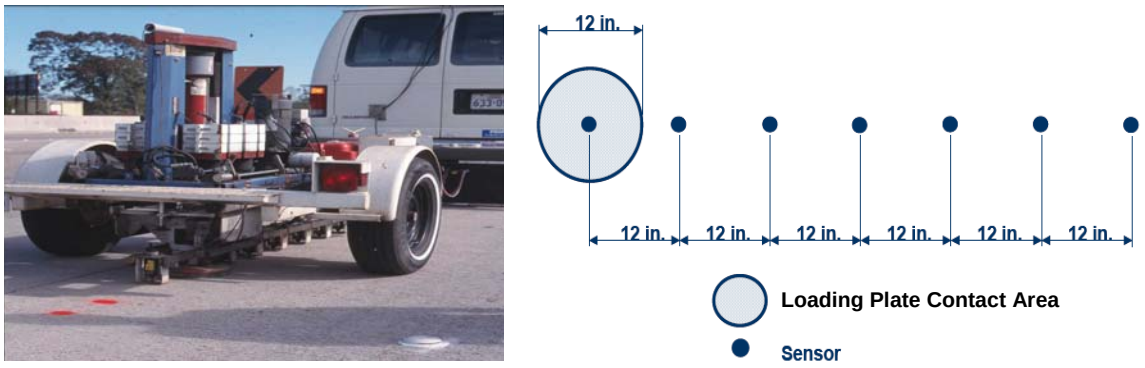

Figure 12. TxDOT's Falling Weight Deflectometer and Sensors.

method, two methods, the CTR (Center for Transportation Research) method (*5*) and the NCHRP (National Cooperative Highway Research Program) method (*6*), were identified as most promising procedures. However, the work done later under NCHRP 10-48: *Void Detection in PCC and Thin Asphalt Overlaid Composite Pavements* (*7*), found that either the existing CTR or NCHRP method could not effectively detect voids beneath experimental slabs. Therefore, the application of the FWD for void detection is not recommended at the current moment.

In contrast to the GPR and RDD, TxDOT pavement engineers in general are more familiar with FWD testing and modulus backcalculation. Therefore, this chapter will briefly discuss modulus backcalculation and then focus on determining LTE using the FWD. Finally, some guidelines are provided for FWD testing, data interpretation, and result reporting.

3.2 BACKCALCULATION OF PAVEMENT STRUCTURAL LAYER MODULUS

FWD backcalculation has been studied for a long time, and different software have been developed to backcalculate pavement structural layer modulus. In Texas, MODULUS 6.0 is commonly used for modulus backcalculation (*8*). An example is presented below to demonstrate the modulus backcalculation for a potential HMA overlay project over a section of JCP on US96 in the Beaumont District.

The section of the JCP on US96 is 10 inch concrete with a 10 inch treated base. The MODULUS 6.0 program was used to backcalculate the layer modulus. Table 1 shows the FWD backcalculated moduli, which are required by the HMA overlay thickness design program being developed, as discussed in Chapter 5.

Table 1. FWD Results for US96.

TTI MODULUS ANALYSIS SYSTEM (SUMMARY REPORT) (Version 6.0)

District:20 (Beaumont)
County :122 (JASPER)
Highway/Road: US0096

	Thickness(in)	MODULI RANGE(psi) Minimum	Maximum	Poisson Ratio Values
Pavement:	10.00	340,000	5,500,000	H1: v = 0.20
Base:	10.00	10,000	550,000	H2: v = 0.35
Subbase:	0.00			H3: v = 0.00
Subgrade:	97.98(by DB)	5,000		H4: v = 0.35

Station	Load (lbs)	Measured Deflection (mils): R1	R2	R3	R4	R5	R6	R7	Calculated Moduli values (ksi): SURF(E1)	BASE(E2)	SUBB(E3)	SUBG(E4)	Absolute Dpth to ERR/Sens	Bedrock	
0.000	11,070	4.55	4.01	3.55	3.00	2.52	1.96	1.59	3457.9	315.2	0.0	10.8	1.20	147.5	
0.197	11,098	3.63	3.18	2.80	2.27	1.87	1.46	1.17	5165.5	163.8	0.0	16.0	0.92	137.0	
0.399	11,051	4.20	3.72	3.25	2.65	2.21	1.80	1.42	3383.0	340.2	0.0	12.4	0.75	130.4	
0.595	11,035	7.87	7.20	6.61	5.60	4.69	3.57	2.70	3037.8	81.1	0.0	5.8	2.53	125.1	
0.797	10,880	5.10	4.41	3.86	3.12	2.54	1.95	1.50	3324.7	114.5	0.0	11.9	1.01	123.3	
0.994	10,943	4.64	4.18	3.78	3.16	2.68	2.01	1.49	5458.4	59.1	0.0	10.8	1.96	102.6	
1.200	10,975	6.05	5.27	4.56	3.61	2.76	1.89	1.20	2825.1	13.6	0.0	13.6	2.77	81.5	*
1.393	11,154	2.85	2.35	1.94	1.52	1.20	0.86	0.67	3437.5	316.6	0.0	28.1	1.11	91.5	
1.601	10,876	4.72	4.09	3.54	2.91	2.37	1.80	1.34	3609.0	125.2	0.0	12.8	0.97	104.2	
1.798	11,074	4.40	4.11	3.96	3.35	2.89	2.24	1.69	5500.0	71.7	0.0	10.4	5.29	108.7	*
1.995	10,979	3.49	3.04	2.66	2.26	1.92	1.56	1.28	3816.0	550.0	0.0	13.5	0.52	145.0	*
2.197	10,864	4.88	4.12	3.60	2.68	2.11	1.59	1.09	2649.9	103.6	0.0	15.3	1.46	92.3	
2.399	11,051	3.67	3.24	2.89	2.39	2.03	1.61	1.24	4262.8	401.1	0.0	13.3	1.04	111.1	
2.588	10,721	4.50	4.02	3.60	3.04	2.40	1.91	1.43	5065.9	60.5	0.0	11.8	1.39	103.7	
2.789	10,947	2.69	2.17	1.78	1.36	1.06	0.74	0.59	3183.2	318.3	0.0	32.0	1.47	84.6	
2.999	10,832	4.28	3.81	3.36	2.72	2.24	1.73	1.44	4323.0	131.4	0.0	13.0	1.04	149.4	
3.200	10,947	2.44	2.03	1.64	1.22	0.93	0.66	0.52	4492.1	149.8	0.0	37.8	0.83	88.9	
3.401	11,066	2.41	2.00	1.69	1.29	0.98	0.83	0.68	5500.0	82.2	0.0	36.6	3.86	300.0	*
3.610	11,039	2.97	2.39	2.01	1.52	1.17	0.84	0.62	3135.3	267.4	0.0	28.8	1.44	95.6	
3.612	10,900	3.16	2.43	1.78	1.31	0.98	0.70	0.50	1743.7	289.0	0.0	35.5	1.48	86.9	
3.796	11,051	1.79	1.41	1.13	0.80	0.58	0.39	0.31	5304.9	148.2	0.0	64.4	1.46	73.5	
4.000	10,939	3.06	2.66	2.30	1.72	1.42	1.01	0.81	5500.0	27.2	0.0	26.9	2.19	96.4	*
4.194	10,943	2.55	2.21	1.83	1.55	1.22	0.99	0.85	4423.2	547.7	0.0	23.3	0.99	300.0	
4.399	10,892	3.08	2.66	2.30	1.74	1.41	1.03	0.73	5500.0	31.5	0.0	26.1	1.84	89.1	*
4.600	10,880	2.70	2.30	1.99	1.65	1.34	1.06	0.87	4273.2	550.0	0.0	21.1	0.50	138.1	*
4.801	10,983	3.06	2.61	2.30	1.90	1.56	1.30	1.10	4096.2	550.0	0.0	17.3	1.22	300.0	*
4.998	10,876	2.80	2.26	1.98	1.52	1.17	0.90	0.75	3419.0	363.8	0.0	26.5	1.48	130.8	
5.199	10,816	2.99	2.57	2.31	1.79	1.41	1.17	0.95	5500.0	103.0	0.0	22.4	2.83	149.6	*
5.400	10,896	3.28	2.91	2.48	1.95	1.64	1.30	1.08	4512.2	259.3	0.0	18.0	1.34	168.8	
5.602	10,991	2.20	1.85	1.56	1.24	1.05	0.81	0.69	5500.0	144.2	0.0	36.5	6.64	118.9	*
5.799	10,717	2.87	2.49	2.15	1.79	1.62	1.11	0.85	4369.7	517.6	0.0	18.2	2.95	300.0	
6.000	10,689	3.24	2.89	2.49	2.01	1.59	1.29	0.99	5161.6	176.3	0.0	18.0	1.00	109.2	
6.204	10,705	3.24	2.69	2.35	1.90	1.51	1.16	0.96	3345.8	364.2	0.0	19.4	1.18	129.3	
6.401	10,816	3.76	3.24	2.83	2.30	1.91	1.41	1.09	4500.3	152.8	0.0	16.1	1.62	109.5	
Mean:		3.62	3.13	2.73	2.20	1.79	1.37	1.06	4199.3	232.1	0.0	21.3	1.77	118.0	
Std. Dev:		1.21	1.14	1.08	0.93	0.79	0.61	0.45	1017.8	169.7	0.0	11.6	1.31	36.3	
Var Coeff(%):		33.41	36.37	39.42	42.28	44.08	44.39	42.60	24.2	73.1	0.0	54.2	73.72	30.7	

3.3 APPLICATION OF FWD TESTING TO DETERMINE LOAD TRANSFER EFFICIENCY

In addition to pavement layer thickness and modulus, LTE is another important parameter that should be characterized for concrete pavement before HMA overlay. Generally, FWD is used to evaluate the LTE of joints in concrete pavements. LTE testing begins with the placement of the FWD load plate 6 inches from the joint, measured from the center of the plate to the joint or crack. An FWD load is then imparted to the pavement while the deflections across the joint or crack are recorded. The sensors for measuring deflections are placed at the center of the plate and 12 inches from the center of the load plate across the joint. LTE tests are usually performed in the outer wheelpath of the outside lane. LTE calculations can be made by placing the FWD load plate on either side of the joint, where the approach side is called upstream and the leave side is called downstream. Downstream measurements require that a deflection sensor be placed behind the load plate. Typically the sensor W4 (36 inches from center of load plate) is placed on the back side of the load plate (-12 inches). Downstream measurements are not typically done in Texas; the upstream measurements are more common.

Testing should be done at a minimum at one load level. It is preferable to test at three load levels—8 kips, 12 kips, and 16 kips. Also, it is recommended that testing should be performed across joints (or cracks) at intervals of no greater than 0.1 mile. It is also recommended that testing be conducted in the cooler part of the day, preferably early morning when the LTE will be smallest.

Figure 13 illustrates the concept of deflection load transfer for two extreme cases: a joint with full load transfer and a joint with no load transfer. Joint deflection LTE values may range from 0 percent (no load transfer) to 100 percent (full load transfer). The LTE described above is the deflection load transfer and is often defined as the ratio of the deflection of the unloaded side to the deflection of the loaded side. The FWD deflection data can be used in three different ways to determine LTE in terms of the measured deflection, which are illustrated in Figure 14. The advantage and disadvantage of each approach are discussed in Table 2. Clearly, Approach 3 is preferred, because both layer moduli of pavement structure backcalculated from FWD testing at slab center and LTE at joints are needed for asphalt overlay thickness design.

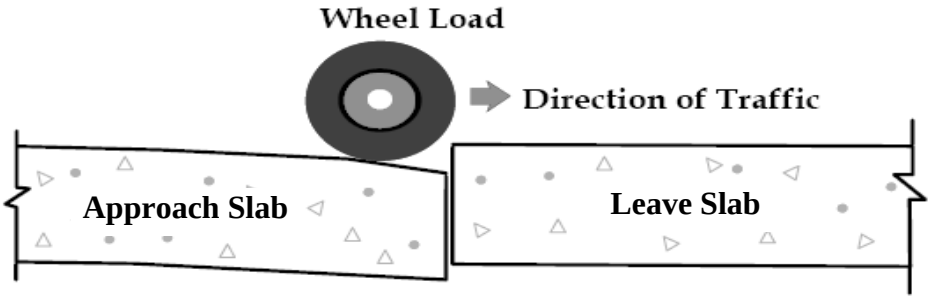

(a) Leave slab deflection: LTE = 0 %

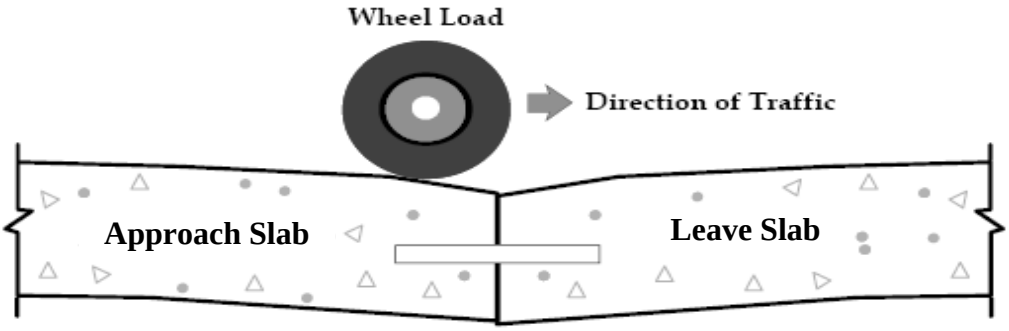

(b) Leave slab deflection (= approach slab deflection): LTE = 100 %

Figure 13. Illustration of Poor and Good Load Transfer across a Joint (9).

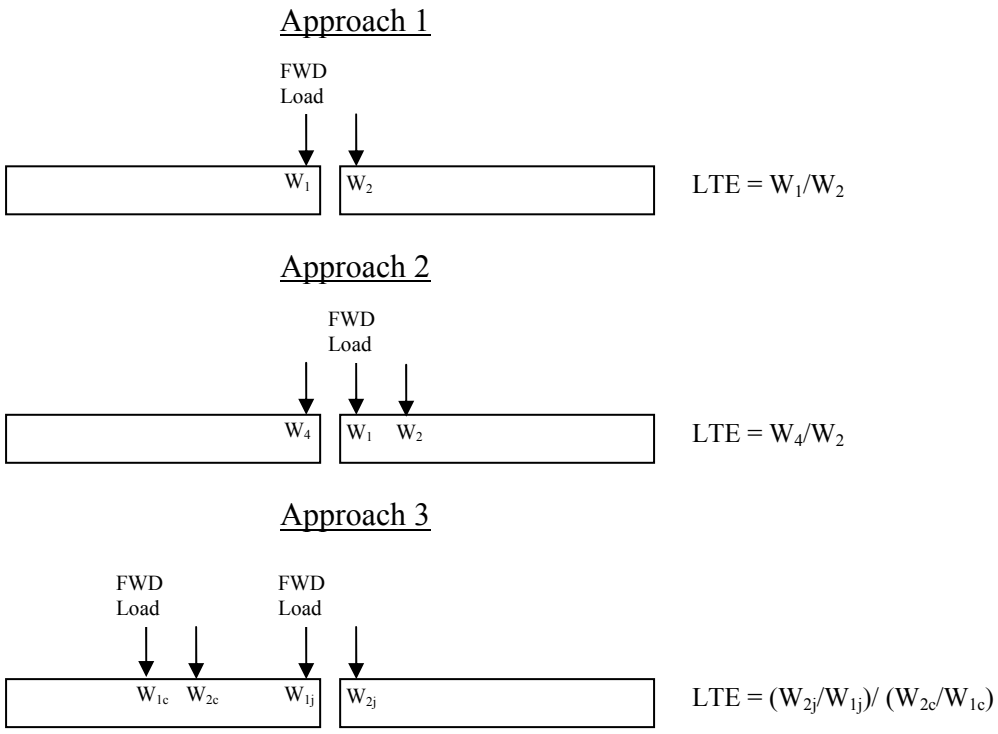

Figure 14. FWD Based LTE Definitions.

Table 2. Advantage and Disadvantage of Each LTE Approach.

Approach	Advantages	Disadvantage(s)
1	Only FWD testing at joint is needed; FWD sensors are not required to change their arrangement.	100 % LTE may never be reached.
2	Conceptually sound: 100 % LTE becomes possible; Only FWD testing at joint is needed.	W4 sensor has to be placed on the back side of the load plate.
3	Conceptually sound: 100 % LTE becomes possible. FWD sensors are not required to change their arrangement. FWD testing at slab center can be used to backcalculate layer moduli of the pavement structure.	Both FWD testing at the center of the slab and joint are required.

The load transfer rating as related to the LTE is shown in Table 3. For joints with LTE rated below fair, joint replacement or improvement (dowel bar retrofit) is recommended before placing HMA overlay.

Table 3. LTE Rating.

Load Transfer Rating	LTE (%)
Good	>80
Fair	60-80
Poor	<60

For the purpose of demonstration, two examples are presented: one with good LTE and the other with both good and poor LTE. For these two examples, the upstream FWD testing was performed where the load plate is placed on one side of the joint and the remaining six sensors are placed on the other side. Detailed information is presented below:

- **Example 1: A Section of JCP with Good LTE**

The raw FWD data are shown in Figures 15a and 15b, and the calculated LTE for each joint using Approach 3 is listed in Table 4. Note that LTEs at some joints may be greater than 100 percent. In these cases, the 100 percent LTE is recommended. Clearly, all joints are in good condition; this section appears to be a good candidate for an overlay.

FWD TEST FILE NAME:E:\5123\reports\2006 report\final version\122U0096-good section.FWD
ROADWAY ID :20122 US0096
District   : 20 (Beaumont)
County   : 122 (JASPER)
Highway/Road: US0096
Total Drops : 1   and drop: 1 is selected

TESTED DATE : 050623   NUMBER OF SENSORS: 7   NUMBER OF STATION : 65
START TIME : 13:42   PLATE RADIUS   : 5.91   FWD OPERATOR   : Acil Diffey
END TIME   : 15:28

No	SENSOR SPACING : STATION	LNE	LOAD	0.0 W1	12.0 W2	24.0 W3	36.0 W4	48.0 W5	60.0 W6	72.0 W7	PVMT TEMP	AIR TEMP	SURF TEMP	TEST TIME	COMMENTS
1	0.000	L	11071	4.55	4.01	3.55	3.00	2.52	1.96	1.59	0	97	0	13:42	First Mid-Stream Drop.
3	0.197	L	11099	3.63	3.18	2.80	2.27	1.87	1.46	1.17	0	95	0	13:52	Test at Mid-stream
5	0.399	L	11052	4.20	3.72	3.25	2.65	2.21	1.80	1.42	0	95	0	13:56	test 3 mid-stream
7	0.595	L	11036	7.87	7.20	6.61	5.60	4.69	3.57	2.70	0	95	0	14:00	test 4 mid-stream.
9	0.797	L	10881	5.10	4.41	3.86	3.12	2.54	1.95	1.50	0	95	0	14:03	test 5 mid-stream.
11	0.994	L	10944	4.64	4.18	3.78	3.16	2.68	2.01	1.49	0	95	0	14:06	test 6 midstream.
13	1.200	L	10976	6.05	5.27	4.56	3.61	2.76	1.89	1.20	0	95	0	14:09	test 7 mid-stream.
15	1.393	L	11155	2.85	2.35	1.94	1.52	1.20	0.86	0.67	0	94	0	14:12	test 8 mid-stream.
17	1.601	L	10877	4.72	4.09	3.54	2.91	2.37	1.80	1.34	0	94	0	14:15	test 9 mid-stream.
19	1.798	L	11075	4.40	4.11	3.96	3.35	2.89	2.24	1.69	0	96	0	14:18	test 10 mid-stream.
21	1.995	L	10980	3.49	3.04	2.66	2.26	1.92	1.56	1.28	0	98	0	14:21	test 11 mid-stream.
23	2.197	L	10865	4.88	4.12	3.60	2.68	2.11	1.59	1.09	0	99	0	14:23	test 12 mid-stream.
25	2.399	L	11052	3.67	3.24	2.89	2.39	2.03	1.61	1.24	0	98	0	14:26	test 13 mid-stream.
28	2.789	L	10948	2.69	2.17	1.78	1.36	1.06	0.74	0.59	0	99	0	14:31	test 15 mid-stream.
30	2.999	L	10833	4.28	3.81	3.36	2.72	2.24	1.73	1.44	0	99	0	14:35	test 16 mid-stream.
32	3.200	L	10948	2.44	2.03	1.64	1.22	0.93	0.66	0.52	0	99	0	14:38	test 17 mid-stream.
34	3.401	L	11067	2.41	2.00	1.69	1.29	0.98	0.83	0.68	0	99	0	14:42	test 18 mid-stream.
36	3.610	L	11040	2.97	2.39	2.01	1.52	1.17	0.84	0.62	0	99	0	14:44	test 19 mid-stream.
38	3.796	L	11052	1.79	1.41	1.13	0.80	0.58	0.39	0.31	0	99	0	14:47	test 20 mid-stream.
40	4.000	L	10940	3.06	2.66	2.30	1.72	1.42	1.01	0.81	0	99	0	14:50	test 21 nid-stream.
42	4.194	L	10944	2.55	2.21	1.83	1.55	1.22	0.99	0.85	0	98	0	14:52	test 22 mid-stream.
44	4.399	L	10893	3.08	2.66	2.30	1.74	1.41	1.03	0.73	0	99	0	14:55	test 23 mid-stream.
46	4.600	L	10881	2.70	2.30	1.99	1.65	1.34	1.06	0.87	0	98	0	14:58	test 24 mid-stream.
48	4.801	L	10984	3.06	2.61	2.30	1.90	1.56	1.30	1.10	0	97	0	15:02	test 25 mid-stream.
50	4.998	L	10877	2.80	2.26	1.98	1.52	1.17	0.90	0.75	0	99	0	15:04	test 26 mid-stream.
52	5.199	L	10817	2.99	2.57	2.31	1.79	1.41	1.17	0.95	0	99	0	15:07	test 27 mid-stream.
54	5.400	L	10897	3.28	2.91	2.48	1.95	1.64	1.30	1.08	0	99	0	15:09	test 28 mid-stream.
56	5.602	L	10992	2.20	1.85	1.56	1.24	1.05	0.81	0.69	0	99	0	15:12	test 29 mid-stream.
58	5.799	L	10718	2.87	2.49	2.15	1.79	1.62	1.11	0.85	0	99	0	15:15	test 30 mid-stream .
60	6.000	L	10690	3.24	2.89	2.49	2.01	1.59	1.29	0.99	0	98	0	15:17	test 31 mid-stream.
62	6.204	L	10706	3.24	2.69	2.35	1.90	1.51	1.16	0.96	0	99	0	15:24	test 32 mid-stream.
64	6.401	L	10817	3.76	3.24	2.83	2.30	1.91	1.41	1.09	0	100	0	15:27	test 33 mid-stream

Figure 15a. Raw FWD Data at Slab Center for a Section of JCP with Good LTE.

FWD TEST FILE NAME:C:\5123\report\122U0096-good LTE.FWD
ROADWAY ID :20122 US0096
District   : 20 (Beaumont)
County   : 122 (JASPER)
Highway/Road: US0096
Total Drops : 1   and drop: 1 is selected

TESTED DATE : 050623   NUMBER OF SENSORS: 7   NUMBER OF STATION : 65
START TIME : 13:42   PLATE RADIUS   : 5.91   FWD OPERATOR   : Acil Diffey
END TIME   : 15:28

No	SENSOR SPACING : STATION	LNE	LOAD	0.0 W1	12.0 W2	24.0 W3	36.0 W4	48.0 W5	60.0 W6	72.0 W7	PVMT TEMP	AIR TEMP	SURF TEMP	TEST TIME	COMMENTS
2	0.002	L	11171	4.08	3.17	2.58	2.06	1.67	1.33	1.05	0	94	0	13:49	Test 1 joint
4	0.199	L	10960	5.28	4.84	3.96	3.11	2.46	1.83	1.39	0	95	0	13:54	Test 2 jiont
6	0.400	L	11111	3.97	3.62	3.19	2.51	2.11	1.69	1.38	0	95	0	13:58	test 3 joint
8	0.597	L	10909	3.84	3.37	2.70	2.02	1.51	1.11	0.78	0	94	0	14:01	test 4 joint.
10	0.799	L	10940	5.03	4.66	3.80	2.93	2.33	1.74	1.36	0	95	0	14:04	test 5 joint.
12	0.995	L	10913	8.60	7.65	6.25	4.73	3.61	2.54	1.59	0	95	0	14:07	test 6 joint.
14	1.201	L	10944	5.12	4.75	3.85	2.85	2.16	1.52	1.09	0	94	0	14:10	test 7 joint.
16	1.394	L	10924	3.86	3.38	2.85	2.22	1.68	1.20	0.86	0	95	0	14:13	test 8 joint.
18	1.603	L	10873	5.61	4.91	4.03	3.15	2.47	1.81	1.37	0	95	0	14:16	test 9 joint.
20	1.799	L	10738	6.54	5.32	4.10	2.70	1.87	1.31	0.99	0	97	0	14:19	test 10 joint.
22	1.997	L	10730	6.17	5.89	5.44	4.58	4.02	3.59	3.31	0	98	0	14:22	test 11 joint.
24	2.199	L	10829	3.60	3.11	2.58	1.95	1.54	1.15	0.90	0	99	0	14:25	test 12 joint.
26	2.401	L	10960	3.83	3.28	2.75	2.22	1.80	1.40	1.15	0	99	0	14:27	test 13 joint.
29	2.790	L	10817	2.92	2.49	2.02	1.51	1.14	0.86	0.63	0	98	0	14:33	test 15 joint.
31	3.001	L	10670	4.29	3.86	3.21	2.54	2.06	1.66	1.33	0	100	0	14:36	test 16 joint.
33	3.202	L	10948	2.11	1.76	1.40	1.05	0.80	0.60	0.49	0	99	0	14:40	test 17 joint.
35	3.403	L	10877	2.45	2.02	1.65	1.29	1.05	0.83	0.69	0	100	0	14:43	test 18 joint.
37	3.612	L	10901	3.16	2.43	1.78	1.31	0.98	0.70	0.50	0	99	0	14:45	test 19 joint.
39	3.797	L	10897	1.78	1.36	1.02	0.71	0.50	0.35	0.25	0	100	0	14:48	test 20 joint.
41	4.002	L	10917	2.97	2.43	2.11	1.53	1.22	0.87	0.69	0	99	0	14:51	test 21 joint.
43	4.196	L	11064	2.52	2.19	1.81	1.43	1.19	0.96	0.79	0	98	0	14:53	test 22 joint.
45	4.401	L	10913	2.66	2.40	1.98	1.56	1.30	0.96	0.76	0	99	0	14:56	test 23 joint.
47	4.601	L	10793	2.78	2.39	1.98	1.53	1.30	1.05	0.91	0	97	0	15:00	test 24 joint.
49	4.803	L	10726	3.04	2.76	2.39	1.92	1.63	1.33	1.12	0	98	0	15:03	test 25 joint.
51	5.000	L	10944	2.65	2.17	1.79	1.39	1.15	0.85	0.76	0	99	0	15:05	test 26 joint.
53	5.201	L	10988	3.03	2.59	2.15	1.73	1.17	1.09	0.84	0	99	0	15:08	test 27 joint.
55	5.402	L	10801	3.23	2.85	2.38	1.87	1.57	1.26	1.02	0	99	0	15:10	test 28 joint.
57	5.603	L	10924	2.10	1.71	1.45	1.14	0.93	0.76	0.65	0	99	0	15:13	test 29 joint.
59	5.800	L	10797	2.82	2.34	1.90	1.39	1.13	0.84	0.74	0	99	0	15:15	test 30 joint.
61	6.001	L	10845	4.06	3.19	2.56	1.89	1.54	1.09	0.86	0	99	0	15:22	test 31 joint.
63	6.206	L	10714	3.26	2.81	2.39	1.91	1.57	1.24	1.01	0	99	0	15:25	test 32 joint.
65	6.403	L	10809	3.80	3.45	2.78	2.14	1.73	1.37	1.07	0	101	0	15:28	test 33 joint.

Figure 15b. Raw FWD Data at Joint for a Section of JCP with Good LTE.

Table 4. Joints with Good LTE on US96.

Joint	FWD Test at Slab Center		FWD Test at Joint		LTE (%)-Approach 3	Rating
	W_{1c} (mils)	W_{2c} (mils)	W_{1j} (mils)	W_{2j} (mils)		
1	4.55	4.01	4.08	3.17	88	Good
2	3.63	3.18	5.28	4.84	100	Good
3	4.20	3.72	3.97	3.62	100	Good
4	7.87	7.20	3.84	3.37	96	Good
5	5.10	4.41	5.03	4.66	100	Good
6	4.64	4.18	8.60	7.65	99	Good
7	6.05	5.27	5.12	4.75	100	Good
8	2.85	2.35	3.86	3.38	100	Good
9	4.72	4.09	5.61	4.91	100	Good
10	4.40	4.11	6.54	5.32	87	Good
11	3.49	3.04	6.17	5.89	100	Good
12	4.88	4.12	3.60	3.11	100	Good
13	3.67	3.24	3.83	3.28	97	Good
15	2.69	2.17	2.92	2.49	100	Good
16	4.28	3.81	4.29	3.86	100	Good
17	2.44	2.03	2.11	1.76	100	Good
18	2.41	2.00	2.45	2.02	99	Good
19	2.97	2.39	3.16	2.43	96	Good
20	1.79	1.41	1.78	1.36	97	Good
21	3.06	2.66	2.97	2.43	94	Good
22	2.55	2.21	2.52	2.19	100	Good
23	3.08	2.66	2.66	2.40	100	Good
24	2.70	2.30	2.78	2.39	100	Good
25	3.06	2.61	3.04	2.76	100	Good
26	2.80	2.26	2.65	2.17	100	Good
27	2.99	2.57	3.03	2.59	99	Good
28	3.28	2.91	3.23	2.85	99	Good
29	2.20	1.85	2.10	1.71	97	Good
30	2.87	2.49	2.82	2.34	96	Good
31	3.24	2.89	4.06	3.19	88	Good
32	3.24	2.69	3.26	2.81	100	Good
33	3.76	3.24	3.80	3.45	100	Good

- **Example 2: A Section of JCP with both Good and Poor LTE**

The raw FWD data of Example 2 are shown in Figures 16a and 16b, and the calculated LTE for each joint using Approach 3 is listed in Table 5. The LTE shown in Table 5 indicates that the beginning section of this JCP has very poor load transfer, and those joints are required to be replaced or improved prior to overlaying. The LTE in the second half of the project are better, but some of the joints (e.g., joint 25) are classified as poor.

FWD TEST FILE NAME:E:\5123\reports\2006 report\final version\124SO136 poor LTE.FWD
ROADWAY ID :20124 SL0136
District : 20 (Beaumont)
County : 124 (JEFFERSON)
Highway/Road: SL0136
Total Drops : 1 and drop: 1 is selected

TESTED DATE : 050624 NUMBER OF SENSORS: 7 NUMBER OF STATION : 69
START TIME : 09:09 PLATE RADIUS : 5.91 FWD OPERATOR : Acil Diffey
END TIME : 11:41

No	SENSOR SPACING : STATION	LNE	LOAD	0.0 W1	12.0 W2	24.0 W3	36.0 W4	48.0 W5	60.0 W6	72.0 W7	PVMT TEMP	AIR TEMP	SURF TEMP	TEST TIME	COMMENTS
1	-8	K	11357	7.40	6.85	6.46	5.49	4.87	4.12	3.68	0	90	0	09:09	TEST 1 MID-STREAM.
3	208	K	11210	7.82	7.36	7.01	6.19	5.59	4.98	4.59	0	89	0	09:12	TEST 2 MID-STREAM.
5	414	K	11222	7.07	6.51	6.11	5.17	4.60	3.91	3.49	0	89	0	09:15	TEST 3 MID-STREAM.
7	602	K	11171	8.64	8.02	7.53	6.72	6.26	5.86	5.67	0	90	0	09:17	TEST 4 MID-STREAM.
9	808	K	11135	7.76	7.10	6.61	5.61	4.81	3.93	3.15	0	91	0	10:06	TEST 5 MID-STREAM.
11	1015	K	11155	6.37	5.83	5.43	4.57	3.87	3.07	2.41	0	91	0	10:13	TEST 6 mid-stream.
13	1202	K	11032	7.61	7.17	6.62	5.67	4.85	3.87	3.06	0	91	0	10:15	TEST 7 mid-stream
15	1408	K	11099	6.80	6.24	5.74	4.91	4.23	3.57	3.01	0	93	0	10:18	TEST 8 mid-streaam.
17	1614	K	11151	6.44	5.93	5.59	4.85	4.28	3.59	3.03	0	93	0	10:20	TEST 9 mid-stream.
19	1800	K	11004	6.77	6.28	5.89	5.11	4.52	3.80	3.20	0	94	0	10:22	TEST 10 mid-stream.
21	2007	K	10964	6.80	6.17	5.66	4.71	4.02	3.35	2.85	0	96	0	10:25	TEST 11 mid-stream.
23	2213	K	10920	7.17	6.44	5.99	5.07	4.29	3.44	2.70	0	93	0	10:27	TEST 12 mid-stream.
25	2440	K	10984	7.79	7.27	6.91	6.01	5.36	4.61	3.95	0	92	0	10:31	TEST 13 mid-stream.
27	2605	K	10857	6.99	6.52	6.22	5.46	4.83	4.04	3.32	0	94	0	10:35	TEST 14 mid-stream.
29	3061	K	10956	7.59	7.10	6.76	5.93	5.31	4.62	4.07	0	95	0	10:39	TEST 15 mid-stream.
31	3535	K	10905	7.88	7.44	7.07	6.05	5.18	4.19	3.30	0	95	0	10:41	TEST 16 mid-stream.
33	4011	K	10881	7.30	6.72	6.22	5.16	4.32	3.46	2.77	0	95	0	10:44	TEST 17 mid-stream.
35	4506	K	10865	6.74	6.17	5.68	4.78	4.04	3.24	2.57	0	96	0	10:46	TEST 18 mid-stream.
37	6053	K	10893	7.03	6.56	6.18	5.21	4.43	3.53	2.76	0	94	0	10:57	TEST 19 mid-stream,
39	7797	K	10821	6.47	5.94	5.61	4.60	3.85	3.01	2.29	0	93	0	11:00	TEST 20 mid-stream.
41	0	K	10909	5.76	5.21	4.85	3.83	3.09	2.37	1.95	0	95	0	11:04	TEST 21 mid-stream.
43	559	K	10825	7.52	6.79	6.17	4.94	4.00	3.08	2.44	0	94	0	11:07	TEST 22 MID-STREAM.
45	990	K	10837	7.04	6.44	6.05	5.05	4.33	3.44	2.67	0	93	0	11:09	TEST 23 mid-stream.
47	1404	K	10813	5.80	5.42	5.27	4.57	4.02	3.28	2.61	0	94	0	11:12	TEST 24 mid-stream.
50	1527	K	10750	8.69	6.81	5.80	4.36	3.53	2.72	2.13	0	94	0	11:18	TEST 25 mid-stream.
52	2015	K	10742	6.30	5.71	5.39	4.35	3.70	2.87	2.11	0	95	0	11:21	TEST 26 mid-stream.
54	2535	K	10897	6.35	5.89	5.61	4.67	3.94	3.01	2.23	0	95	0	11:24	TEST 27 mid-stream
56	3029	K	10913	5.19	4.79	4.48	3.69	3.08	2.44	1.92	0	95	0	11:26	TEST 28 mid-stream.
58	3547	K	10646	8.02	6.38	5.15	3.92	2.94	2.06	1.44	0	95	0	11:28	TEST 29 mid-stream.
60	4022	K	10821	8.61	8.07	7.62	6.37	5.44	4.30	3.43	0	95	0	11:31	TEST 30 mid-stream.
62	4519	K	10797	7.79	6.78	5.93	4.92	4.04	3.06	2.24	0	95	0	11:33	TEST 31 mid-stream.
64	5016	K	10674	7.72	6.97	6.30	5.34	4.52	3.52	2.61	0	94	0	11:36	TEST 32 mid-stream.

Figure 16a. Raw FWD Data at Slab Center for a Section of JCP with Both Good and Poor LTE.

FWD TEST FILE NAME:C:\5123\report\124S0136 poor LTE.FWD
ROADWAY ID :20124 SL0136
District   : 20 (Beaumont)
County   : 124 (JEFFERSON)
Highway/Road: SL0136
Total Drops : 1   and drop: 1 is selected

TESTED DATE : 050624   NUMBER OF SENSORS: 7   NUMBER OF STATION : 69
START TIME : 09:09   PLATE RADIUS   : 5.91   FWD OPERATOR   : Acil Diffey
END TIME   : 11:41

No	SENSOR SPACING : STATION	LNE	LOAD	0.0 W1	12.0 W2	24.0 W3	36.0 W4	48.0 W5	60.0 W6	72.0 W7	PVMT TEMP	AIR TEMP	SURF TEMP	TEST TIME	COMMENTS
2	9	K	11079	15.17	5.61	5.01	4.12	3.56	2.94	2.47	0	89	0	09:11	TEST 1 JOINT.
4	217	K	10909	24.02	5.11	4.75	4.00	3.48	3.03	2.69	0	89	0	09:13	TEST 2 JOINT.
6	424	K	10909	20.72	5.43	4.93	4.02	3.53	2.96	2.33	0	89	0	09:16	TEST 3 JOINT.
8	610	K	10750	23.64	2.38	2.37	1.93	1.93	1.78	1.65	0	90	0	10:03	TEST 4 JOINT.
10	817	K	11032	12.26	8.48	7.38	6.06	5.07	4.13	3.34	0	92	0	10:12	TEST 5 joint.
12	1024	K	11028	9.67	7.37	6.25	4.94	4.01	3.15	2.55	0	91	0	10:14	TEST 6 joint.
14	1209	K	10829	13.90	7.00	5.91	4.71	3.85	3.03	2.45	0	91	0	10:16	TEST 7 joint
16	1417	K	10805	14.70	4.74	4.29	3.58	3.13	2.65	2.23	0	92	0	10:19	TEST 8 joint.
18	1622	K	10837	14.45	5.73	5.03	4.08	3.41	2.83	2.32	0	93	0	10:21	TEST 9 joint.
20	1807	K	10785	14.47	6.18	5.39	4.28	3.56	2.81	2.39	0	94	0	10:23	TEST 10 joint.
22	2014	K	10714	12.94	6.19	4.90	3.54	2.88	2.71	2.37	0	94	0	10:26	TEST 11 joint.
24	2221	K	10595	14.58	5.50	4.81	3.76	3.14	2.61	2.17	0	92	0	10:28	TEST 12 joint.
26	2449	K	10619	16.60	5.00	4.52	3.80	3.25	2.80	2.44	0	94	0	10:33	TEST 13 joint.
28	2614	K	10809	11.33	7.04	6.11	5.11	4.35	3.61	3.00	0	95	0	10:37	TEST 14 joint.
30	3068	K	10654	16.77	6.28	5.57	4.66	4.08	3.45	3.00	0	94	0	10:40	TEST 15 joint.
32	3543	K	10746	9.73	8.07	6.87	5.50	4.53	3.68	2.99	0	95	0	10:42	TEST 16 joint.
34	4017	K	10845	10.11	8.23	7.00	5.57	4.55	3.62	2.97	0	97	0	10:44	TEST 17 joint.
36	4514	K	10857	8.56	8.03	6.80	5.39	4.38	3.48	2.80	0	95	0	10:47	TEST 18 joint.
38	6061	K	10698	12.60	6.76	5.84	4.61	3.84	2.99	2.52	0	93	0	10:58	TEST 19 joint.
40	7806	K	10825	9.71	7.89	6.59	4.86	3.80	2.86	2.27	0	94	0	11:01	TEST 20 joint.
42	7	K	10722	8.26	6.58	5.57	3.95	3.32	2.44	2.01	0	95	0	11:06	TEST 21 JOINT.
44	566	K	10627	11.41	7.39	6.31	4.63	3.74	2.81	2.33	0	94	0	11:08	TEST 22 joint.
46	999	K	10817	8.02	7.67	6.61	5.18	4.23	3.39	2.76	0	93	0	11:10	TEST 23 joint.
48	1412	K	10642	8.00	5.21	4.59	3.64	3.06	2.52	2.07	0	93	0	11:14	TEST 24 joint.
51	1537	K	10706	10.76	5.36	4.62	3.54	2.85	2.20	2.03	0	94	0	11:19	TEST 25 joint.
53	2024	K	10678	8.96	6.39	5.45	4.21	3.40	2.69	2.17	0	97	0	11:22	TEST 26 joint.
55	2542	K	11167	8.25	7.22	5.96	4.66	3.70	2.91	2.34	0	96	0	11:25	TEST 27 joint.
57	3037	K	10869	6.90	6.22	5.33	4.10	3.37	2.59	2.17	0	94	0	11:27	TEST 28 joint.
59	3555	K	10674	8.77	7.03	5.74	4.91	3.81	3.40	1.66	0	96	0	11:30	TEST 29 joint.
61	4031	K	10710	8.81	7.44	6.43	5.20	4.25	3.34	2.60	0	94	0	11:32	TEST 30 joint.
63	4528	K	10805	7.01	5.88	4.87	3.81	3.05	2.30	1.72	0	94	0	11:34	TEST 31 joint.
65	5025	K	10690	6.87	5.89	4.95	3.98	3.21	2.51	1.93	0	96	0	11:37	TEST 32 joint.

Figure 16b. Raw FWD Data at Joints for a Section of JCP with Both Good and Poor LTE.

Table 5. Joints with Both Good and Poor LTE.

Joint	FWD Test at Slab Center		FWD Test at Joint		LTE (%)-Approach 3	Rating
	W_{1c} (mils)	W_{2c} (mils)	W_{1j} (mils)	W_{2j} (mils)		
1	7.40	6.85	15.17	5.61	40	Poor
2	7.82	7.36	24.02	5.11	23	Poor
3	7.07	6.51	20.72	5.43	28	Poor
4	8.64	8.02	23.64	2.38	11	Poor
5	7.76	7.10	12.26	8.48	76	Fair
6	6.37	5.83	9.67	7.37	83	Good
7	7.61	7.17	13.90	7.00	53	Poor
8	6.80	6.24	14.70	4.74	35	Poor
9	6.44	5.93	14.45	5.73	43	Poor
10	6.77	6.28	14.47	6.18	46	Poor
11	6.80	6.17	12.94	6.19	53	Poor
12	7.17	6.44	14.58	5.50	42	Poor
13	7.79	7.27	16.60	5.00	32	Poor
14	6.99	6.52	11.33	7.04	67	Fair
15	7.59	7.10	16.77	6.28	40	Poor
16	7.88	7.44	9.73	8.07	88	Good
17	7.30	6.72	10.11	8.23	88	Good
18	6.74	6.17	8.56	8.03	100	Good
19	7.03	6.56	12.60	6.76	57	Poor
20	6.47	5.94	9.71	7.89	89	Good
21	5.76	5.21	8.26	6.58	88	Good
22	7.52	6.79	11.41	7.39	72	Fair
23	7.04	6.44	8.02	7.67	100	Good
24	5.80	5.42	8.00	5.21	70	Fair
25	8.69	6.81	10.76	5.36	64	Fair
26	6.30	5.71	8.96	6.39	79	Fair
27	6.35	5.89	8.25	7.22	94	Good
28	5.19	4.79	6.90	6.22	98	Good
29	8.02	6.38	8.77	7.03	100	Good
30	8.61	8.07	8.81	7.44	90	Good
31	7.79	6.78	7.01	5.88	96	Good
32	7.72	6.97	6.87	5.89	95	Good

3.4 GENERAL GUIDELINES FOR FWD TESTING, DATA INTERPRETATION, AND REPORTING

Generally, an FWD survey is proposed for projects where a structural overlay is to be designed. Note that functional HMA overlays applied to improve surface friction (such as HMA overlays over Continuously Reinforced Concrete Pavements [CRCP]) are not included in this discussion. Based on the information presented above, some general guidelines for FWD testing, data interpretation, and data reporting are recommended as follows:

- FWD testing: For JCP (including JCP pavements with thin AC overlays), an FWD test is performed initially at the center of the slab and then move forward to the next joint location. At a joint (or crack), perform an upstream test where the load plate is placed on one side of the joint, and the remaining six sensors are placed on the other side, as shown in Figure 14 (Approach 3). Test at a minimum of 30 locations along the project, but do not collect data at intervals of greater than 0.1 mile. For very long projects, for example greater than 10 miles, at the engineer's discretion, the data collection interval can be extended to every 0.2 miles.

  For structural overlays of CRCP, in general, the same testing process proposed above for JCP evaluation is applicable for deteriorated CRCP. The only difference is that structurally deteriorated CRCP can have severe cracks instead of joints. In reality, the LTE on most CRCP pavements is not typically a problem; in the testing conducted to date, the LTEs are typically greater than 90 percent. However, as being described later on the IH20 project, low LTE values can be obtained on deteriorated CRCP. In addition, to ensure that the computed LTE reflects the actual LTE at joints and/or cracks, FWD testing temperature should be considered during testing. Testing should be avoided during hot portions of the day (after 11 am, typically) to avoid joint lockup. On cool, overcast days, deflection testing may be performed throughout the day.

  For flexible pavements dominated by transverse cracking, the similar FWD testing procedure proposed for JCP can be followed. However, it

should be noted that cracks in flexible pavements may be random, and consequently, it may be difficult to determine LTE based on FWD testing. If this is the case, it is proposed to simply classify the LTE as the following three classifications based on severity of cracks:

  - Good: crack width is less than 3/8 inch;
  - Fair: crack width is between 3/8 inch and 3/4 inch or filled crack surrounded by random cracking; and
  - Poor: crack width is over 3/4 inch or filled crack surrounded by medium or high severity random cracking.

  Note that for all FWD testing, the temperatures at mid-depth slab for concrete pavements or at mid-depth of the HMA layer should be measured at the start and end of the test.

- FWD data interpretation: The MODULUS 6.0 program should be used to backcalculate layer moduli of existing pavements, and the average value of backcalculated modulus for each layer is also provided by the MODULUS 6.0 program. Regarding the LTE at joints and/or cracks, Approach 3, shown in Figure 14, is recommended to determine the LTE (= $(W_{2j}/W_{1j})/ (W_{2c}/W_{1c})$). Then an average value of the LTE should be calculated for the whole project. The next step is to rate the LTE as good, fair, or poor based on the recommendation in Table 3. Note that for those joints and/or cracks rated below fair (Table 3), joint (or crack) replacement or improvement is recommended before placing the HMA overlay.
- FWD data reporting: The expected data from FWD testing are 1) average modulus for each pavement layer, 2) rating of average LTE, and 3) number of joints or cracks needed to replace or improve.

Additionally, it should be noted that FWD testing is only at discrete points, and it is time consuming and sometimes difficult to use the FWD to determine the load transfer at joints and/or cracks. The best the FWD can do is to provide a sample of LTEs along a project. For a long project (e.g., >10 miles), this limitation is more significant. In order to better evaluate existing PCC pavements, continuous measurements of pavement surface deflections are desired and discussed in the next chapter.

CHAPTER 4

APPLICATION OF ROLLING DYNAMIC DEFLECTOMETER ON EVALUATING EXISTING PCC PAVEMENTS

4.1 BACKGROUND

The RDD shown in Figure 17 was developed in the 1990s at the Center for Transportation Research in Austin under the direction of Drs. Ken Stokoe and Jim Bay (*10*). The RDD places a cyclic load on the pavement as it rolls along at 1.5 mph; for pavement testing, the load is usually fixed at 10,000 lb with a frequency of 30 Hz. One innovative feature of the RDD is the four rolling geophones, which continuously measure the movement of the pavement surface at different offsets from the load wheels shown in Figure 18.

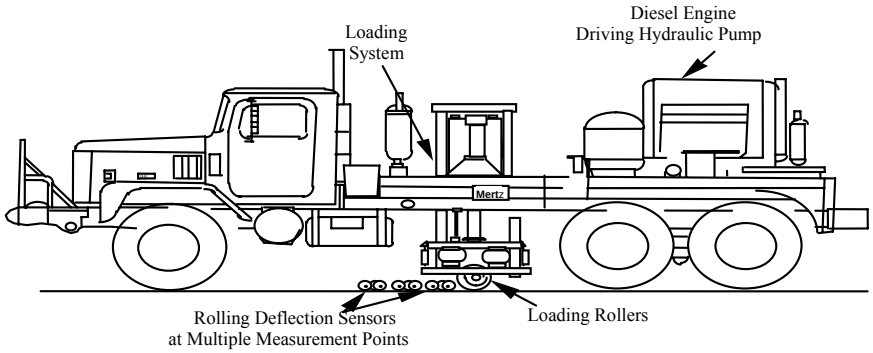

Figure 17. TxDOT's Rolling Dynamic Deflectometer (*10*).

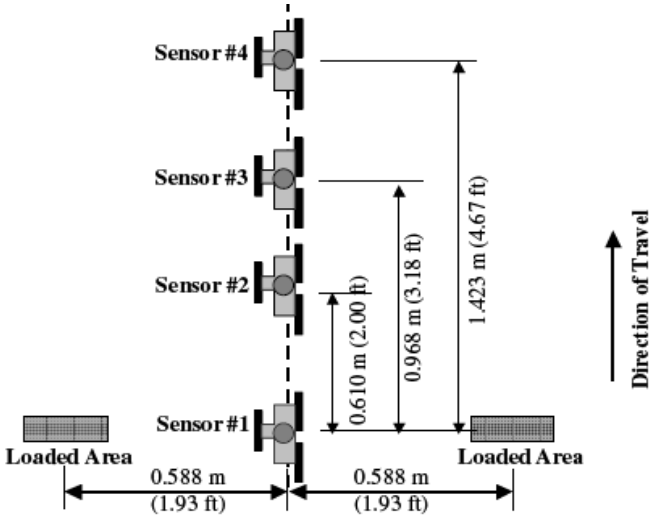

Figure 18. RDD Loading and Sensor Locations (*11*).

The RDD is the only known operational rolling deflection system that provides sufficient data to make project-level decisions on a JCP. The current data-acquisition system collects continuous pavement deflections at a frequency of 30 Hz. The operator typically summarizes the data into a 2-second window and calculates an average pavement deflection for that time interval. Under normal operating speed, this calculation corresponds to an average deflection measurement for every 2 to 3 feet of pavement. The data are supplied for analysis in a spreadsheet form, and a typical data set (for three channels) with the distance offsets is shown in Table 6 (*12*).

Table 6. Raw RDD Data (*12*).

Distance (ft)			Deflection (mils / 10-Kips)		
Sensor #1	Sensor #3	Sensor #4	Sensor #1	Sensor #3	Sensor #4
0	2.9037	4.4067	1.7649	1.3903	1.1012
2.2775	5.4545	6.9575	1.9229	1.3593	1.1347
5.3749	8.5519	10.0549	2.1639	2.0186	0.5949
9.5655	12.7425	14.2455	1.9461	1.8017	1.1240
12.0252	15.2022	16.7052	1.7440	1.8722	1.5215
14.6671	17.8441	19.3471	1.6259	1.7863	1.3603
17.4912	20.6682	22.1712	1.9699	1.8906	1.1890
21.4085	24.5855	26.0885	1.8131	1.2739	0.8443
24.2326	27.4096	28.9126	2.0740	1.5786	1.0307
27.4211	30.5981	32.1011	1.8679	1.8578	1.2118

The operator also provides a log of distances and markers along the roadway, as shown in Table 7 (*12*). This information permits the engineer to locate areas of interest in the field. More details on the RDD operation can be found in a paper by Lee et al. (*11*).

Table 7. Event Log Produced by RDD Operators (*12*).

File	Start	End	Length (ft)
TC4	Sign: 200 ft South of Milepost 9	Sign: End Road Work	199.6
TC6	Sign: End Road Work	Sign: EXIT 7 Off-Ramp	4114
TC7	Sign: EXIT 7 Off-Ramp	Sign: EXIT 6 Off-Ramp	6450.8
TC8	Sign: EXIT 6 Off-Ramp	Sign: EXIT 5 Frontage Road 1/4 mile	4469.2

Since the RDD was first developed, RDD continuous deflection profiles have primarily been used to identify "critical" sections and joints or cracks, which are required to replace or improve. This chapter discusses interpretation of RDD data and the approaches to identifying critical joints or cracks. In contrast to GPR and FWD, no RDD data analysis and interpretation software is available right now. Therefore, some basics of interpreting RDD data are first discussed. Then, the RDD deflection and the observed reflective cracking performance on IH20 are presented, and the relationship between RDD deflection and reflective cracking rate is further investigated. Finally, guidelines for evaluating PCC pavements using RDD are proposed.

4.2 INTERPRETATION OF RDD DEFLECTION DATA

The RDD is ideal for testing JCP or cracked CRCP, with a purpose of HMA overlay, where it is important to assess load transfer efficiency and identify the joints and/or cracks requested for replacement or improvement. Thousands of joints have been tested with the RDD on more than 10 projects in Texas. As an example, Figure 19 shows a typical RDD data set collected from a short section of JCP on IH 45 in Houston under TxDOT research project 0-4517 (*12*). However, as noted above, the RDD data interpretation criterion is under development, and no specific software is available to interpret the RDD data. After reviewing large amounts of RDD data collected on both JCP and CRCP, several common patterns have been identified, and associated interpretations have been proposed. The findings from these investigations are presented in the following sections. Note that although the RDD has the capabilities of monitoring four rolling sensors, in all studies described in this report only Sensors–1 (between loading wheels) and 3 (38 inches from Sensor 1) were used. Sensor 2 was not collected in most runs because of mounting problems, and Sensor 4 is judged to be too far away from the loading plate. Therefore, the RDD data interpretation focused on Sensors 1 and 3.

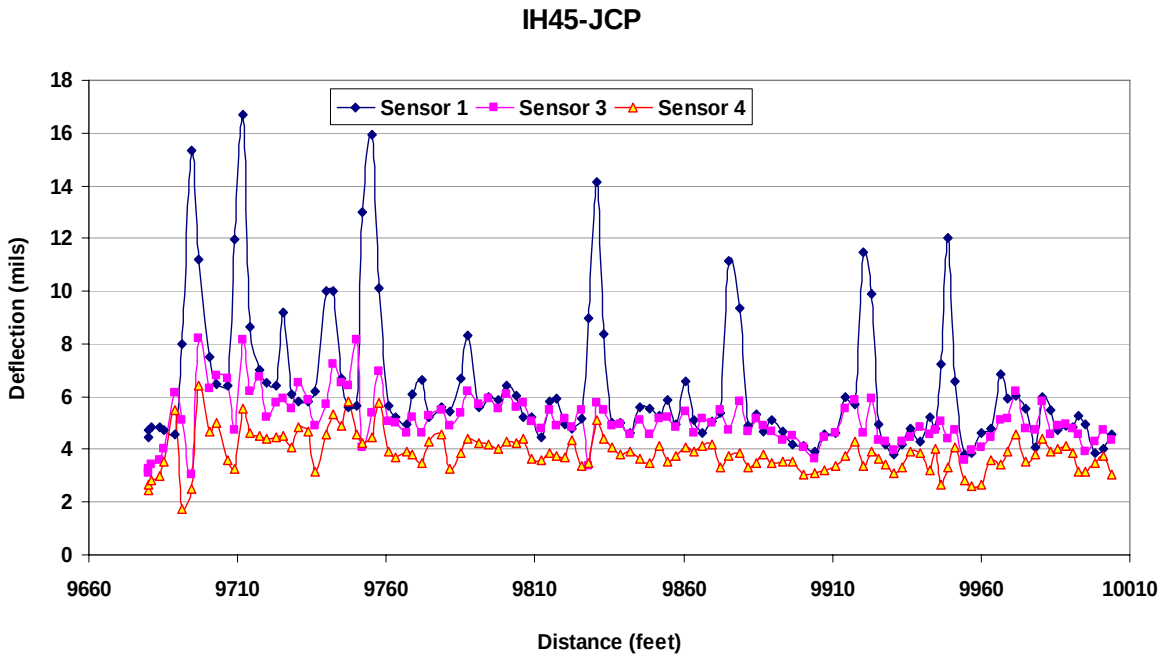

Figure 19. Typical RDD Three-Channel Deflection Plot for a Section of JCP *(12)*.

4.2.1 Periodic Increase in Sensor 1 Deflection/Location and Number of Joints and/or Cracks

In Figure 19, the blue line indicates the deflections measured between the load wheels, and the pink and yellow lines are deflections measured at offsets of 38 and 56 inches from the center of the load wheels (sensors 1, 3, and 4 from Figure 18), respectively. The large periodic increases in Sensor 1 (blue line) are the deflections measured as the load wheels pass over a joint or crack. The difference between Sensors 1 and 3 is related to the LTE of the joint; the higher the difference, the worse the LTE. This observation is very important and useful for a long project (e.g. > 5 miles) to estimate the number of joints and/or cracks in JCP and/or CRCP where counting the number of joints and/or cracks is tedious and sometimes impossible. This interpretation will be demonstrated later in analyzing HMA overlay performance on IH20.

4.2.2 Complexity of Sensors 1 and 3 Deflections at Joints or Cracks/ Load Transfer Efficiency

It has been proposed that the difference between the Sensor 1 maximum deflection over the joint (or crack) and the deflection measured at Sensor 3 is an indication of the LTE at the joint (or crack). This concept is simple, easy to understand, and theoretically sound. However, in some cases, it is a mistake to only simply interpret the differential deflection between Sensors 1 and 3 as the LTE, because the real RDD deflection data are much more complicated than what has been normally imagined. Several examples are presented below to demonstrate the complexity and illustrate the patterns of RDD deflections.

- **Harmonized deflection pattern of Sensors 1 and 3/variable LTE**

As shown in Figures 20, 21, and 22, there are large increases in both RDD sensors as the load wheels pass over the joint and both deflections peak at the same time. For this deflection pattern, where Sensor 1 peaks, it is assumed that this is equivalent to the upstream FWD tests location, with the FWD plate on one side of the joint and the other sensors on the other. With the current level of understanding, researchers propose that the instantaneous difference in deflection (between Sensors 1 and 3) when Sensor 1 peaks is a good measure of the load transfer efficiency of the joint. Furthermore, the different magnitude of the Sensor 1 deflection over the joint is an indication of subgrade quality or of potential broken slab. Based on the data reviewed to date, the interpretation for Figure 20 would be low overall deflection at the joint, very good load transfer, and strong subgrade support. Similar RDD deflection data have also been observed on other highways. For example, Figure 23 shows the RDD deflection data collected from a section of JCP on US82 under TxDOT research project 0-4517 (*12*). To further validate the interpretation of this type of deflection pattern, field testing was conducted with both FWD and dynamic cone penetrometer (DCP) on US82. In the location shown in Figure 23, the LTE determined based on FWD testing were all 95 percent and above, and the rate of penetration of the DCP through the subgrade ranged from 0.5 to 0.8 inches/blow (*12*). This type of deflection pattern is an ideal case for HMA overlay.

In contrast to Figure 20, Figure 21 indicates that the joint has a good load transfer but potentially weak support. Furthermore, the supports beneath the slab at locations of

113,725 and 113,804 feet on IH20 are worse, as shown in Figure 22. These observations indicate that a harmonized deflection pattern does not always mean a good LTE. Generally, the higher Sensor 1 deflection, the poorer the support is, and consequently the poorer the LTE.

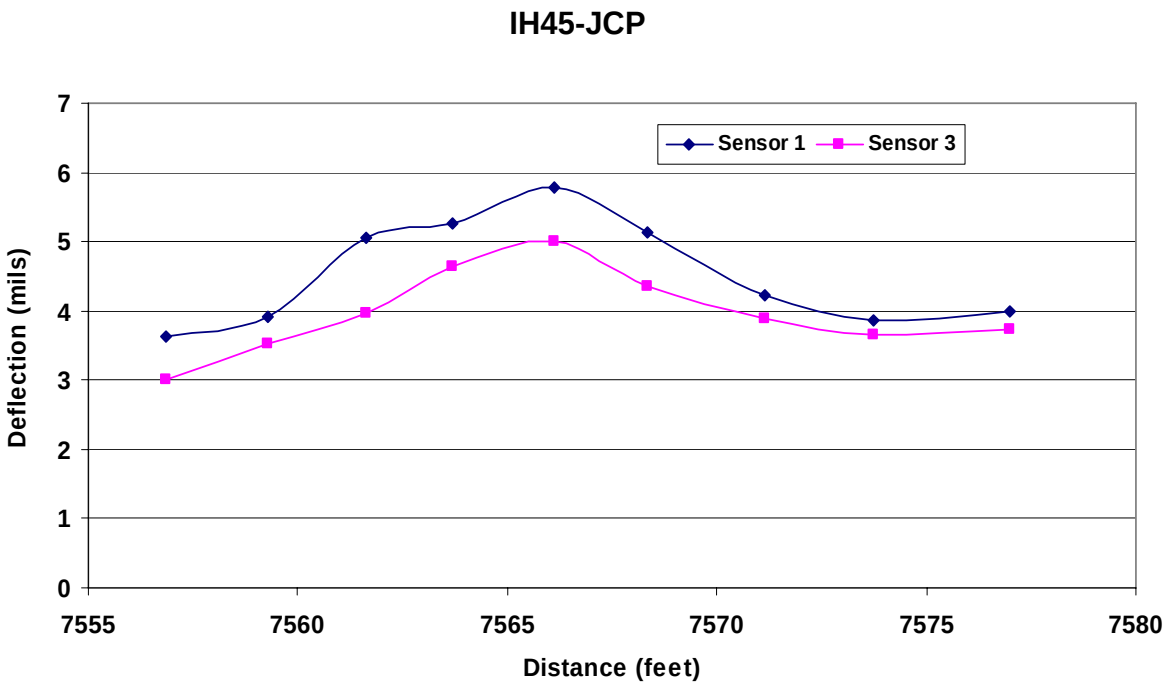

Figure 20. RDD Deflection Plot for a JCP Section on IH45.

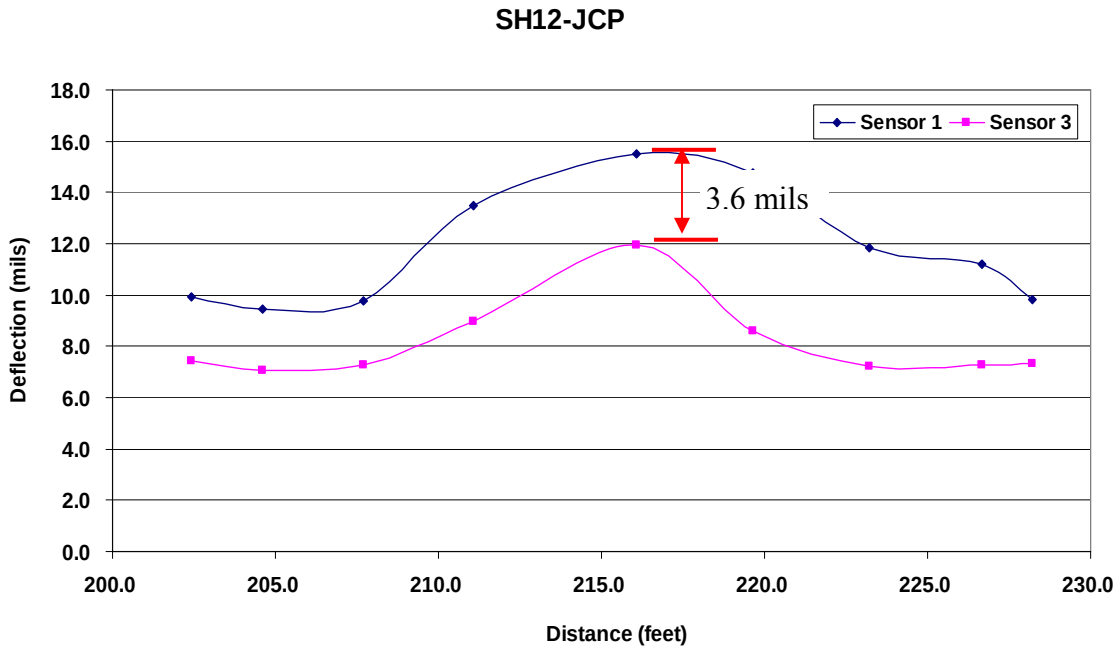

Figure 21. RDD Deflection Plot for a JCP Section on SH12.

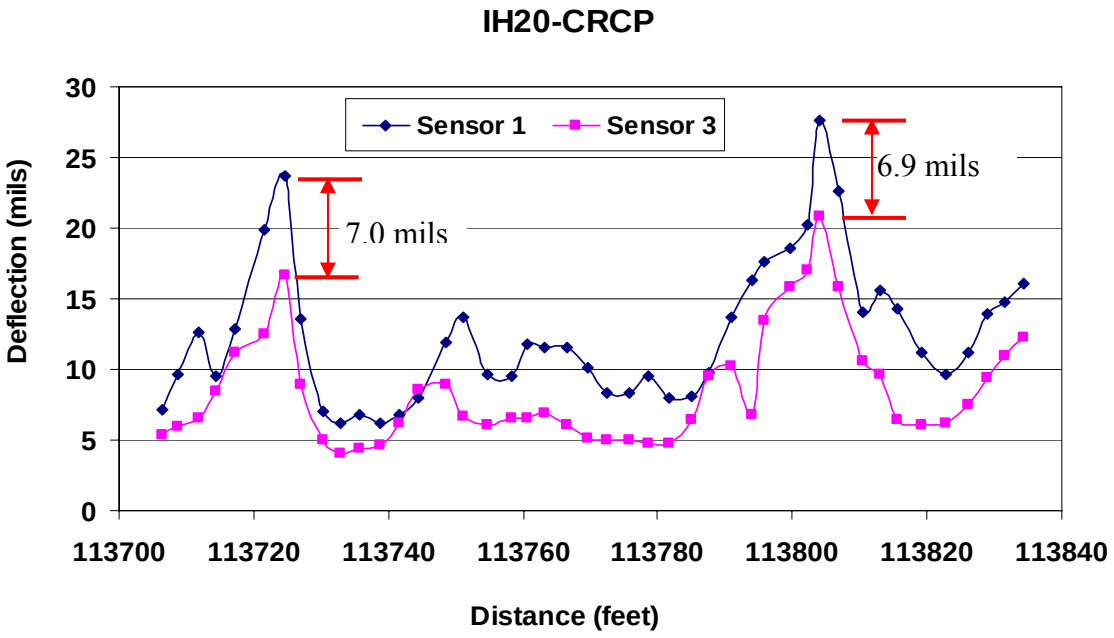

Figure 22. RDD Deflection Plot for a CRCP Section on IH20.

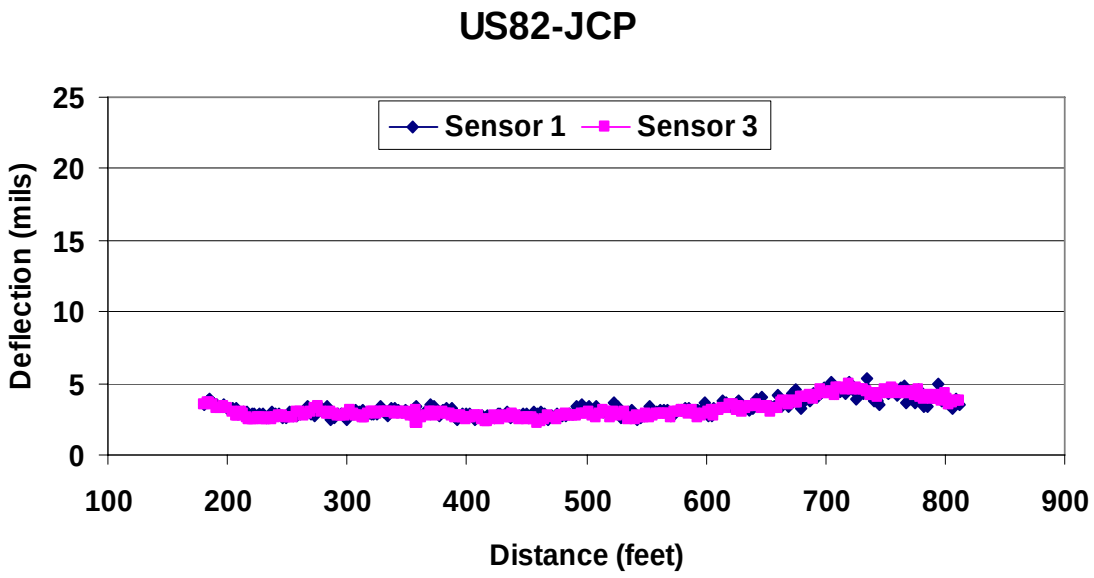

Figure 23. RDD Deflection Plot for a JCP Section on US82.

- **Non-harmonized deflection pattern of Sensors 1 and 3/poor LTE**

This type of deflection pattern is shown in Figure 24. Different from the harmonized deflection pattern where Sensors 1 and 3 both increase when approaching a joint (or crack) and peaks instantaneously, Sensor 3 deflection, for the non-harmonized deflection pattern, does not continuously increase but decreases first and then reaches its peak ("V" shape). The Sensor 1 deflection, however, becomes larger and larger when approaching the joint (or crack). The key to interpreting this non-harmonized deflection pattern is to understand the locations of Sensors 1 and 3 and the joint (or crack), when Sensor 3 reaches its valley and peak.

Figure 25 shows a sketch of the moving process of Sensors 1 and 3 when approaching a joint. It is clear that only the differential deflection between Sensors 1 and 3 at Stage B can be used to evaluate the LTE at the joint, where Sensor 1 is at the loading side, while Sensor 3 locates at the other side of the joint. In general, Sensor 3 at Stage B should have the smallest deflection because of the joint. Sensor 3 deflection normally is larger at either Stage A or C, because Sensor 3 is at the same side of the joint at either Stage A or C. Furthermore, this non-harmonized deflection pattern generally indicates

poor LTE, because Sensor 3 deflection should not show "V" shape but "Λ" shape when crossing a joint with good LTE. The poor LTE is further verified by the larger differential deflection between Sensors 1 and 3, as shown in Figure 24 as well. Note that the "V" shape of the Sensor 3 deflection is also observed in other highways such as IH45, as shown in Figures 26. For the joints with the non-harmonized deflection pattern, necessary improvement is generally needed.

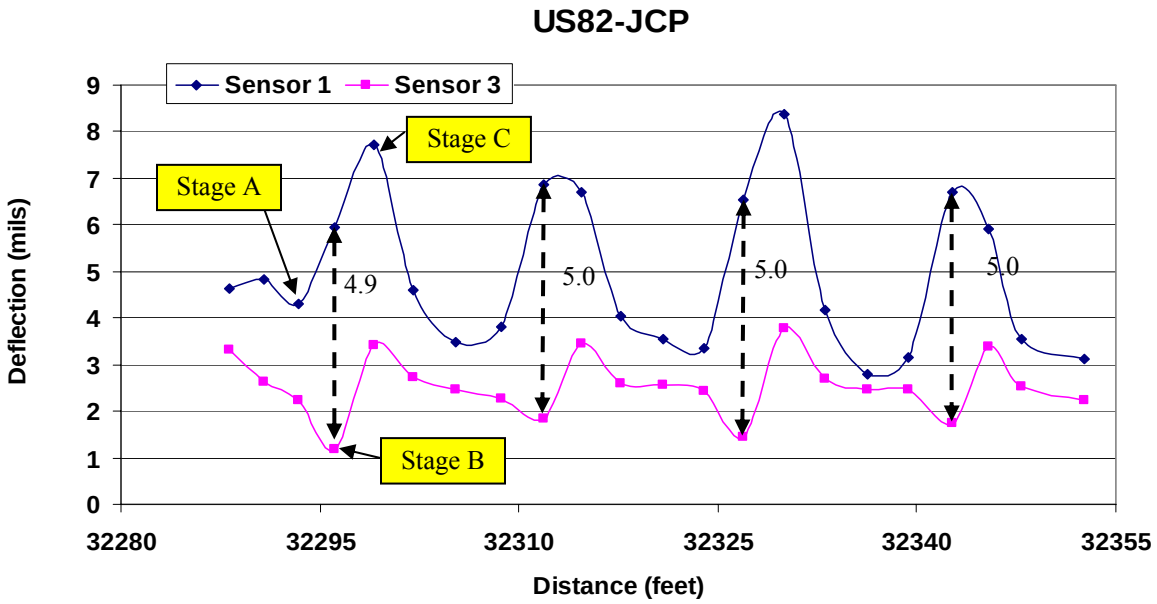

Figure 24. Non-harmonized Deflection Pattern from a Section of JCP on US82.

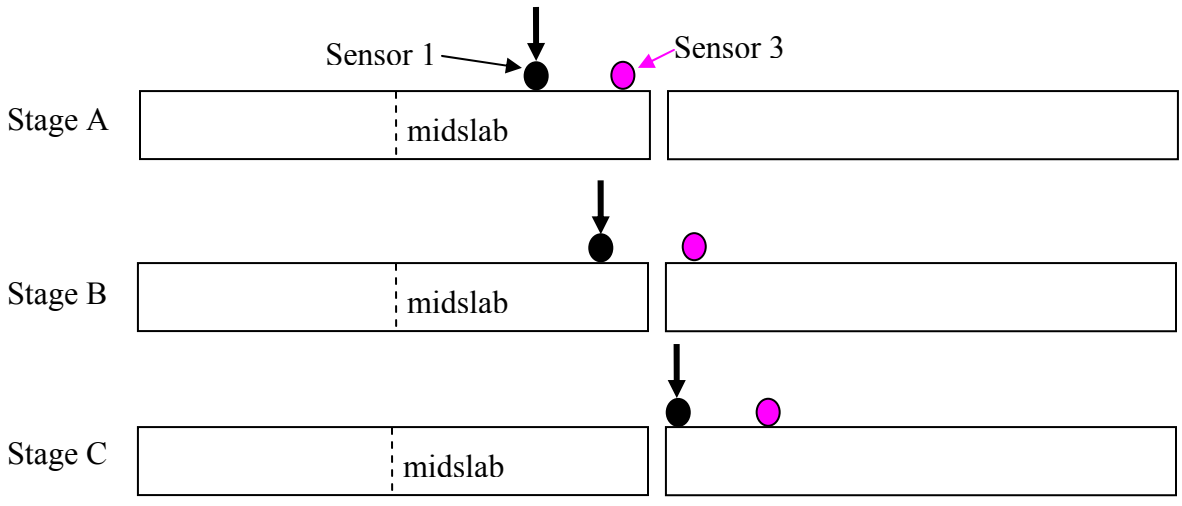

Figure 25. Sketch of Moving Process of Sensors 1 and 3.

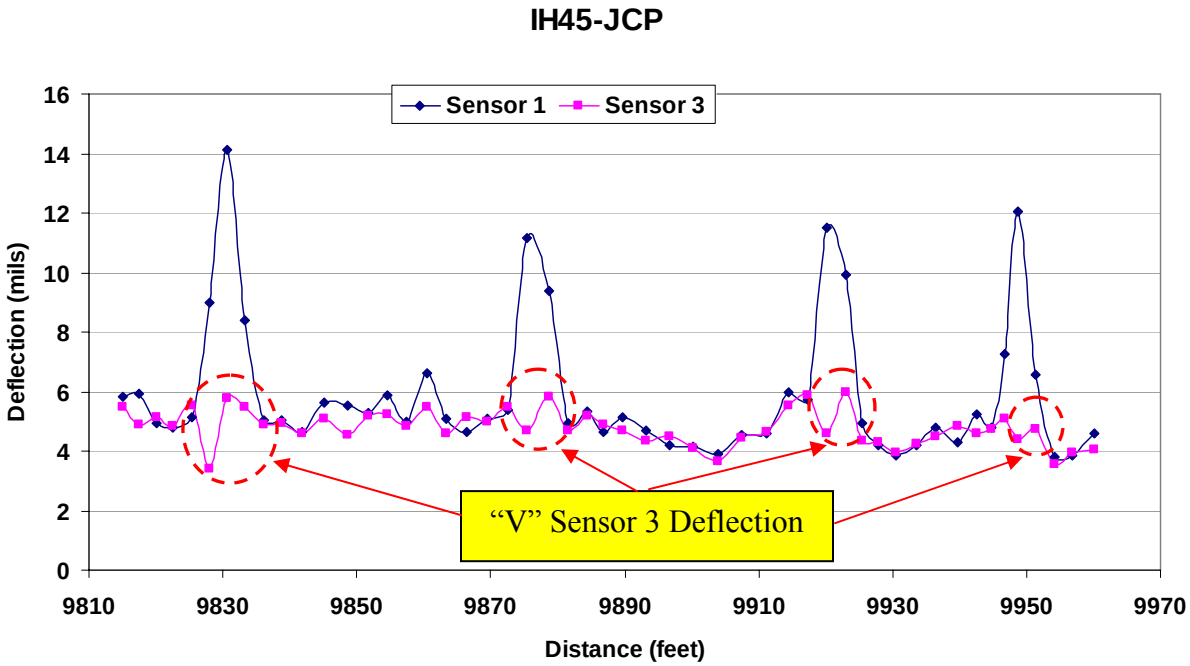

Figure 26. Non-harmonized Deflection Pattern: Scenario 1 on IH45.

4.2.3 Reversal deflections between Sensors 1 and 3/rocking slab

In general, the deflection in Sensor 1 should be larger than that of Sensor 3, as shown above, because Sensor 1 is between the load wheels, and Sensor 3 is 38 inches away. However, some RDD data collected on US82 under TxDOT research project 0-4517 (*12*) show reversal phenomena that the deflections in Sensor 3 are larger than that measured at Sensor 1, as indicated in Figure 27. Similar phenomena have also been observed on IH45, which is plotted in Figure 28. In these sections, there is no visual distress on the surface of slabs, as shown in Figure 29. It is not difficult to imagine that these slabs are rocking under the RDD dynamic loading, as demonstrated in Figure 30. This type of deflection pattern also indicates poor support beneath the slab. To further validate this interpretation, DCP testing was conducted at this section on US82. It was found that the top of the subgrade penetrations ranged from 2.2 to 3.2 inches/blow, which is much higher than that at section under strong subgrade support (shown in Figure 23). If this is the case, slab undersealing or other treatments must be performed before HMA overlay; otherwise, no HMA overlay will work for these active and rocking slabs.

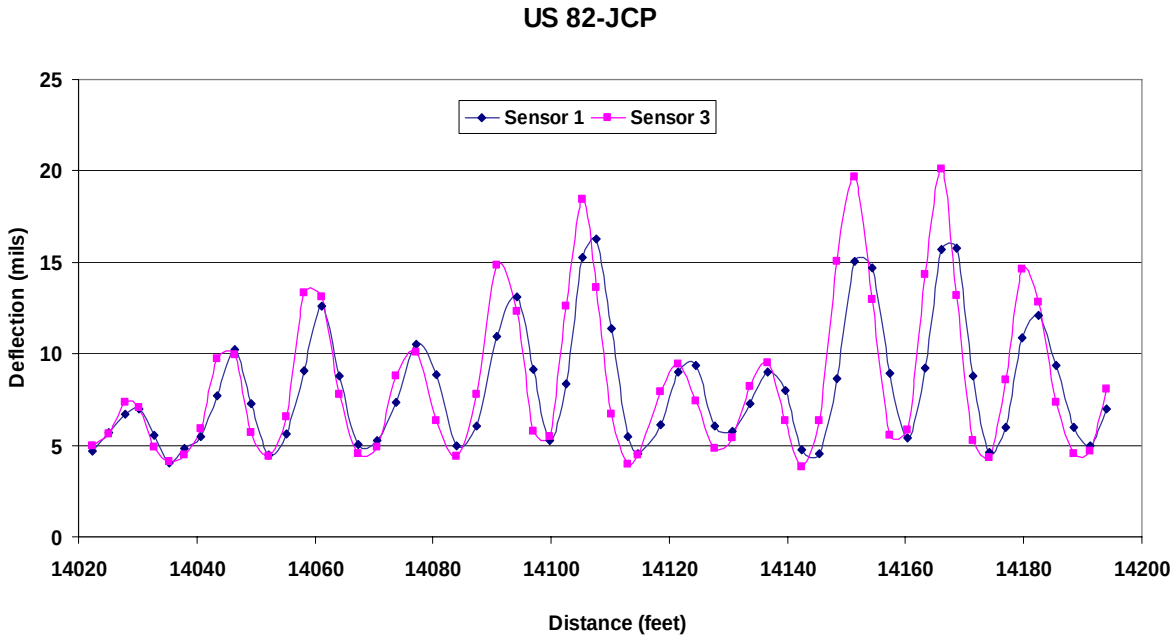

Figure 27. Reversal RDD Deflection Data Collected on US82.

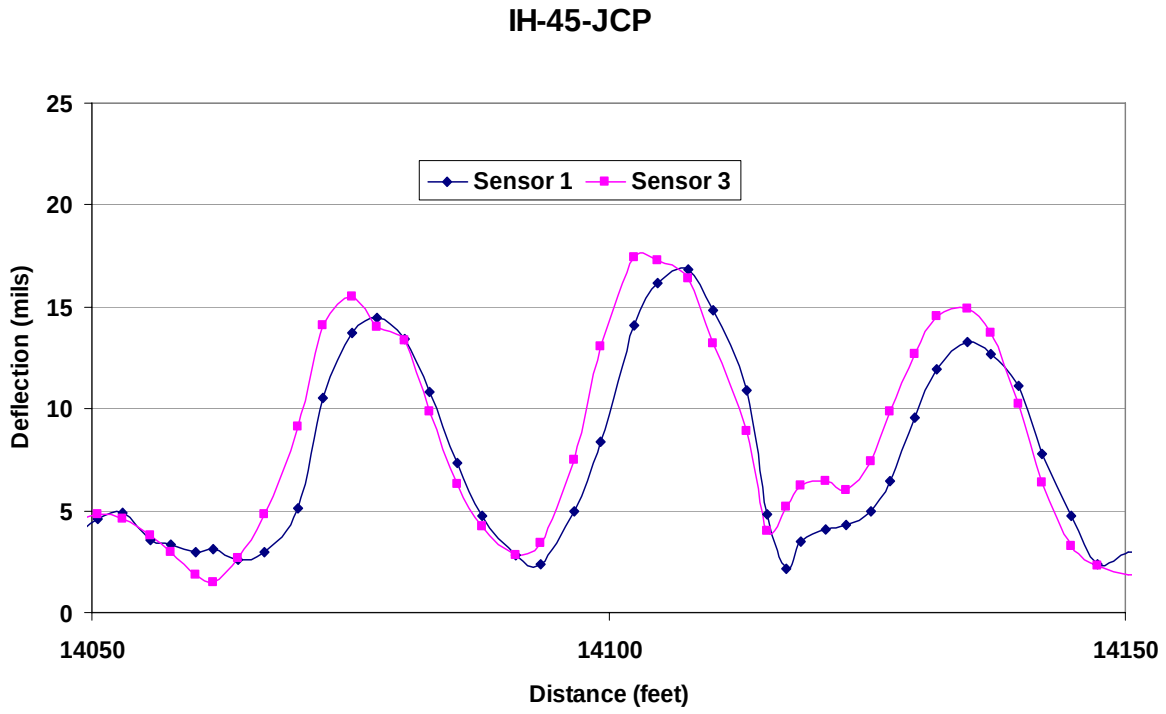

Figure 28. Reversal RDD Deflection Data Collected on IH45.

Figure 29. In-situ Conditions of Reversal Deflection Site on US82 *(12)*.

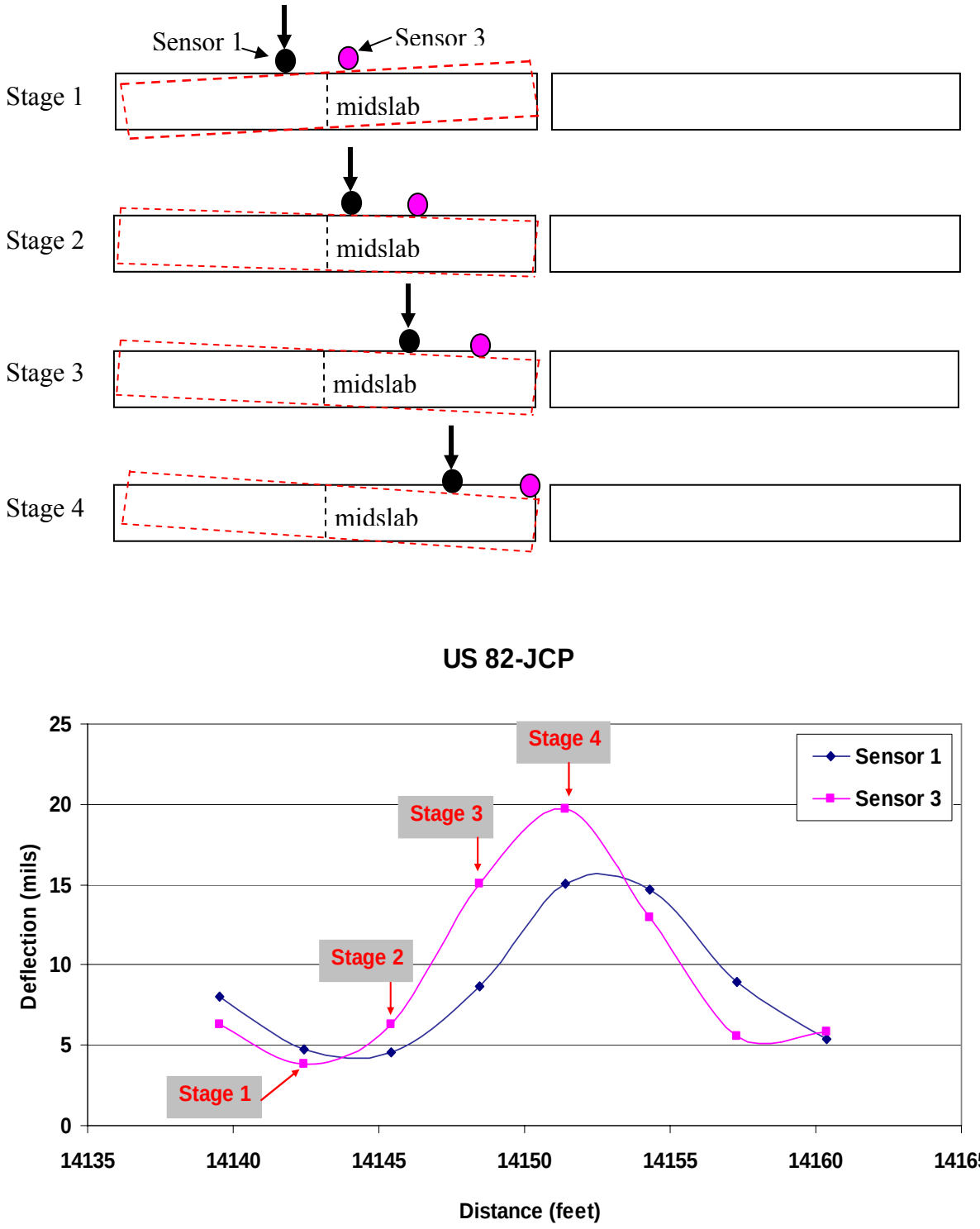

Figure 30. Sketch for Demonstration of Rocking Slab under RDD Dynamic Loading.

4.2.4 Brief Summary

Based on the above discussion, the following information related to HMA overlay can be interpreted from RDD deflection data (Sensors 1 and 3):

- number of joints and/or cracks;
- LTE at joints, including both harmonized deflection pattern and non-harmonized deflection pattern; and
- number of active slabs.

The information above provides pavement engineers an overview of existing concrete pavement, such as LTE at joints. However, the information about LTE at joints represented by differential deflection between Sensors 1 and 3 is qualitative rather than quantitative. The RDD provides a wealth of information about the condition of each joint in the pavement. However, our ability to interpret this information must be improved. Future studies should consist of testing on controlled slabs where the LTE and support condition under the slab are known. These slabs should contain upstream and downstream voids of known dimensions. This field evaluation should be supported by a finite element modeling of the observed deflection profile. In addition, a quantitative relationship between RDD deflections of Sensors 1 and 3 and field performance (reflective cracking rate) of HMA overlay is still needed for better selecting the HMA overlay strategy, which is discussed in the next section.

4.3 RELATIONSHIP BETWEEN RDD DEFLECTION AND REFLECTIVE CRACKING RATE

To establish a quantitative relationship between RDD deflection data and reflective cracking rate, both RDD deflection data collected on existing pavements before HMA overlay and reflective cracking conditions after HMA overlay must be available. Up to now, the only HMA overlay project in which both RDD deflection data and reflective cracking rate are available is the HMA overlay project on IH20. Therefore, researchers will establish the quantitative relationship based on the data from IH20, which can be verified and/or refined when data from other HMA overlay projects are available. Detailed information is presented next.

4.3.1 RDD Deflection Data Collected from an HMA Overlay Project on IH20

The original pavement on IH20 was a composite pavement, and its typical section consisted of: (1) 4 inch HMA overlay, (2) 8 inch CRCP, (3) 7 inch cement-stabilized base, (4) 6 inch of cement-treated base, and (5) subgrade. The rehabilitation scheme was first to mill off the 4 inch existing HMA overlay; then full-depth repairs to the CRCP were made at selected locations, followed by placement of a new 4 inch HMA overlay. The rehabilitation was completed in November 2001. Detailed construction information of the HMA overlay project has been well documented by Chowdhury et al. (*13*). RDD deflection data were collected after milling the existing 4 inch HMA overlay. As an example, Figure 31 shows part of the RDD deflections measured after milling the 4 inch HMA overlay on westbound IH20. These values are high, indicating that at this location the CRCP pavement is badly deteriorated. Detailed RDD deflection data on both westbound and eastbound IH20 are presented in Appendix B.

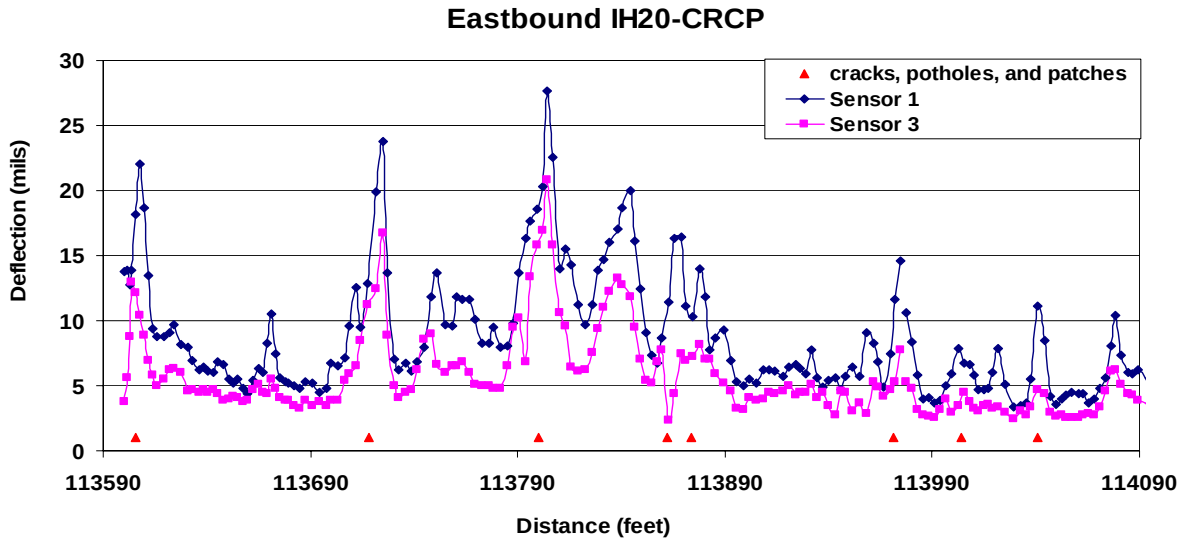

Figure 31. Example of RDD Deflection Data and Observed Distresses on Westbound IH20.

4.3.2 Reflective Cracking Observed from the HMA Overlay Project on IH20

The distresses including reflected cracks, potholes, and patches on this HMA overlay project on IH20 have been continuously monitored by Yildirim and Kennedy (*14*) and personnel from the TxDOT pavement section (*15*) for 25 months. Any visible cracks,

potholes, and patches that were observed during the 25 month monitoring are considered as reflective cracking-related distresses in the following analysis, because the potholes and patches were initiated by reflective cracking. Specifically, locations of these observed distresses are also recorded and identified in the plot of the RDD deflection profile, as indicated in Figure 31. Detailed reflective cracking data are presented in Appendix B, as well. In view of Figure 31, it is difficult to determine that either Sensor 1 deflection or the differential deflection between Sensors 1 and 3 or both control(s) reflective cracking rate. Therefore, in the following analysis, both Sensor 1 deflection and the differential deflection between Sensors 1 and 3 are considered as controlling factors for potential reflective cracking.

4.3.3 Relationships between the RDD Deflections of Sensors 1 and 3 and the Observed Reflective Cracking Rate

Two relationships are discussed below. One is the relationship between Sensor 1 deflection and the reflective cracking rate. The other is the relationship between the differential deflection between Sensors 1 and 3, which cross the joint (or crack) and reflective cracking rate. These two relationships are discussed below.

4.3.3.1 Relationship between Sensor 1 deflection and reflective cracking rate

The approach used to develop the relationship is outlined as follows.

1. Determine the number of existing cracks (NEC) on existing CRCP before the HMA overlay.

   This is a difficult task, because existing cracks were not counted before the HMA overlay. In this case, an alternative approach was used. As discussed previously, each deflection peak of Sensor 1 generally corresponds to one joint (or crack). Using this approach, the NEC on both eastbound and westbound IH20 are determined and presented in Table 8. Note that the NEC is counted and accumulated when the Sensor 1 deflection goes down. For example, the NEC (= 8) corresponding to the Sensor 1 deflection being larger than 23 mils is included in the NEC (= 11) corresponding to the Sensor 1 deflection being larger than 21 mils, which is detailed in Table 9.

2. Determine the number of reflected cracks (NRC) based on the 25 months condition survey.

   After counting the NRC shown in Figure 31 and those presented in Appendix B, the NRC are determined and listed in Table 8, as well.

3. For a selected minimum deflection (e.g., 21 mils), calculate the reflected cracking rate (RCR):

$$RCR(\%) = \frac{NRC}{NEC} \times 100\% \qquad (5)$$

Table 8. Sensor 1 Deflection vs. Reflective Cracking Rate Data on IH20 Including both Eastbound and Westbound.

Sensor 1 Deflection Data			Observed Reflective Cracking Data		
D_1 condition	D_{1ave} (mils)	D_{1std} (mils)	NRC	NEC	RCR (%)
$D_1 > 23$	26.5	2.6	6	8	75.0
$D_1 > 21$	25.2	3.2	8	11	72.7
$D_1 > 20$	23.9	3.5	10	15	66.7
$D_1 > 19$	23.0	3.6	12	19	63.2
$D_1 > 18$	21.4	3.6	19	29	65.5
$D_1 > 17$	20.5	3.6	24	38	63.2
$D_1 > 16$	19.9	3.6	27	45	60.0
$D_1 > 15$	18.8	3.7	35	60	58.3
$D_1 > 14$	17.8	3.7	42	77	54.5
$D_1 > 13$	16.7	3.7	52	103	50.5
$D_1 > 12$	15.6	3.7	61	141	43.3
$D_1 > 11$	14.4	3.6	70	196	35.7
$D_1 > 10$	13.0	3.5	85	301	28.2
$D_1 > 9$	12.1	3.4	102	412	24.8
$D_1 > 8$	11.1	3.3	116	566	20.5
$D_1 > 7$	10.1	3.2	130	790	16.5

Table 9. Detailed Example of Demonstrating the Process of Calculation.

Sensor 1 Deflection (mils)	30.5	28.9	27.7	27.2	27.1	23.8	23.7	23.4	22.1	21.5	21.3	20.9
Reflective Cracking	No	Yes	Yes	Yes	Yes	Yes	Yes	No	Yes	No	Yes	Yes
D_1>23	D_{1ave} = 26.5, D_{1std}=2.6; NRC=6, NEC=8, and RCR= 6/8*100%=75 %											
D_1>21	D_{1ave} = 25.2, D_{1std}=3.2; NRC=8, NEC=11, and RCR= 8/11*100%=72.7 %											

4. For each determined RCR, determine the average and associated standard deviation of Sensor 1 deflection, as shown in Table 9.

5. For a specified reflective cracking rate, calculate the RDD Sensor 1 deflection value at a given reliability using the following relationship:

$$D_{1R} = D_{1ave} - Z_r * D_{1std} \quad (6)$$

where:

D_{1R} = Sensor 1 deflection with a specified reliability (Z_r) (mils);

D_{1av} = Average of D_1;

D_{1std} = Standard deviation of D_1; and

Z_r = Reliability coefficient, as given in Table 10.

Table 10. Z_r Values for Various Reliability Levels (*16*).

Reliability (%)	50	80	85	90	95
Z_r value	0	0.842	1.036	1.282	1.645

Take the results shown in Table 9 as an example. For the case of D_1 > 23 and RCR = 75 percent, the corresponding D_{1ave} and D_{1std} are 26.5 and 2.6 mils, respectively. Using Equation 6, the RDD Sensor 1 deflection with 95 percent reliability should be 22.2 mils

(=26.5 − 1.645 * 2.6), which means that when Sensor 1 deflections at joints (or cracks) are larger than 22.2 mils, the probability of reflective cracking rate at these joints (or cracks) being less than 75 percent is 5 percent.

Following the above procedure, the relationships between the reflective cracking rate and Sensor 1 deflection have been established for different levels of confidence (or reliabilities). Figure 32 shows the established relationships at three levels of reliability: 50, 90, and 95 percent. Note that TxDOT generally uses a reliability of 90 to 95 percent (*16*). If the reflective cracking rate of 50 percent is chosen, the corresponding minimum Sensor 1 deflections are 11.9 and 10.6 mils for reliabilities of 90 and 95 percent, respectively. For practical applications, the recommended threshold value for Sensor 1 deflection is 11.0 mils. The joints and/or cracks having deflections of higher than 11.0 mils need to be treated in order to reduce the probability of premature reflective cracking within a short period. Note that this threshold value of Sensor 1 deflection is recommended based on the HMA overlay project on IH20 with a short performance period of 25 months.

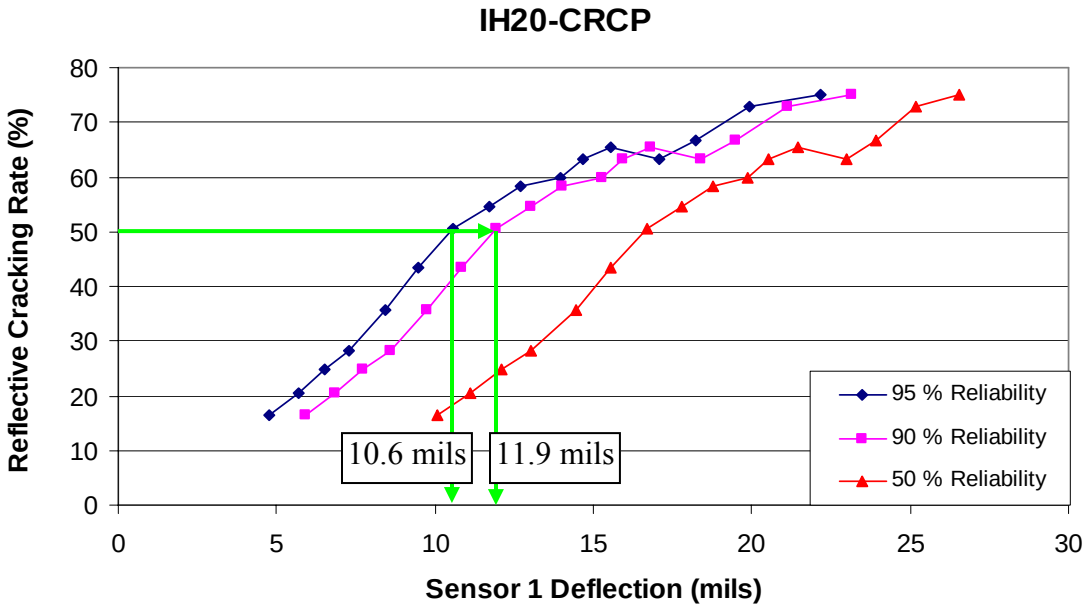

Figure 32. Relationships between Sensor 1 Deflection and Reflective Cracking Rate at Three Levels of Reliabilities.

4.3.3.2 Relationship between differential deflection between Sensors 1 and 3 and reflective cracking rate

The same approach used above is used to develop the relationships between differential deflection between Sensors 1 and 3 and the reflective cracking rate. Table 11 presents the results, and Figure 33 shows the relationships at different levels of reliabilities. Again, if the reflective cracking rate of 50 percent is chosen, the corresponding minimum differential deflections between Sensors 1 and 3 are 7.5 and 8.3 mils for reliabilities of 90 and 95 percent, respectively. For practical application, the recommended threshold value for differential deflection between Sensors 1 and 3 is 8.0 mils. Furthermore, the joints and/or cracks having differential deflections of higher than 8.0 mils are proposed to have poor LTE and need to be treated in order to reduce premature reflective cracking within a short period. Additionally, the differential deflection of 5.0 mils is proposed for rating the LTE of the joints (or cracks) as either good (< 5.0 mils) or fair (5.0 – 8.0 mils). Currently, researchers are collecting more data from other highways (e.g., SH12, US82, and US96) to verify these recommendations.

Table 11. Differential Deflection vs. Reflective Cracking Rate Data on IH20 Including both Eastbound and Westbound.

Differential Deflection between Sensors 1 and 3			Observed Reflective Cracking Data		
DD_1 condition	DD_{1ave} (mils)	DD_{1std} (mils)	NEC	NRC	RCR (%)
$DD_1 > 11$	13.0	1.9	17	27	63.0
$DD_1 > 10$	12.1	2.0	26	43	60.5
$DD_1 > 9$	11.3	2.1	33	62	53.2
$DD_1 > 8$	10.3	2.1	41	95	43.2
$DD_1 > 7$	9.3	2.2	52	150	34.7
$DD_1 > 6$	8.2	2.2	73	236	30.9
$DD_1 > 5$	7.3	2.2	84	363	23.1
$DD_1 > 4$	6.4	2.3	105	531	19.8
$DD_1 > 3$	5.7	2.3	116	708	16.4
$DD_1 > 2$	5.4	2.4	119	765	15.6

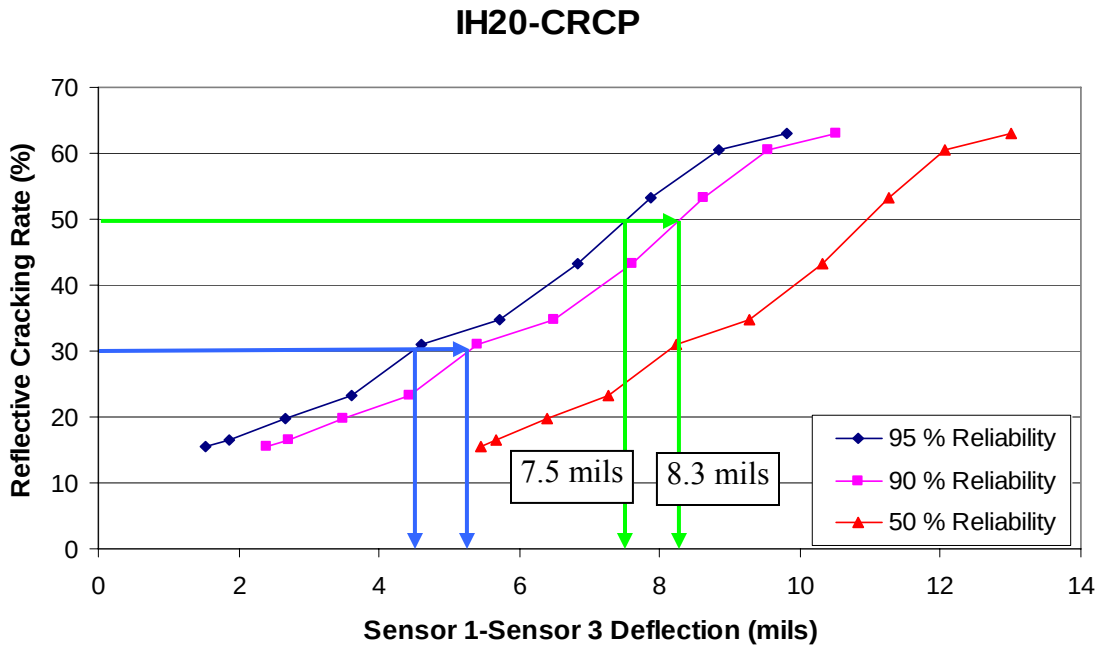

Figure 33. Relationships between Differential Deflection between Sensors 1 and 3 and Reflective Cracking Rate at Three Levels of Reliabilities.

4.4 GENERAL GUIDELINES FOR RDD TESTING, DATA INTERPRETATION, AND REPORTING

In general, the RDD testing is proposed to evaluate the LTE at joints and/or cracks and the support condition beneath the slabs. The major advantage the RDD has over other discrete NDT devices is that it measures continuous deflection profiles along the pavement. Based on the information presented above, some general guidelines for RDD testing, data interpretation, and data reporting are recommended as follows.

- RDD testing on PCC pavements: Conduct the RDD testing in the outside lane of the entire project. However, the slow-moving speed of the current RDD testing should be noted. The current data collection speed of 1 to 1.5 mph can be dangerous in urban situations, especially at on-ramps and off-ramps.
- RDD data interpretation: Currently, there is no software available to automatically interpret the RDD data. After reviewing thousands of RDD data collected on different PCC pavements including both JCP and CRCP, the

researchers make several important recommendations on the RDD data interpretation, which include determination of the number of joints and/or cracks, LTE, and active slab. Furthermore, researchers establish relationships between RDD deflections and field reflective cracking performance on IH20. They further recommend a threshold value for RDD Sensor 1 deflection and the differential deflection between Sensors 1 and 3:

  - Maximum Sensor 1 deflection: 11 mils and
  - Maximum differential deflection between Sensors 1 and 3: 8 mils.

  If either Sensor 1 deflection or the differential deflection between Sensors 1 and 3 is larger than the proposed thresholds, the corresponding joints and/or cracks are recommended to repair before placing a new HMA overlay. Potential problematic areas, joints, and cracks can be identified with the above preliminary threshold values.
- RDD data reporting: The main expectation from the RDD testing is the locations of potential problematic areas such as rocking slabs, poor support beneath the slabs, and joints and cracks with poor LTE.

In addition, several limitations of the current RDD operation and data-processing system should be also discussed. The limitations identified and some recommendations are listed below:

- Traveling speed: One of the main limitations of the current RDD system is the speed of travel. The data collection speed of 1 to 1.5 mph can be dangerous in urban situations, especially at on-ramps and off-ramps. The current system is built on a 30-year-old vibrosies frame, which frequently breaks down.
- Data interpretation software: Thousands of RDD data have been collected; however, no software is available to interpret these data. A user-friendly RDD data interpretation software is urgently needed in order to efficiently use the RDD testing tool on evaluating existing PCC pavements.
- Data acquisition and processing system: The current RDD data-acquisition system urgently needs to be upgraded. Currently, it collects data in a time mode and reports data as average deflections in 2 to 3 feet intervals, which

significantly increases the difficulty to identify the exact locations between Sensors 1 and 3 and the joints (or cracks). More work is required here, especially in the area of reporting deflections over joints.

- Combined video system: Another limitation of the RDD on long runs is that it is very difficult to locate individual problematic joints in the field just after data collection. This problem could best be solved by incorporating a video system as part of the data-acquisition unit.
- Temperature correction: The impact of temperature on RDD joint deflections should be studied.
- RDD field calibration and verification: As described earlier, an RDD field calibration verification site should be established where the LTE and support conditions are known. This site should include areas of known upstream and downstream voids. RDD data should be collected and interpreted with the use of advanced mechanistic response models.

CHAPTER 5
GUIDELINES FOR EVALUATION OF EXISTING PAVEMENTS FOR ASPHALT OVERLAYS

Based on previous discussion of different NDT tools for evaluating existing pavements for asphalt overlay, guidelines for the most often used NDT tools including GPR, FWD, and RDD have been provided in previous chapters. General guidelines for using these NDT tools to evaluate existing pavements and others are provided below.

1. **Assemble all existing project information.** This information includes typical sections and recent maintenance history. For PCC pavements, it is important to know if the slab is reinforced, the type of joint, type of shoulders, and the type of base beneath the slab.
2. **Conduct GPR survey and visual inspection.** The GPR data should be collected in the outside lane/outside wheel path of the project with a data collection interval of 1 foot per trace. Basically, the GPR data can be used to determine existing pavement layer thickness and check section uniformity. Additionally, the GPR data can also identify areas of high reflection, indicating possible trapped moisture. For composite pavement, the GPR can measure the thickness of the overlay and determine if there is any deterioration (such as stripping) in the overlay. Note that the layer thickness information is required by the HMA overlay thickness design being developed, as indicated later in this chapter. Also, the information generated from the GPR will be used to assist in interpreting the FWD and RDD data.

   During the GPR survey, collect a video of the pavement surface (especially existing cracks), and use it to make a log of pavement conditions, which is extremely important to monitor reflective cracking performance after the HMA overlay. For existing flexible pavements, the pavement surface cracking conditions can be used to classify the overall LTE, if the cracks are random. Consequently, it may be difficult to determine LTE based on FWD testing. The proposed three levels of LTE classifications shown below are based on the severity of cracks:

- Good: crack width is less than 3/8 inch;
- Fair: crack width is between 3/8 inch and 3/4 inch or sealed crack surrounded by random cracking; and
- Poor: crack width is over 3/4 inch or filled crack surrounded by medium or high severity random cracking.

3. **For existing PCC pavements, conduct an RDD survey.** Conduct RDD testing in the outside lane on the entire project to evaluate every joint or crack. Then, identify the potential problematic joints, cracks, and rocking slabs based on the threshold values of both RDD Sensor 1 deflection and the differential deflection between Sensors 1 and 3 proposed in Chapter 4. These potential problematic joints, cracks, and rocking slabs should be treated before a new HMA overlay. Additionally, the differential deflection between Sensors 1 and 3 can also be used to evaluate the LTE at joints and/or cracks based on the proposed criteria:
    - LTE = Good: differential deflection < 5 mils;
    - LTE = Fair: differential deflection 5 − 8 mils; and
    - LTE = Poor: differential deflection > 8 mils.

    Note that the LTE has significant influence on load-induced reflective cracking and is an important parameter for HMA overlay designs.

4. **Conduct an FWD survey.** Conduct an FWD survey of the entire project regardless of existing flexible, PCC, and composite pavements. Test at a minimum of 30 locations along the project (< 10 miles), but do not collect data at intervals of greater than 0.1 mile. For very long projects, for example greater than 10 miles, at the engineer's discretion, the data collection interval may be extended to every 0.2 miles. Specifically, for existing JCP pavements, perform an FWD test initially at the center of the slab at each location, and then move forward to the next joint location. At the joint, perform an upstream test where the load plate is placed on one side of the joint and the remaining six sensors are placed on the other side. Note that all FWD data should be collected in the outside lane and outside wheel path. Mid-depth slab temperatures should be measured at the start and end of the test.

The FWD data can be used to backcalculate pavement layer moduli, which are definitely required by the HMA overlay thickness design being developed, as indicated later in this chapter. Also, if the FWD testing is conducted across joints and/or cracks, the ratio of unloaded deflection to loaded deflection can be used to evaluate the LTE at the joints and/or cracks. As noted previously, for existing flexible pavements, FWD testing may not be applicable for random cracks to determine the LTE. If this is the case, the overall LTE can be classified based on the severity level of cracks.

5. **Conduct validation testing.** All projects require additional testing to validate both the GPR and RDD interpretations. It is normal to select at least one location in each project segment to validate that the correct interpretations have been made. For example, if the GPR also indicated possible voiding, access holes should be drilled through the concrete to validate what is beneath the slab.

All above information will assist pavement engineers to make decisions on choosing HMA overlay strategies including pretreatments, and part of the information collected by these NDT tools is required by the HMA overlay thickness design program being developed. For the purpose of demonstration, Figure 34 shows the framework of the HMA overlay thickness design in which the existing pavement evaluation plays an important role in predicting potential reflective cracking and thickness design. As shown in Figure 34, four major inputs required to make an HMA overlay thickness design in Step I are as follows:

- HMA overlay information: This information includes trial overlay thickness and associated material properties (dynamic modulus, fracture properties: A and n). As noted below, dynamic modulus will affect the stress intensify factor and fracture properties, A and n, have influence on crack propagation. Note that default values for material properties will be provided in the overlay thickness system. However, if laboratory tests are preferred, these properties can be determined by the dynamic modulus test and overlay tester. Detailed information will be provided in the final report of this research project.

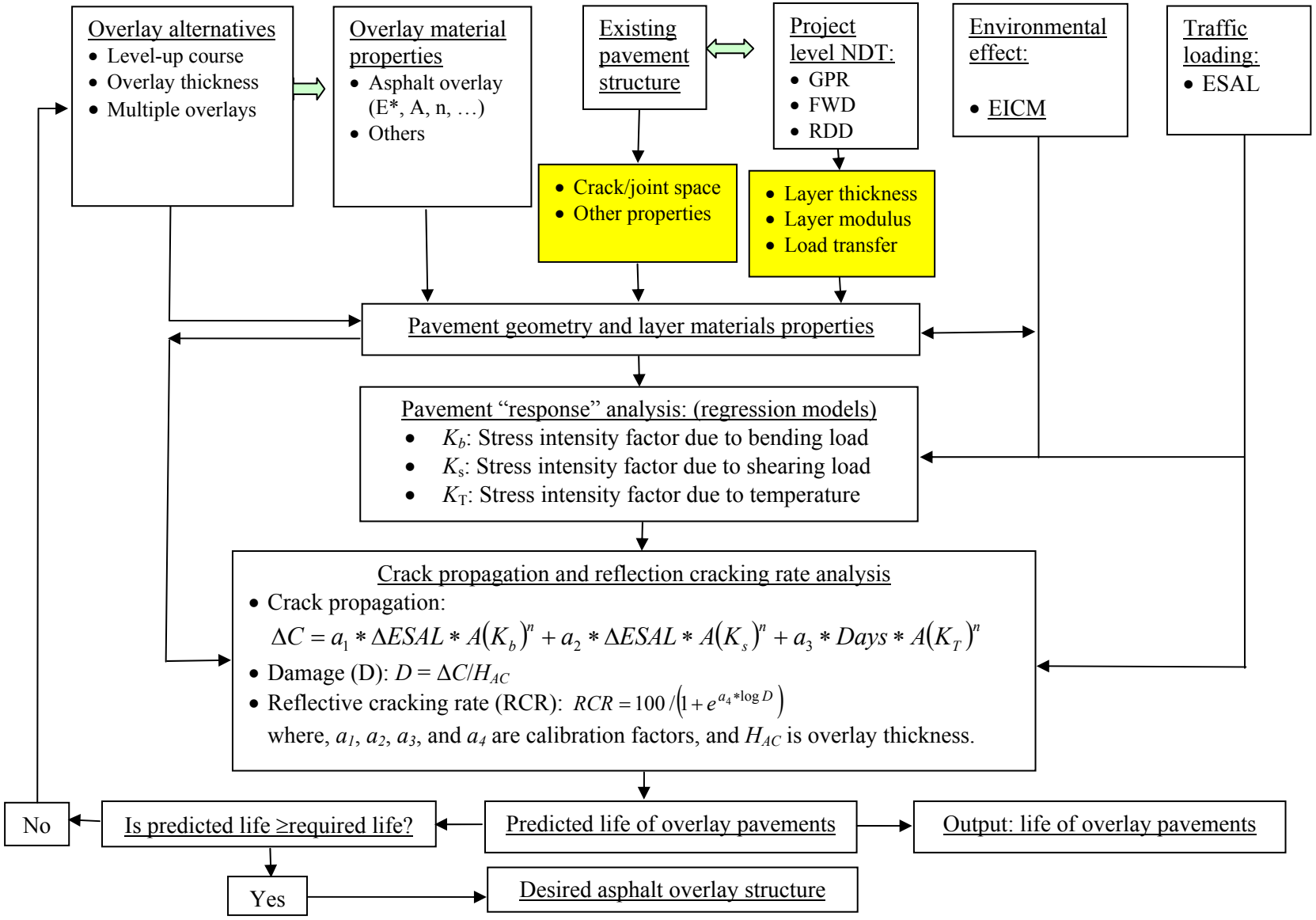

Figure 34. Pavement Evaluation and HMA Overlay Thickness Design.

- Existing pavement structural information: This information includes layer thickness, layer modulus, joint (or crack) space, and LTE, which, as noted below, has influence on the stress intensity factor. Note that one of the purposes of developing evaluation guidelines, as presented above, is to obtain the existing pavement structural information.
- Environmental information: This information is used for predicting daily and monthly temperature profiles and variations in depth direction. Based on the predicted temperature profiles, monthly HMA overlays stiffness can be determined. Additionally, the temperature variations have an effect on the thermal stress intensity factor. Note that environmental information for each district will be provided in the HMA overlay thickness design program being developed.
- Traffic information: An equivalent standard single axle load, 18 kips, is used in the HMA overlay thickness design program.

With these four types of information, HMA overlay "responses" at the crack tip can be calculated in Step II. Note that HMA overlay "responses" refer to stress intensity factors. For further illustration, an HMA overlay on an existing JCP shown in Figure 35 is taken as an example to demonstrate the calculation of these stress intensity factors. When the wheels are right on top of the crack (or joint), the traffic load will induce a stress intensity factor in the bending mode (K_b) at the tip of the crack; when the wheels are at either side of the crack (or joint), the traffic load will induce a stress intensity factor in the shearing mode (K_s) at the tip of the crack. Additionally, daily temperature variations also induce a stress intensity factor in the tension mode (K_T). For easy implementation in the design program, regression equations are developed for each stress intensity factor and presented below.

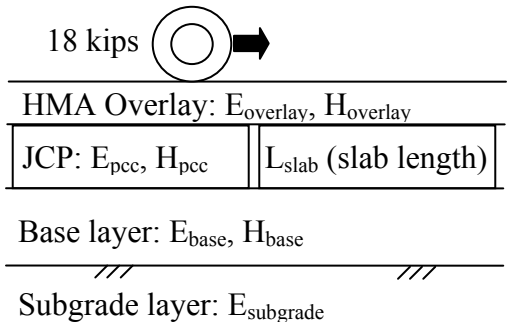

Figure 35. An Example of an HMA Overlay on a JCP.

- K_b: Stress intensity factor due to bending load
- For this case (Figure 35), K_b is negative and the bending load will not induce crack propagation, because the HMA overlay stiffness is far smaller than that of the PCC slab so that the HMA overlay is always in the compression zone.
- K_s: Stress intensity factor due to shearing load

  It is well known that LTE has a significant influence on the shear stress intensity factor; the better the LTE, the less the shear stress intensity factor is. In case of poor LTE, the follow equation has been developed to predict the shear stress intensity factor. It can be seen that both the HMA overlay and the existing pavement structural thickness and layer moduli, in addition to crack length, are required to calculate the shear stress intensity factor.

$$K_s = 2.0*(70.97 + C^{0.485} - 8.619*\ln H_{overlay} + 4.842*\ln E_{overlay} - 3.212*\ln H_{pcc} - 2.314*\ln E_{pcc} - 1.108*\ln H_{base} - 2.439\ln E_{base} - 0.223\ln E_{subgrade})*(0.0918 - 0.0249*\frac{C}{H_{overlay}} - 0.0515*(\frac{C}{H_{overlay}})^2 + 0.158*(\frac{C}{H_{overlay}})^3)$$

  where, C = crack length in HMA overlay.

- K_T: Stress intensity factor due to temperature variation

  In addition, a regression equation, as presented below, has also been developed for the thermal stress intensity factor. Two additional factors are included in this equation: thermal stress, σ_T and L_{slab}. Note that σ_T is a function of the temperature variation and relaxation modulus of the HMA overlay. As illustrated in Figure 35, L_{slab} is the length of the PCC slab.

$$\frac{K_T}{\sigma_T} = (-14.342 + C^{0.446} - 5.09\ln H_{Overlay} + 3.333\ln E_{pcc} + 1.432L_{slab})*(1.795 - 1.105*\frac{C}{H_{Overlay}} - 0.113*(\frac{C}{H_{Overlay}})^2 + 1.927*(\frac{C}{H_{Overlay}})^3)$$

Then, as shown in Figure 34, crack propagation (ΔC) will be predicted by Paris' law ($\Delta C = [A*(K)^n]*\Delta N$) in Step III (*17*). Note that crack propagation is composed of bending crack propagation, shearing crack propagation, and thermal crack propagation. Furthermore, the damage caused by crack propagation is defined as the ratio of accumulated crack propagation to the HMA overlay thickness. Finally, the relationship between the damage and observed field reflective cracking rate will be established by field calibration. More detailed information will be documented in the final report at the end of this research project.

CHAPTER 6
SUMMARY

This report discussed the application of NDT tools for evaluating existing pavements for asphalt overlays. The NDT tools covered in this report include GPR, FWD, and RDD. The GPR is generally used for identifying the layer thickness of existing pavement layers, section break, and potential trapped moisture problems. The FWD is often used to evaluate the structural capacity of existing pavements, and layer modulus can also be backcalculated from FWD data. The FWD can also be used to evaluate the LTE at joints and/or cracks. However, it is tedious and sometimes difficult to determine the LTE using the FWD.

Additionally, this report describes applications of RDD on evaluating existing PCC pavements. The major advantage the RDD has over other discrete NDT devices (e.g., FWD) is that it measures continuous deflection profiles along the pavement. However, no software is available to automatically interpret the RDD data. After reviewing thousands of RDD data collected on different concrete pavements, researchers developed some basics of interpreting RDD data. Furthermore, based on RDD deflection data and field reflective cracking performance on IH20, the threshold values for RDD Sensor 1 deflection and the differential deflection between Sensors 1 and 3 are recommended. If either the Sensor 1 deflection or differential deflection between Sensors 1 and 3 is larger than the proposed thresholds, the corresponding joints and/or cracks are recommended for pretreatment before placing a new HMA overlay. Finally, general guidelines for evaluating existing pavements for HMA overlays are proposed in this report. Note that the criteria and/or threshold values established in the report are based on limited data; further validation and verification are definitely needed.

REFERENCES

1. T. Scullion and T. Saarenketo, *Implementation of Ground Penetrating Radar Technology in Asphalt Pavement Testing*, 9th International Conference on Asphalt Pavement, Copenhagen, Denmark, Aug. 17-22, 2002.
2. T. Saarenketo and T. Scullion, *Using Electrical Properties to Classify the Strength Properties of Base Course Aggregates*, Texas Transportation Institute, Report 0-1341-2, Texas Transportation Institute, College Station, TX, Nov. 1995.
3. T. Saarenketo, Using GPR and Dielectric Probe Measurements in Pavement Density Quality Control, *Transportation Research Board Record*, Jan. 1997.
4. T. Scullion and Y. Chen, *COLORMAP Version 2 User's Guide with Help Menus*, Research Report 0-1702-4, Texas Transportation Institute, Texas A&M University, College Station, TX, June 1999.
5. E. A.Ricci, et al., "The Falling Weight Deflectometer for Nondestructive Evaluation of Rigid Pavements," Research Report 387-3F, Center for Transportation Research, The University of Texas, Austin, TX, Nov. 1985.
6. J. A. Crovetti, and M. I. Darter, "Void Detection Procedures," NCHRP Report 1-21, Appendix C, Mar. 1985
7. Y. R. Kim, *Void Detection in PCC and Thin Asphalt Overlaid Composite Pavements, NCHRP 10-48 Appendix E*, North Carolina State University, Raleigh, NC, Oct. 2000.
8. W. Liu and T. Scullion, MODULUS 6.0 for Windows: User's Manual, Research Report 0-1869-2, Texas Transportation Institute, Texas A&M University, College Station, TX, Oct. 2001.
9. American Association of State Highway and Transportation Officials (1993). *AASHTO Guide for Design of Pavement Structures—1993*, Washington, D.C.
10. J. Bay and K. Stokoe, "Development of a Rolling Dynamic Deflectometer for Continuous Deflection Measurements of Pavements," Center of Transportation Research, Report 1422-3F, University of Texas, Austin, TX, 1998.
11. J. Lee, D. Chen, and K. Stokoe, "Evaluating the Potential for Reflection Cracking Using the Rolling Dynamic Deflectometer," Transportation Research Board, *Journal of Transportation Research Record* No. 1869, pp16-24, 2004.

12. T. Scullion, "*Using Rolling Deflectometer and Ground Penetrating Radar Technologies for Full Coverage Testing of Jointed Concrete Pavements*," FHWA/TX-05/0-4517-2, Texas Transportation Institute, College Station, TX, Apr. 2006.
13. A. Chowdhury, A. Bhasin, and J. Button, "*As-Built Properties of Test Pavements on IH20 in Atlanta District*," FHWA/TX-03/0-4203-2, Texas Transportation Institute, College Station, TX, Mar. 2003.
14. Y. Yildirim and T. W. Kennedy, "*Hamburg Wheel Tracking Device Results on Plant and Field Cores Produced Mixtures*," FHWA/TX-04/0-4185-2, Center for Transportation Research, Austin, TX, Sept. 2002.
15. D. Chen, Personal communication, 2006.
16. G. Keller, *Applied Statistics with Microsoft Excel*, 1st edition, Pacific Grove, 2001.
17. P.C. Paris and F. Erdogan, "A Critical Analysis of Crack Propagation Laws," *Transactions of the ASME, Journal of Basic Engineering*, Series D, 85, No. 3, 1963.

APPENDIX A
GPR TEST DATA ON IH20

This appendix presents color-coded representations of the GPR data collected by TTI researchers along the IH20 overlay project near Marshall, Texas. The reflections from the layer interfaces detected from GPR are labeled in the figures. Note that the surface reflection has been removed, and only the interfaces appearing below the surface are shown.

The color bar at the left side of each figure shows the color coding of the reflection amplitudes. These amplitudes are expressed in volts and range from ±1 volt. Voltages around 1 volt are coded red, while voltages around -1 volt are coded blue. Amplitudes between these limits are assigned the color shown on the bar. The depth scale at the right side of each figure gives the predicted depth of each interface detected by GPR. From this scale, one can determine the thickness of each layer.

At the bottom of each figure is the distance scale expressed in miles and feet. The distance corresponding to each GPR trace is recorded during the measurement. The upper number on the distance scale shows the miles traversed, while the lower number is the distance traveled in feet since the last mile. For example, 6287 feet corresponds to 1 mile and 1007 feet. Also shown above the distance scale is the predicted dielectric profile of the existing AC surface mix on the lane surveyed. This profile may be used to locate possible changes in the surface mix along the length surveyed.

The figures included in this appendix, therefore, provide all relevant information from the GPR testing. Each figure shows:

- the variation of the pavement layering along the length surveyed, as determined from radar;
- the amplitudes of the reflections from the layer interfaces;
- the thickness of each layer; and
- the computed dielectric values of the surface material.

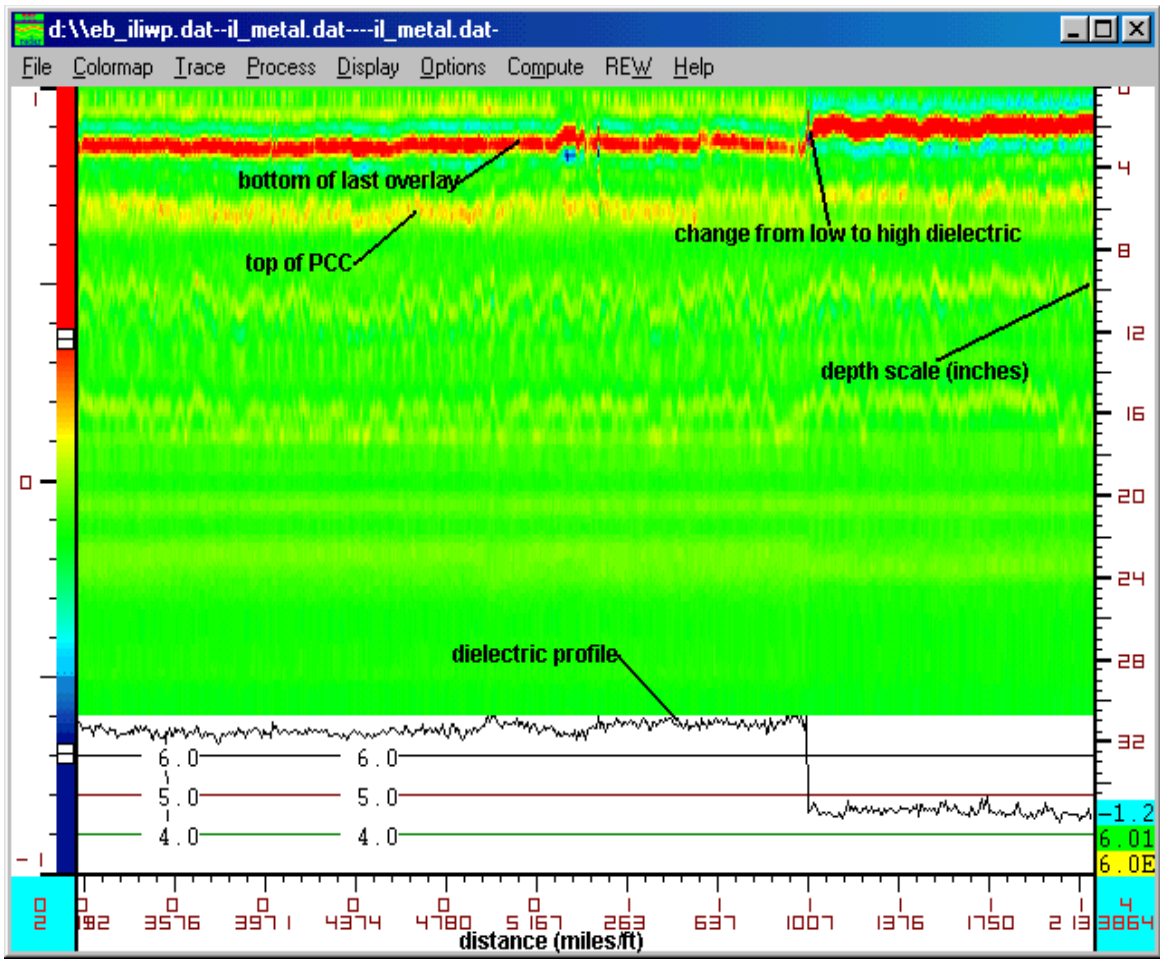

Figure A1. GPR Data Collected along Eastbound Inside Lane of IH20 Project (1/4).

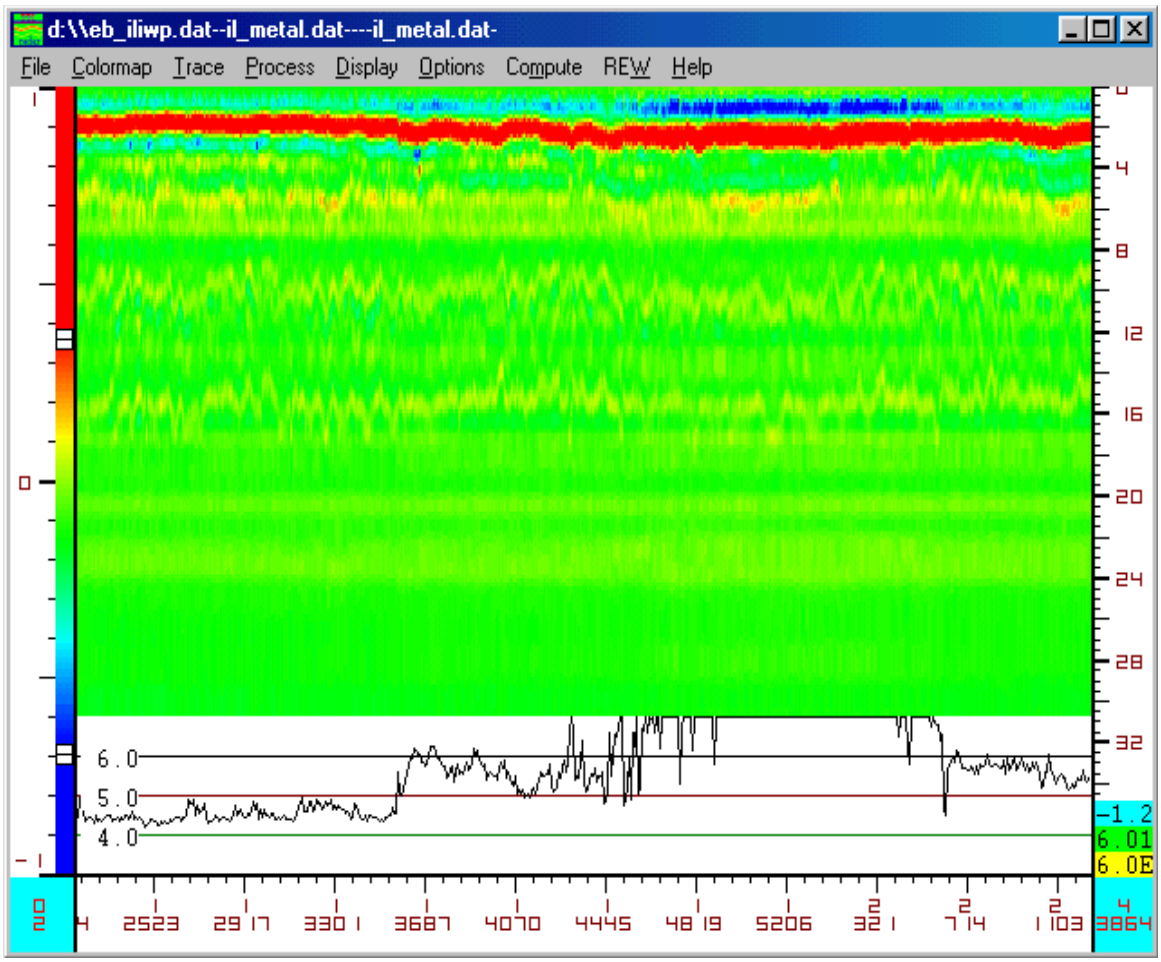

Figure A2. GPR Data Collected along Eastbound Inside Lane of IH20 Project (2/4).

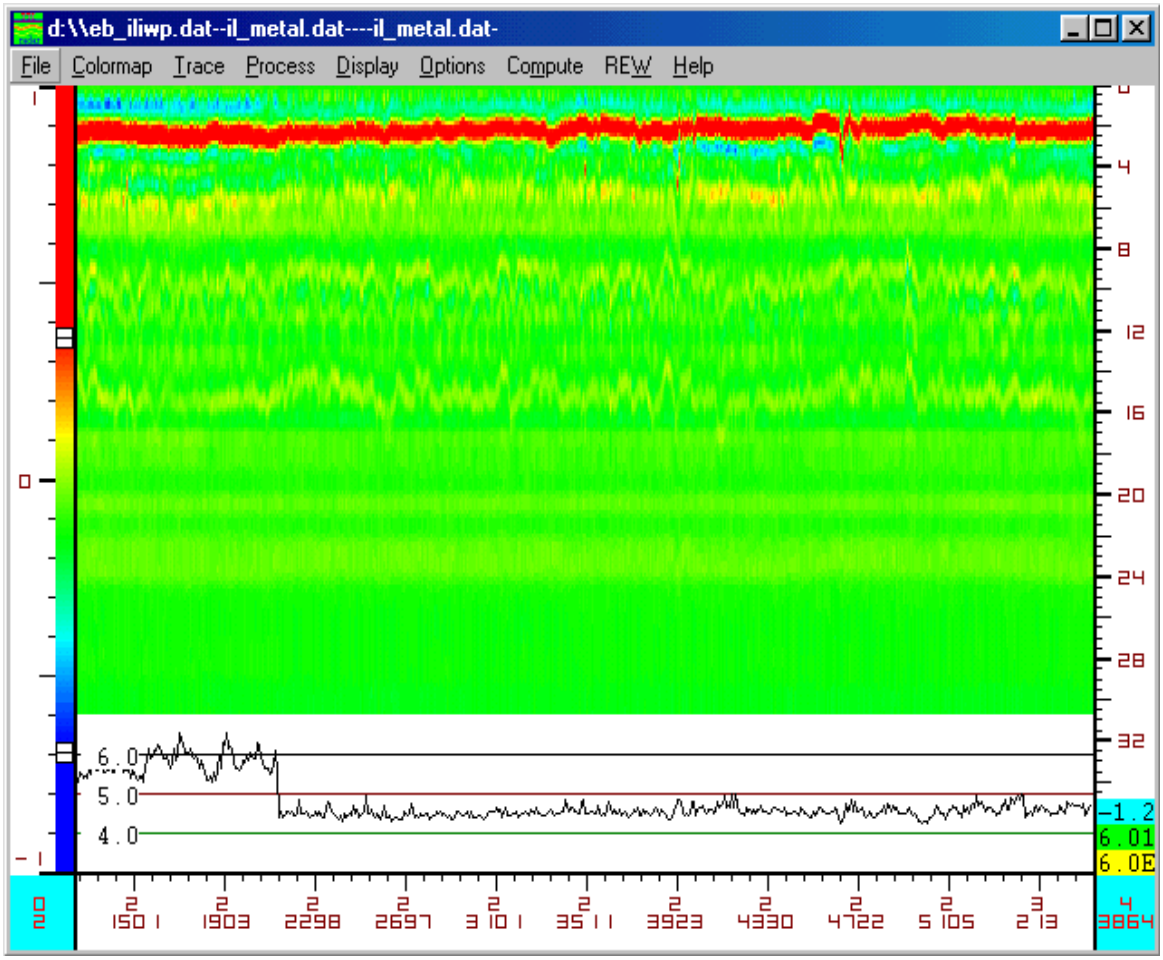

Figure A3. GPR Data Collected along Eastbound Inside Lane of IH20 Project (3/4).

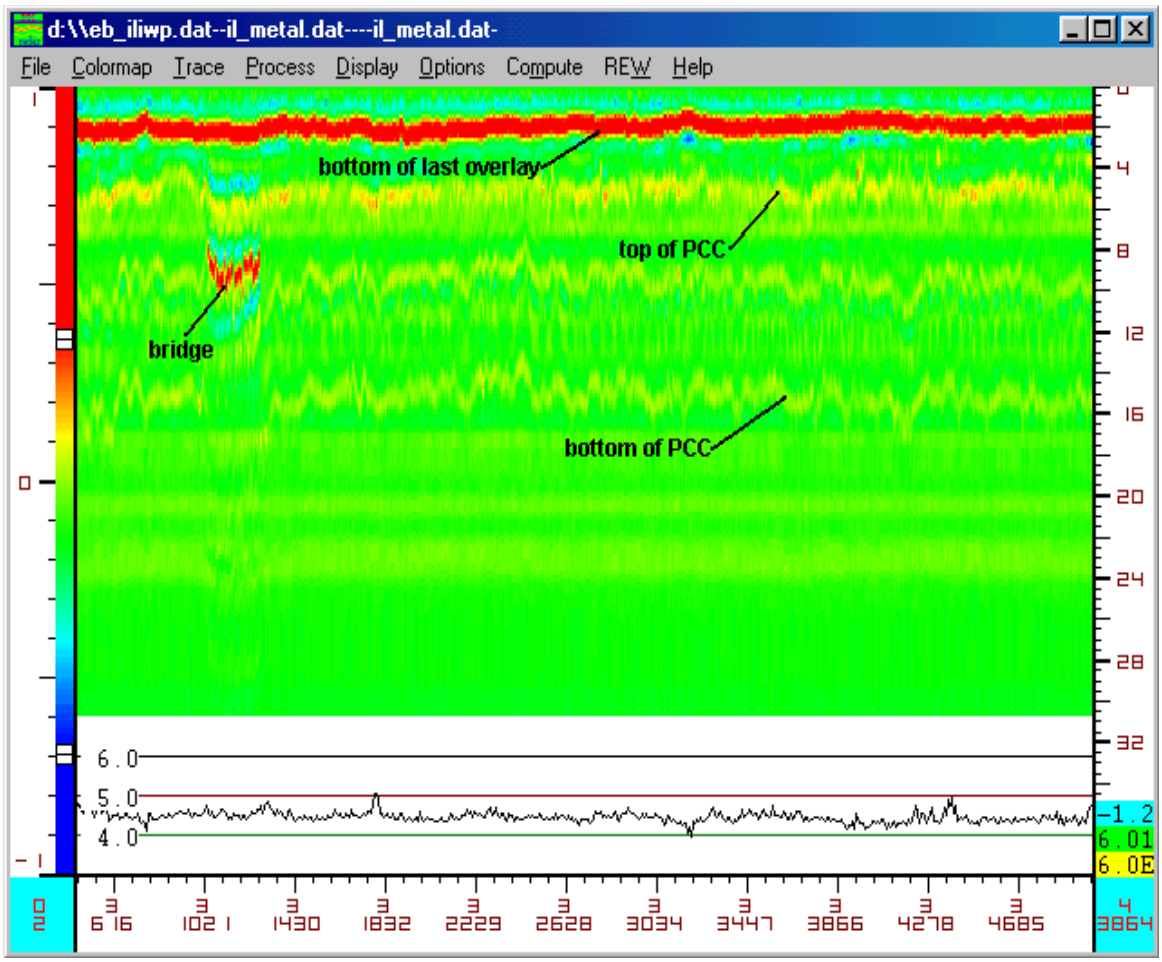

Figure A4. GPR Data Collected along Eastbound Inside Lane of IH20 Project (4/4).

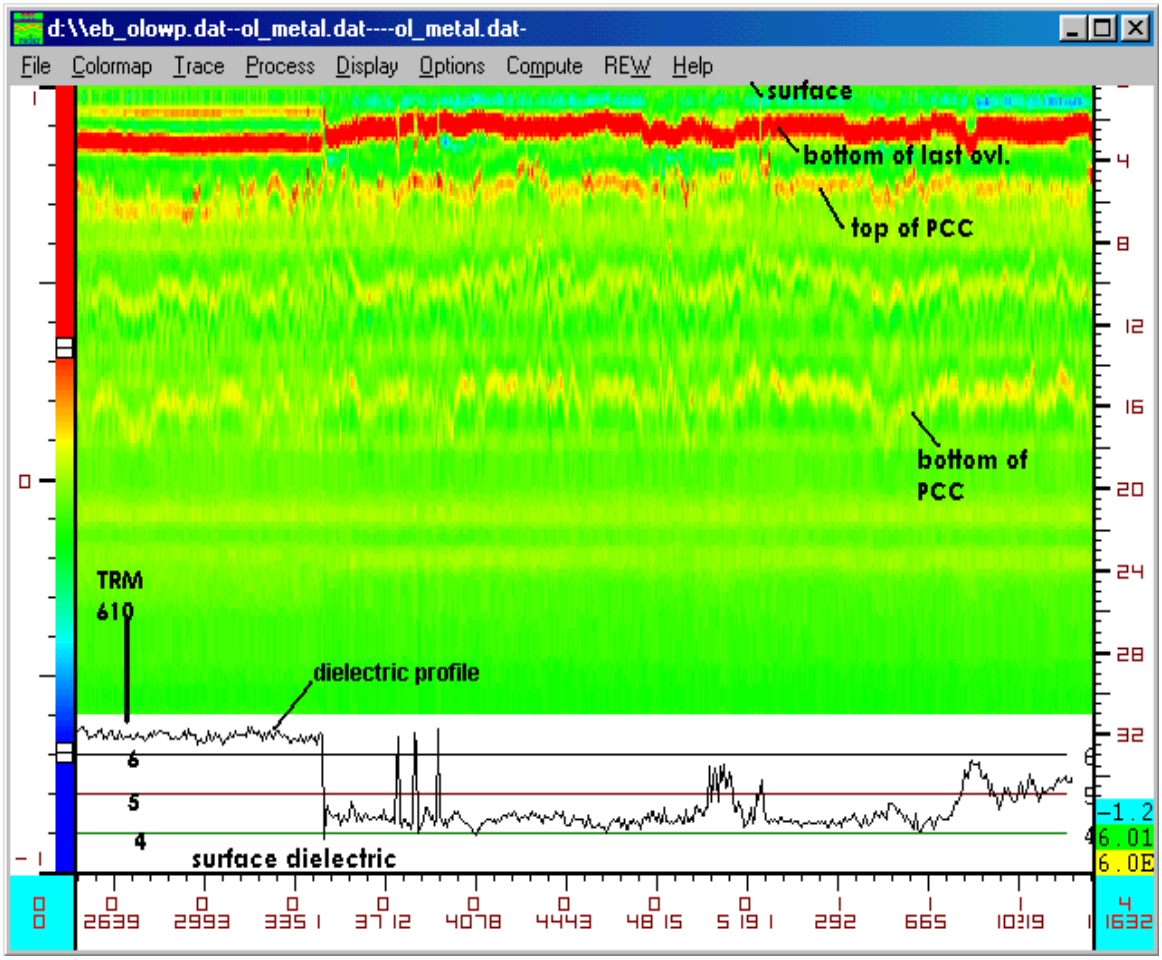

Figure A5. GPR Data Collected along Eastbound Outside Lane of IH20 Project (1/4).

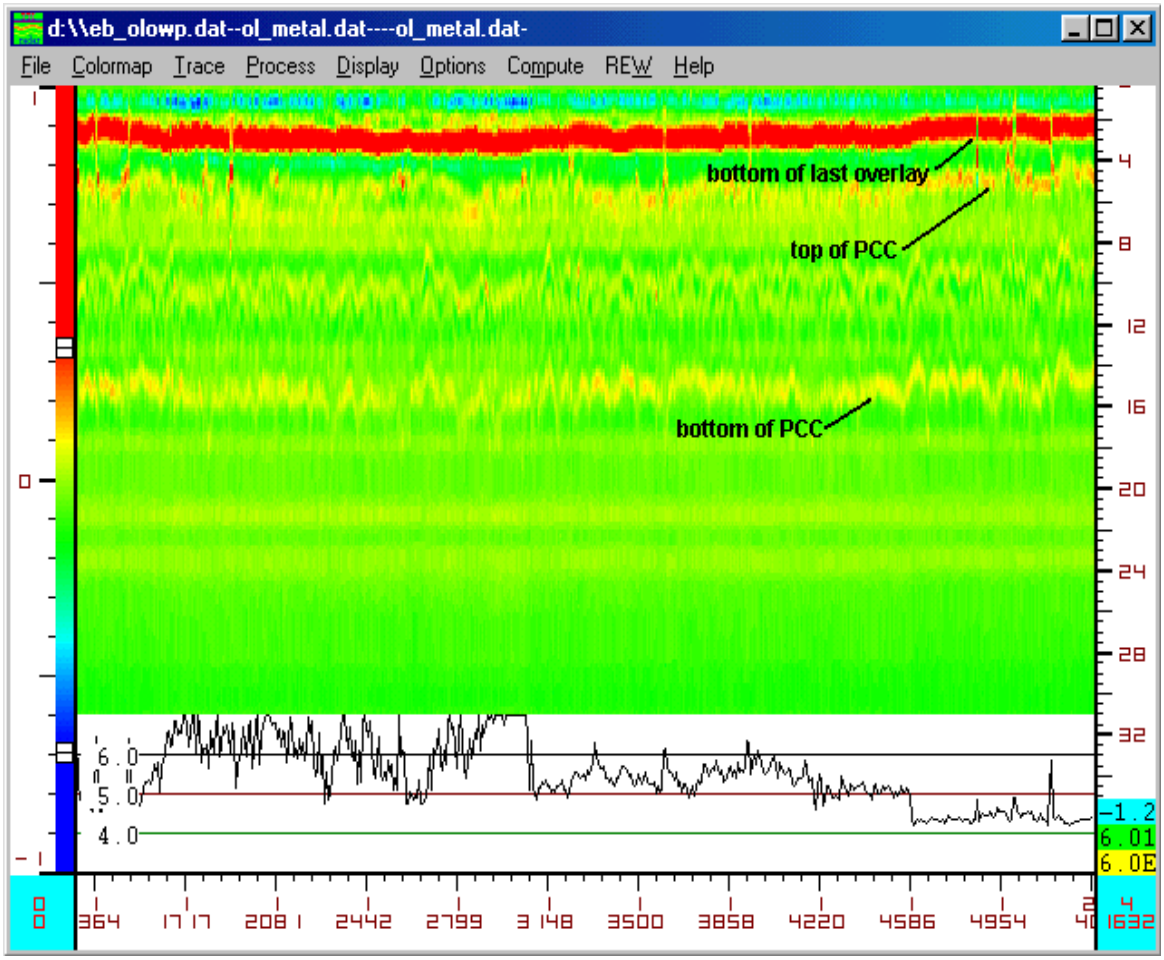

Figure A6. GPR Data Collected along Eastbound Outside Lane of IH20 Project (2/4).

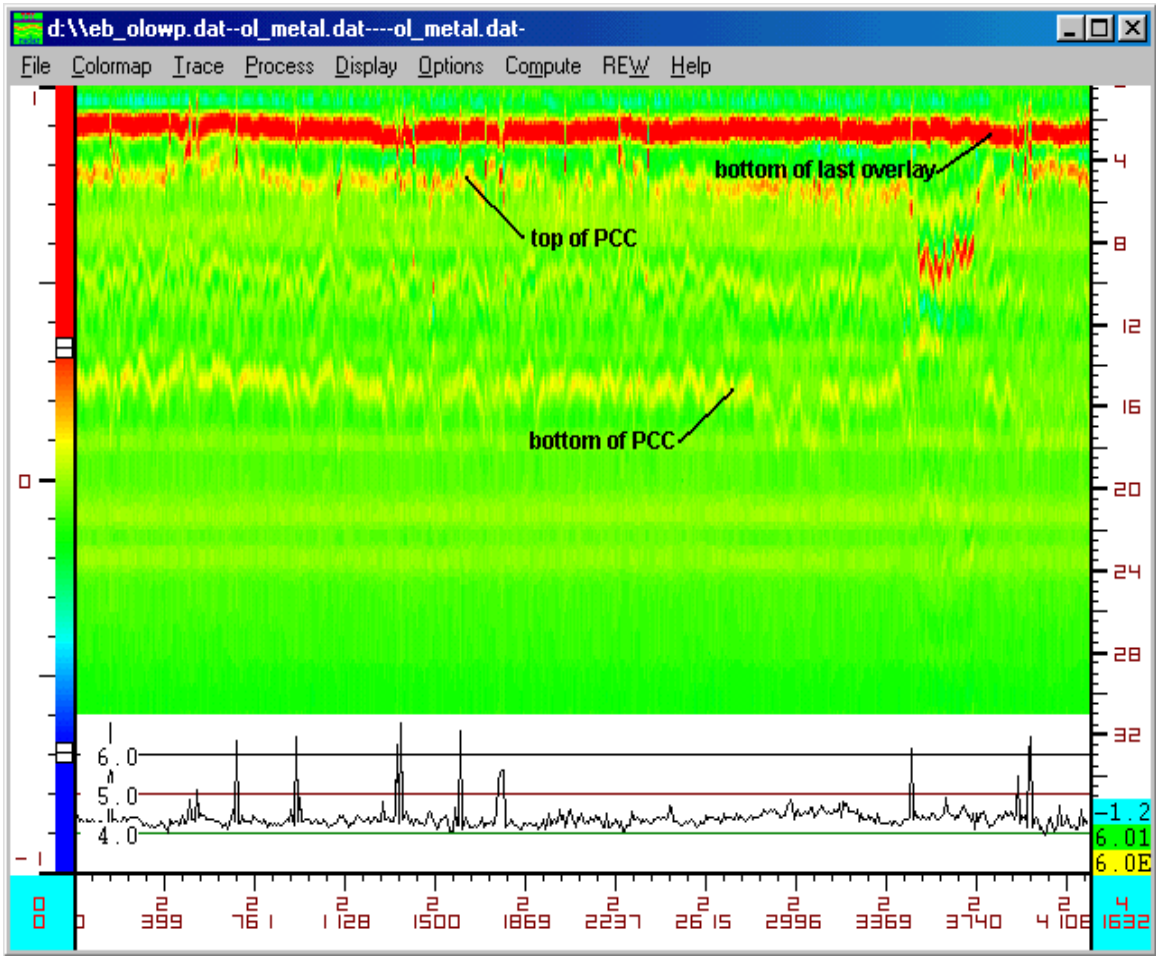

Figure A7. GPR Data Collected along Eastbound Outside Lane of IH20 Project (3/4).

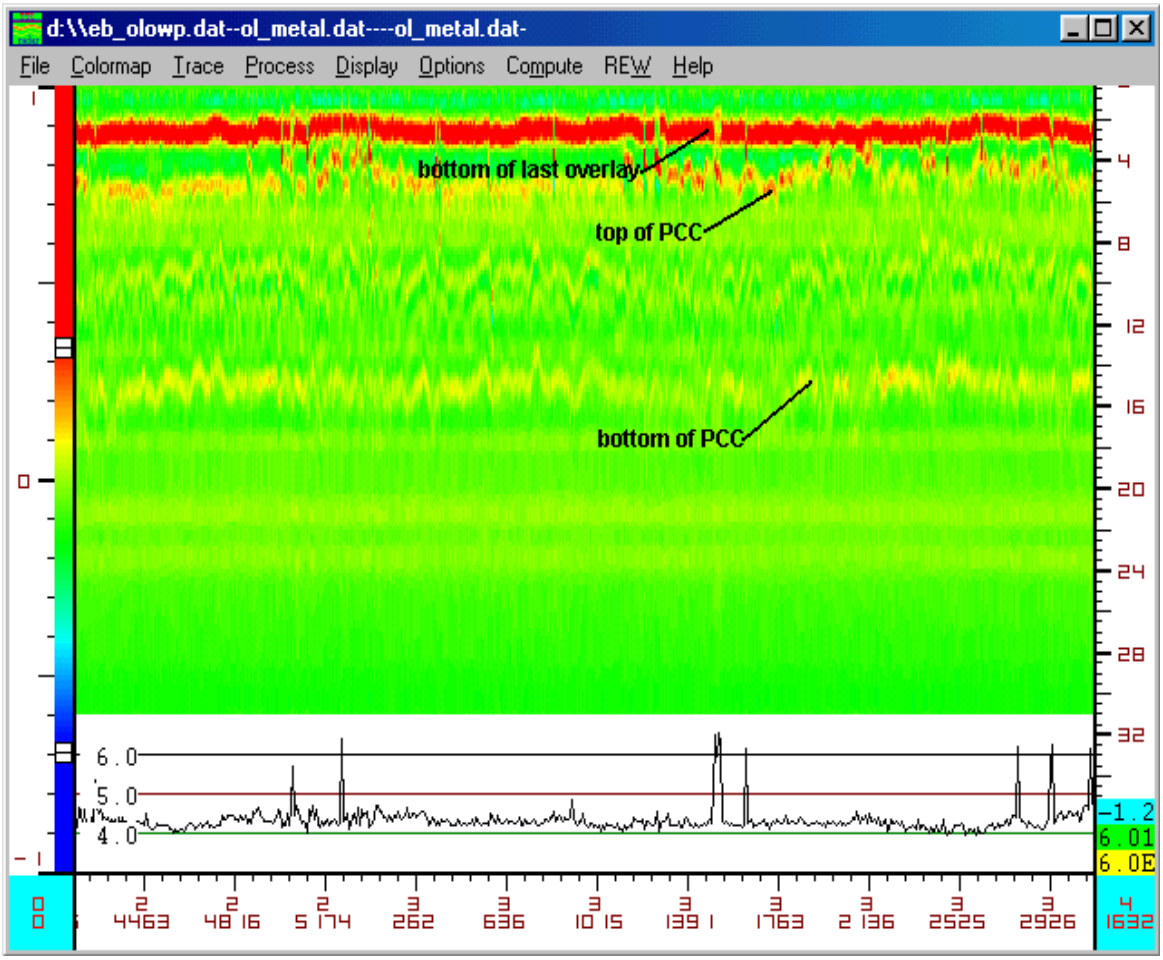

Figure A8. GPR Data Collected along Eastbound Outside Lane of IH20 Project (4/4).

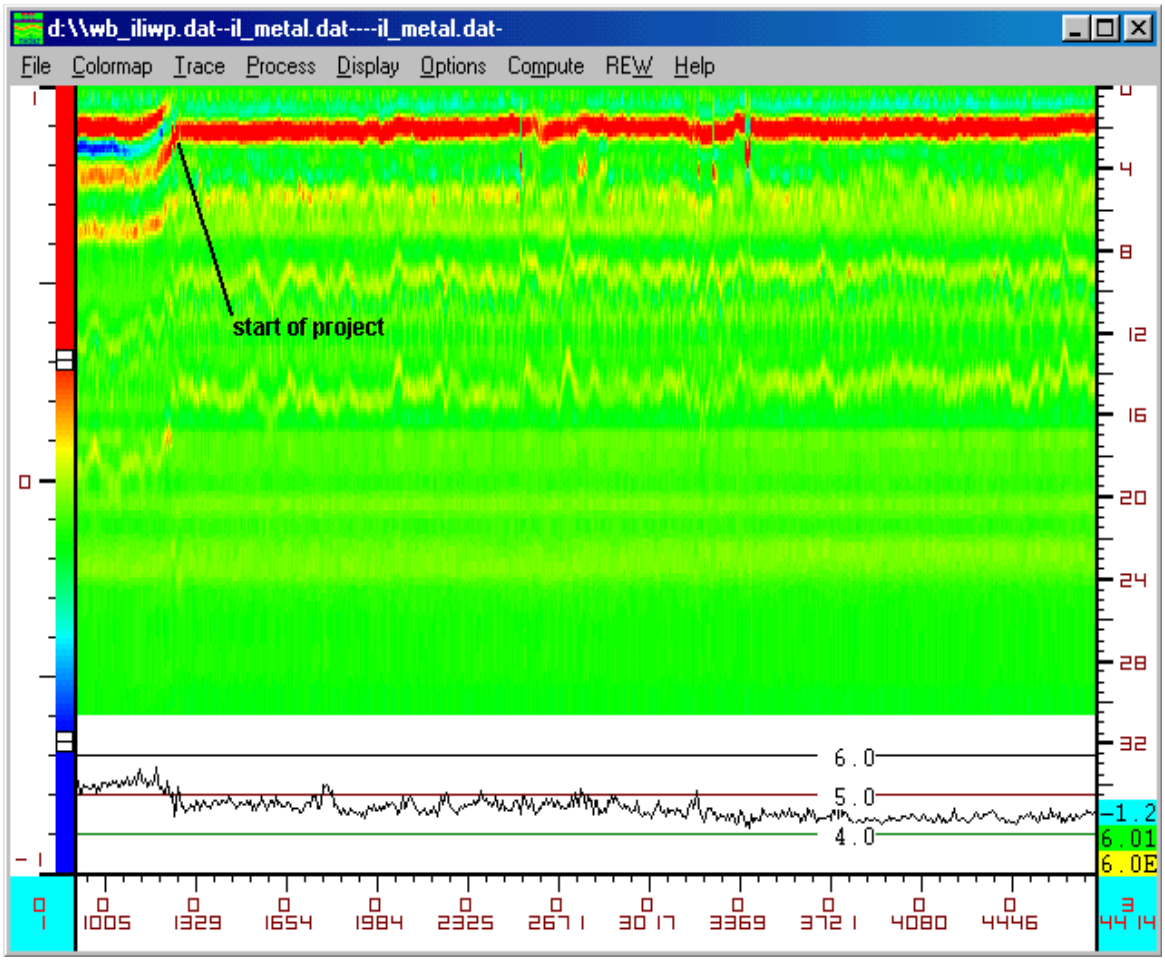

Figure A9. GPR Data Collected along Westbound Inside Lane of IH20 Project (1/4).

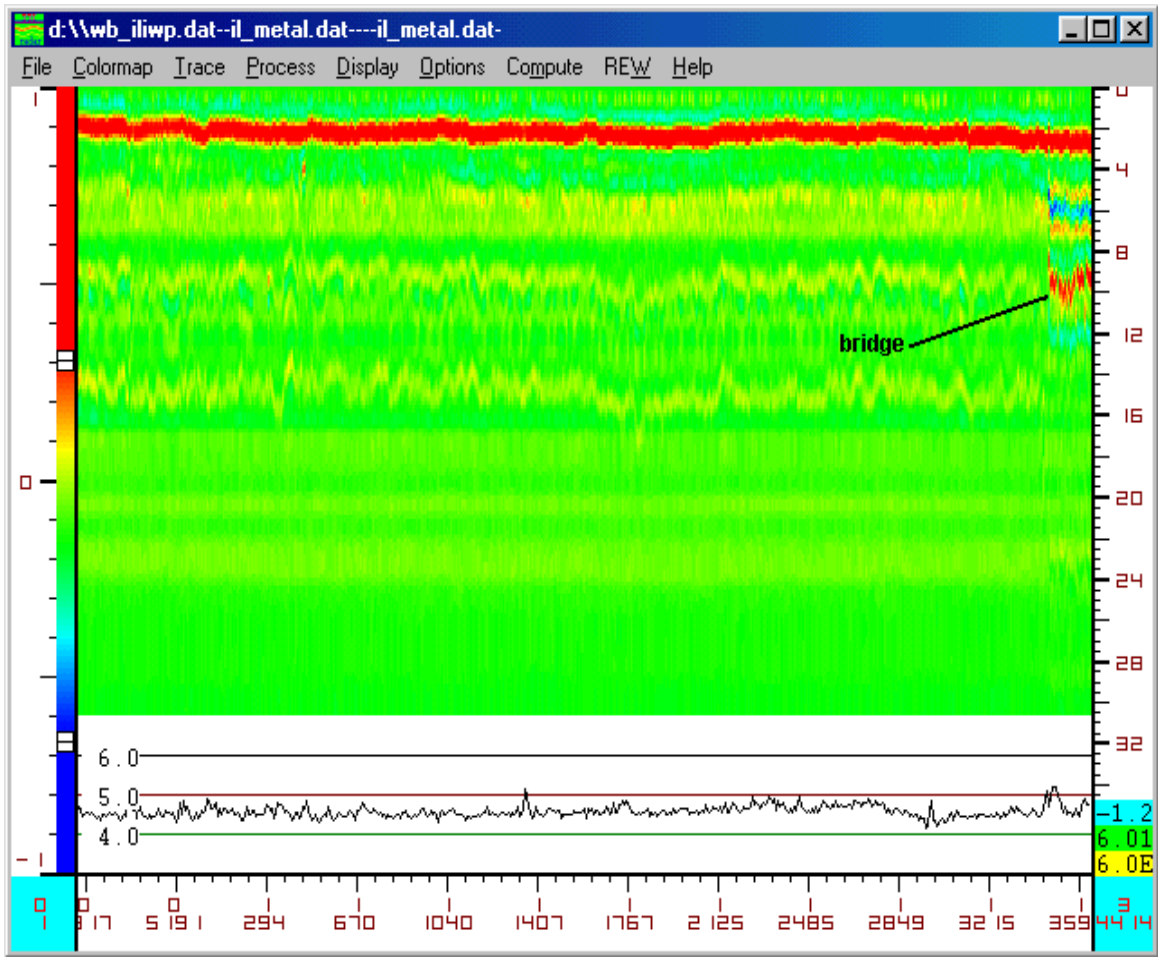

Figure A10. GPR Data Collected along Westbound Inside Lane of IH20 Project (2/4).

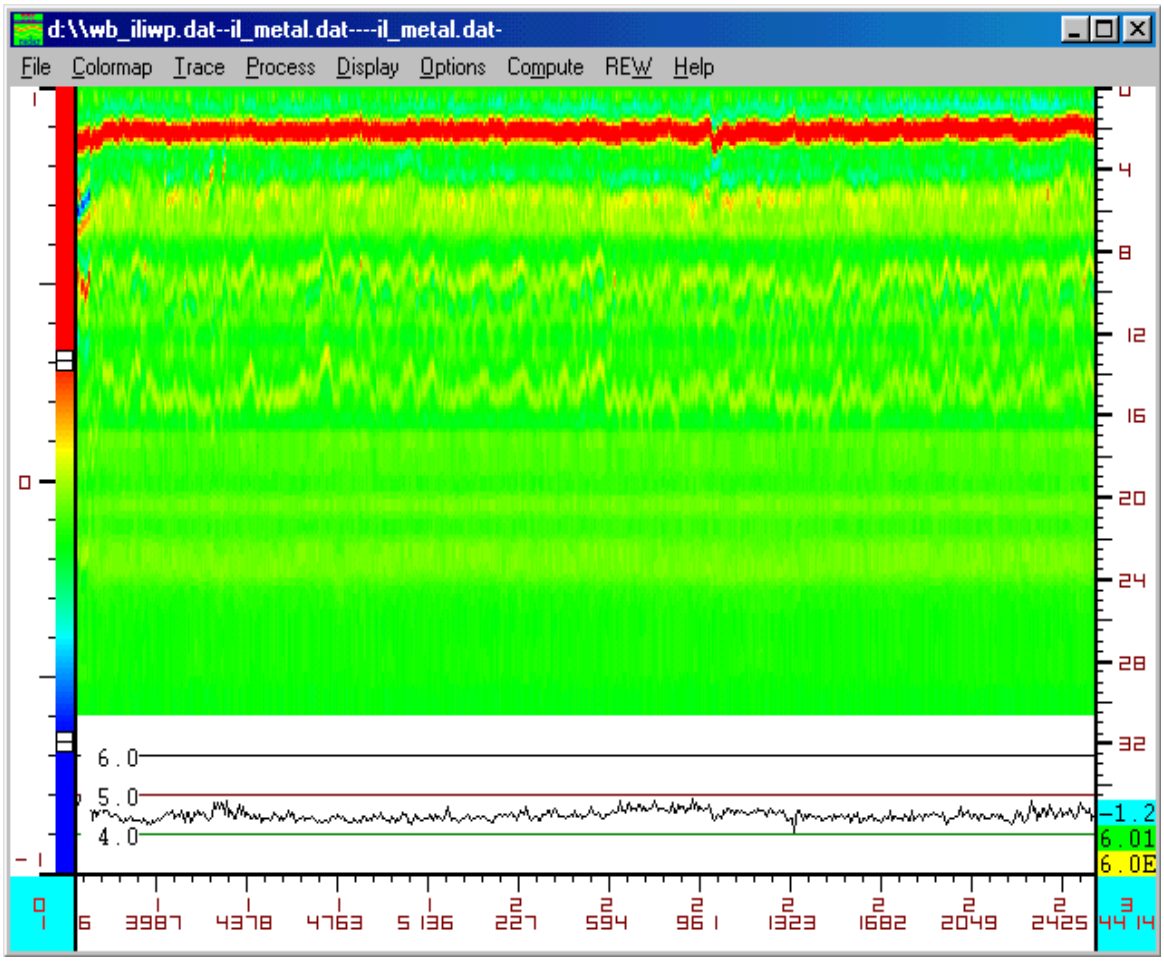

Figure A11. GPR Data Collected along Westbound Inside Lane of IH20 Project (3/4).

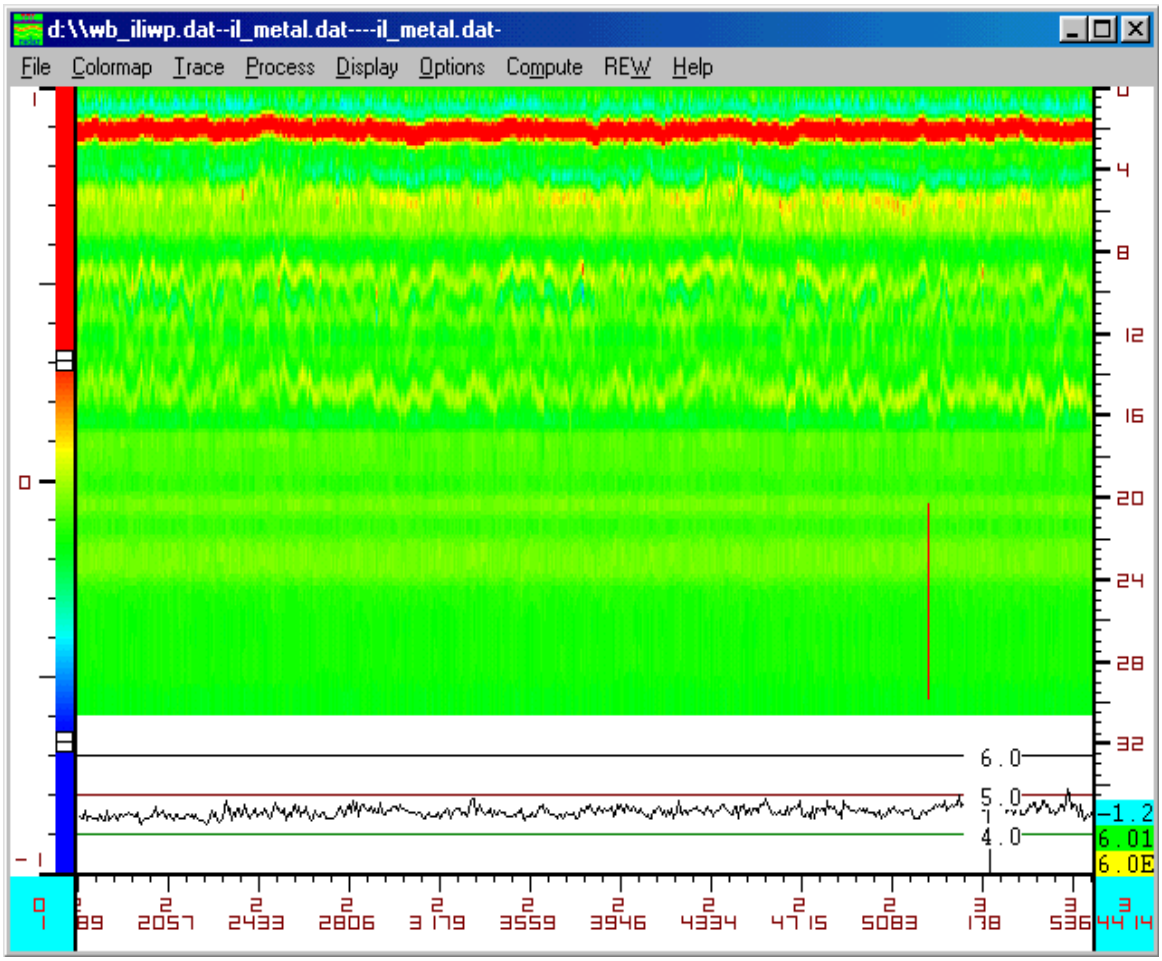

Figure A12. GPR Data Collected along Westbound Inside Lane of IH20 Project (4/4).

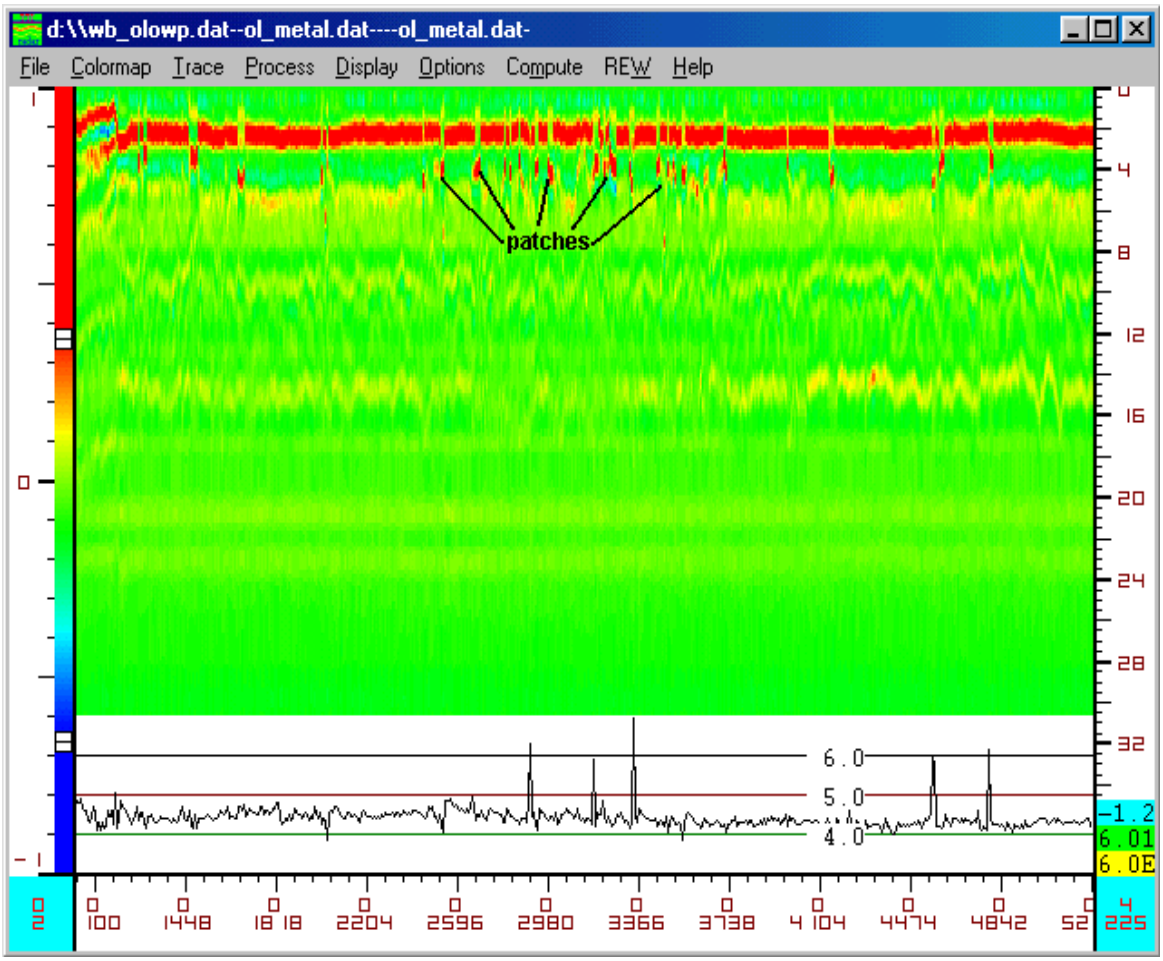

Figure A13. GPR Data Collected along Westbound Outside Lane of IH20 Project (1/4).

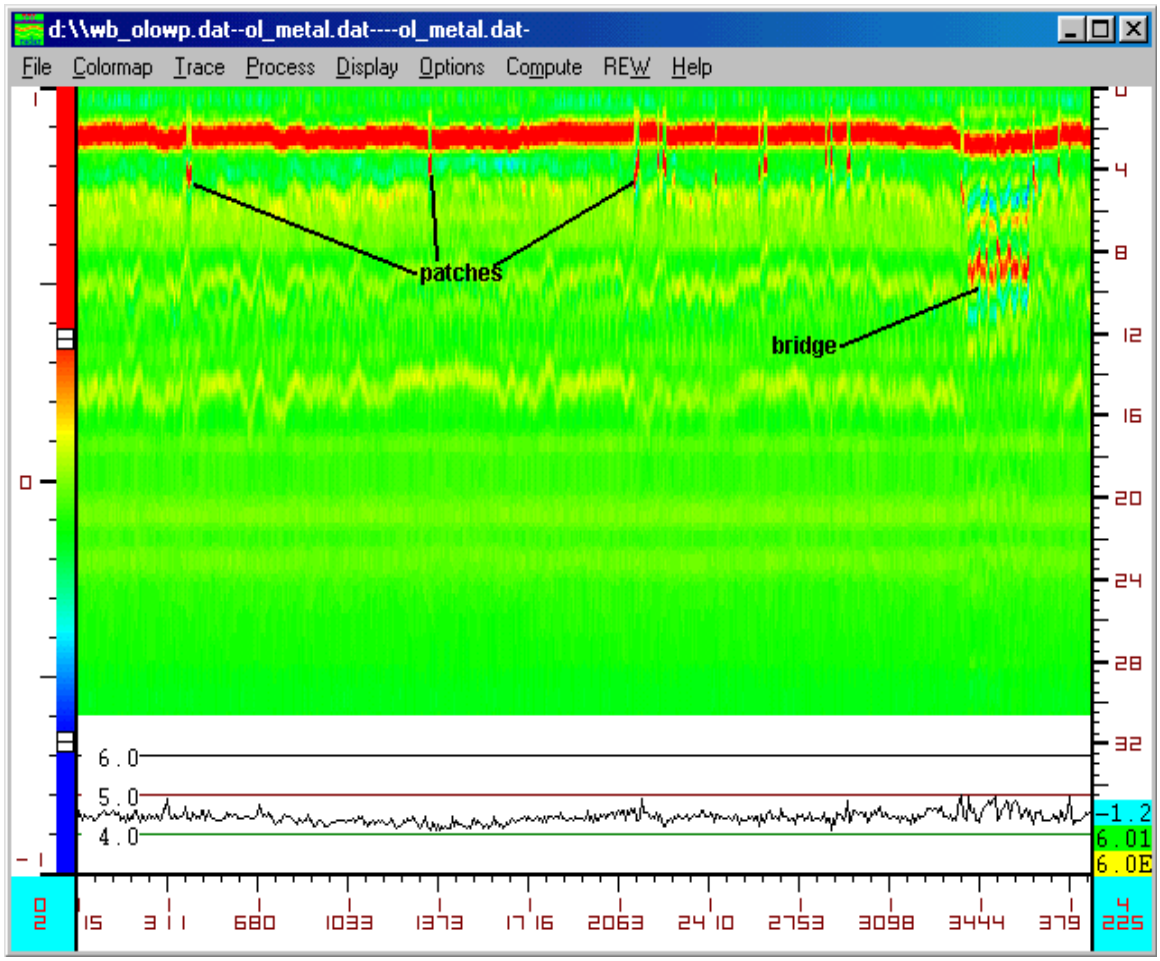

Figure A14. GPR Data Collected along Westbound Outside Lane of IH20 Project (2/4).

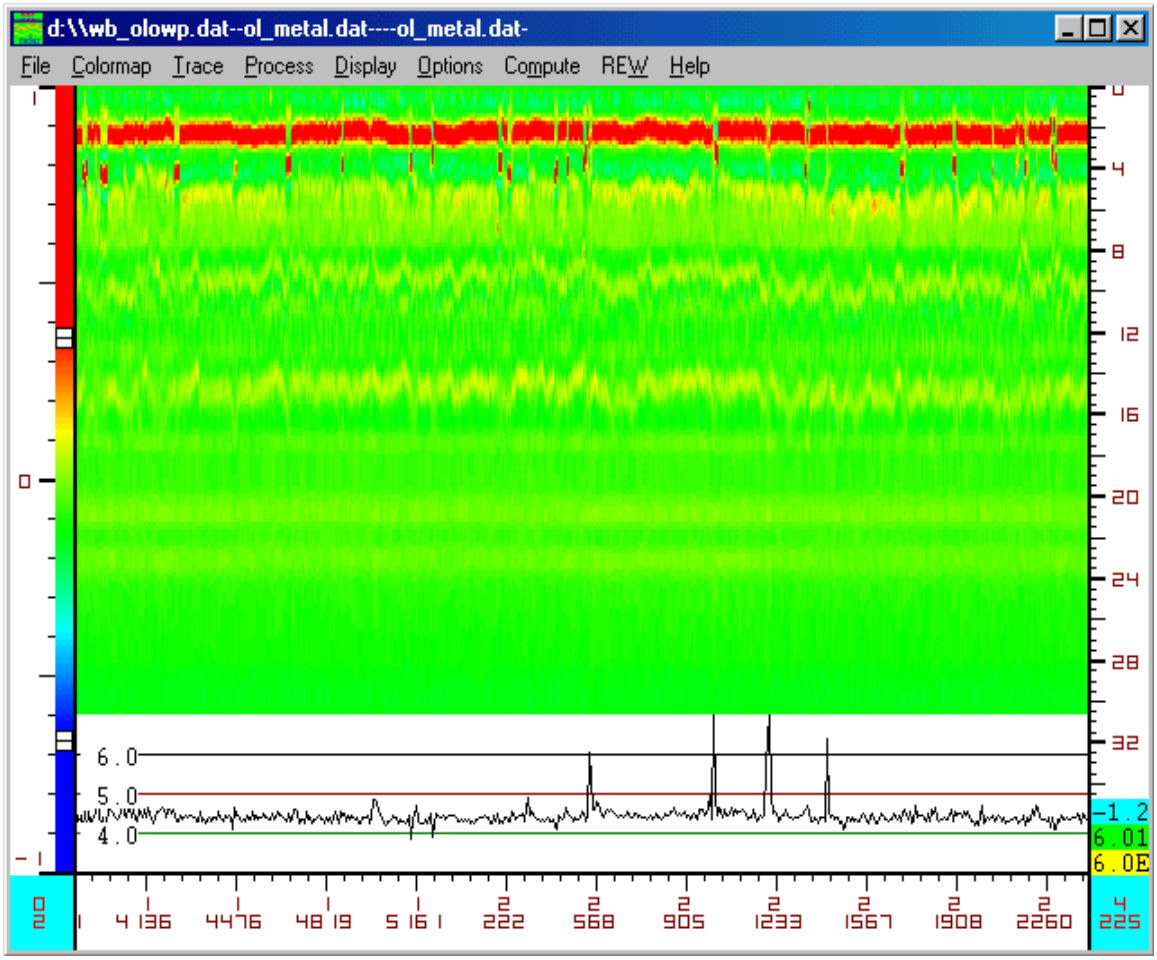

Figure A15. GPR Data Collected along Westbound Outside Lane of IH20 Project (3/4).

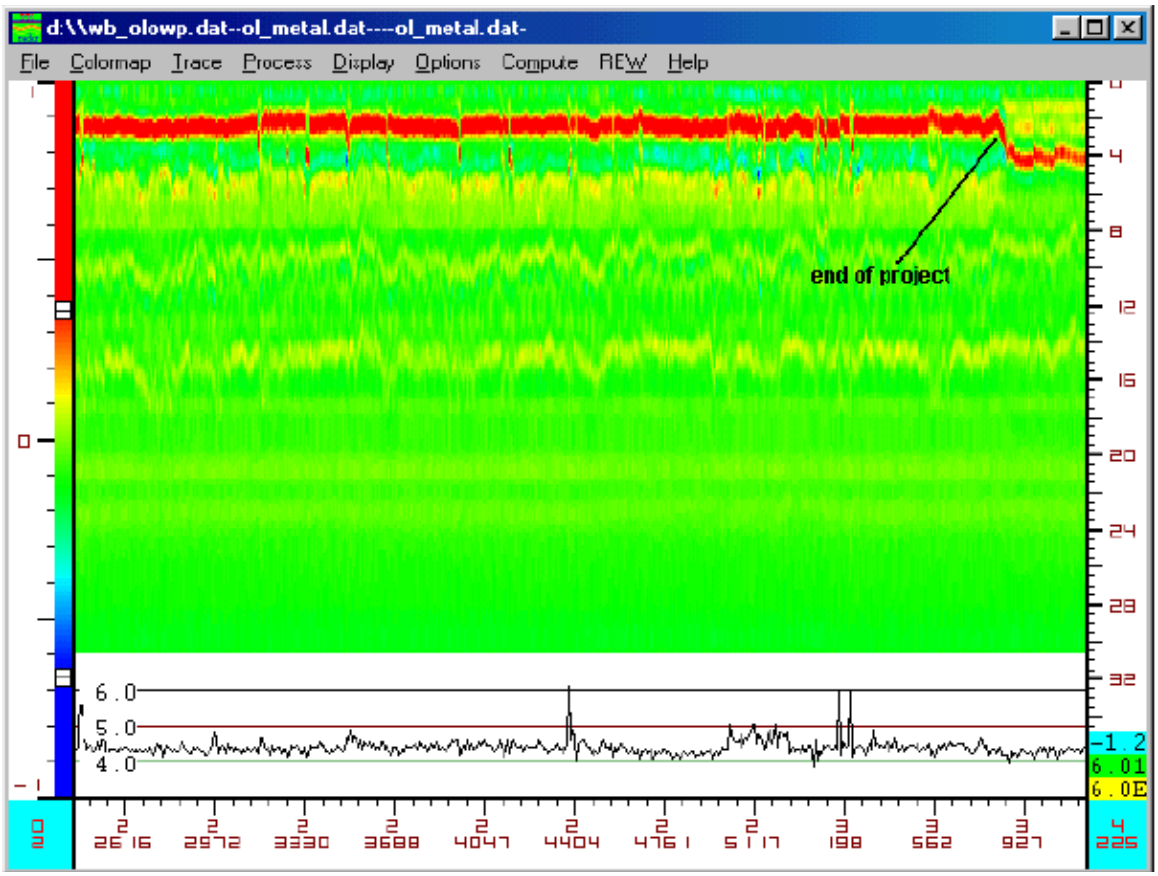

Figure A16. GPR Data Collected along Westbound Outside Lane of IH20 Project (4/4).

APPENDIX B

RDD DATA AND OBSERVED DISTRESS ON IH20

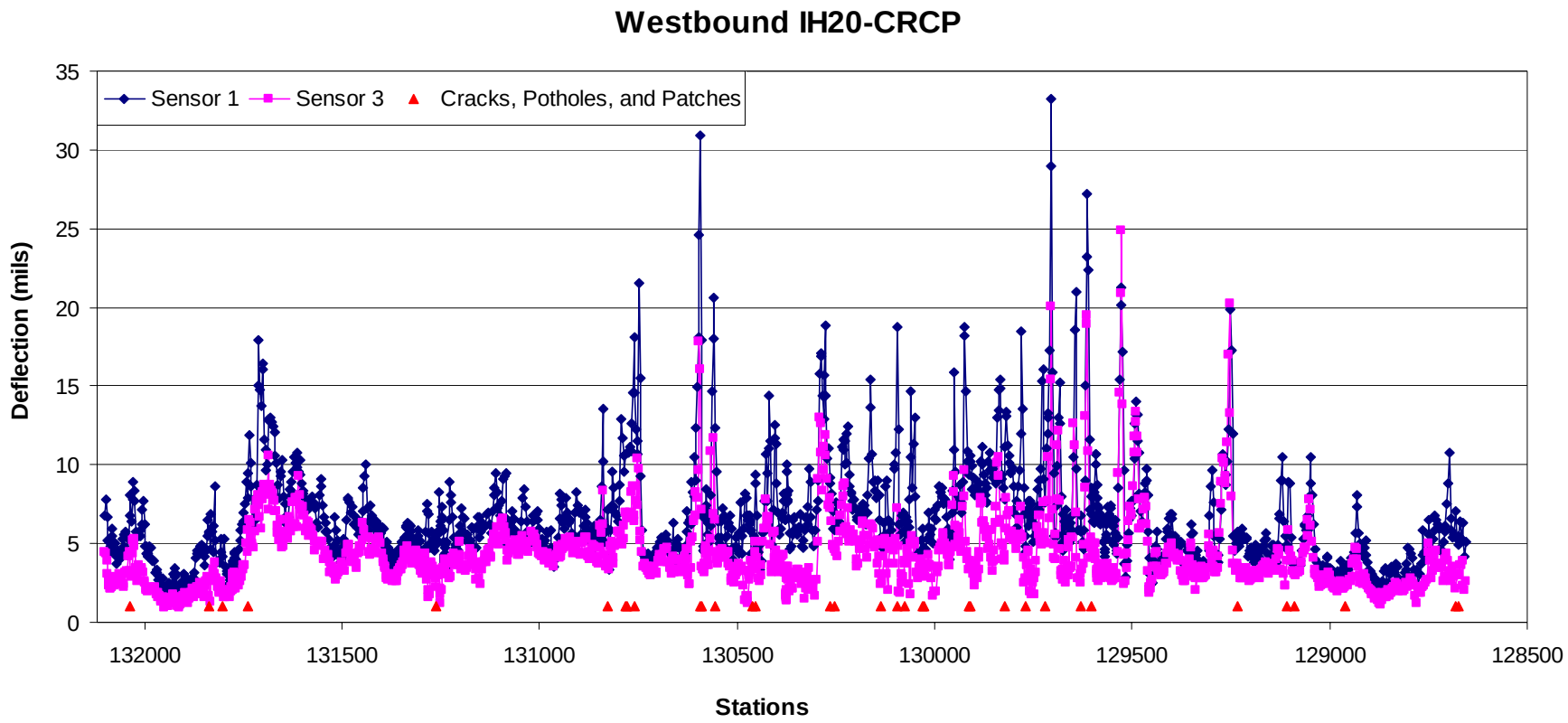

Figure B1. RDD Deflection Data and Observed Distresses on Westbound IH20 (1/4).

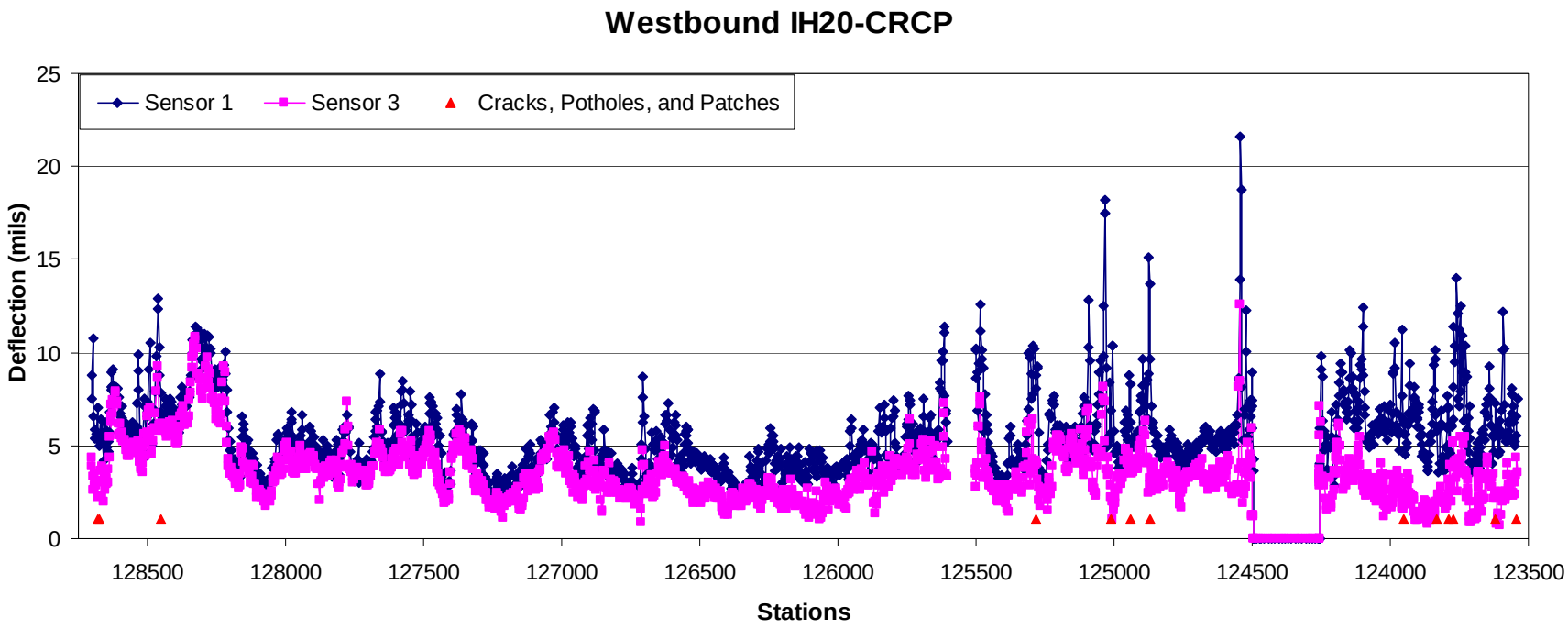

Figure B2. RDD Deflection Data and Observed Distresses on Westbound IH20 (2/4).

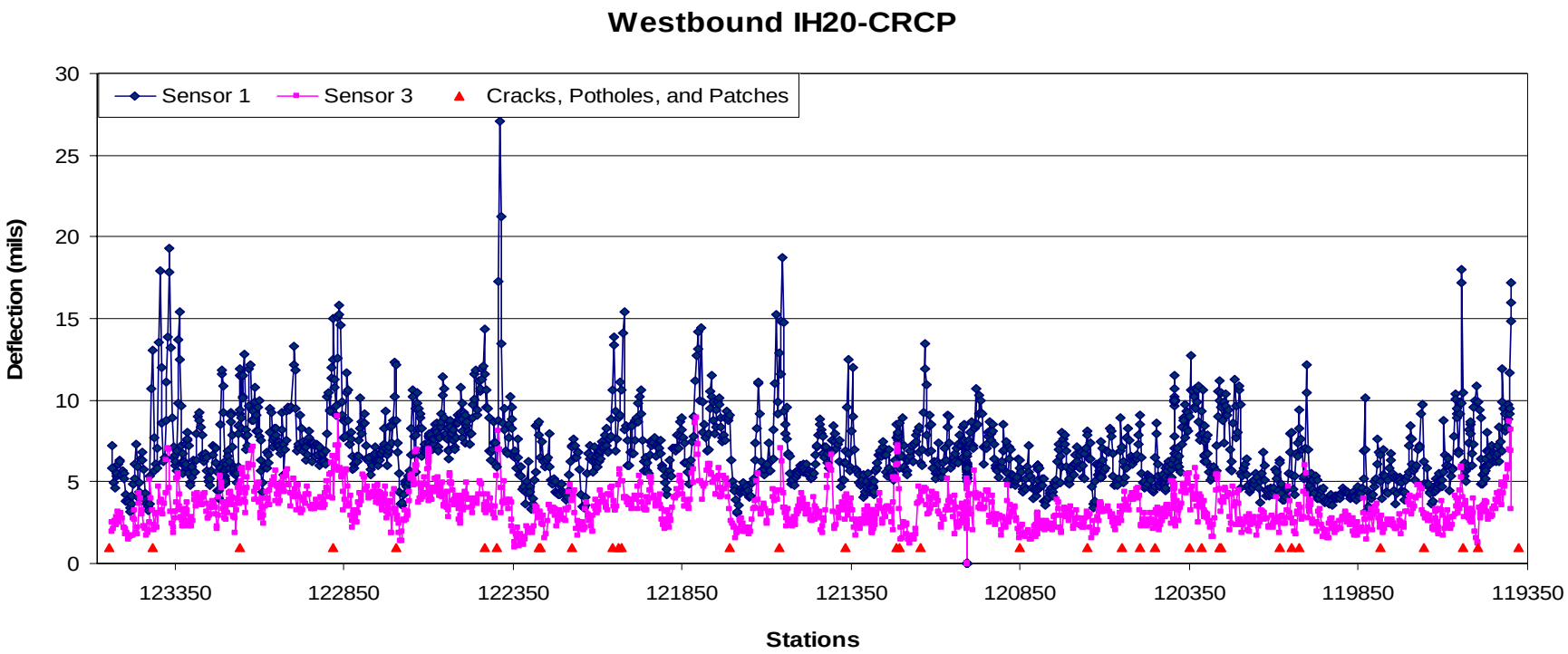

Figure B3. RDD Deflection Data and Observed Distresses on Westbound IH20 (3/4).

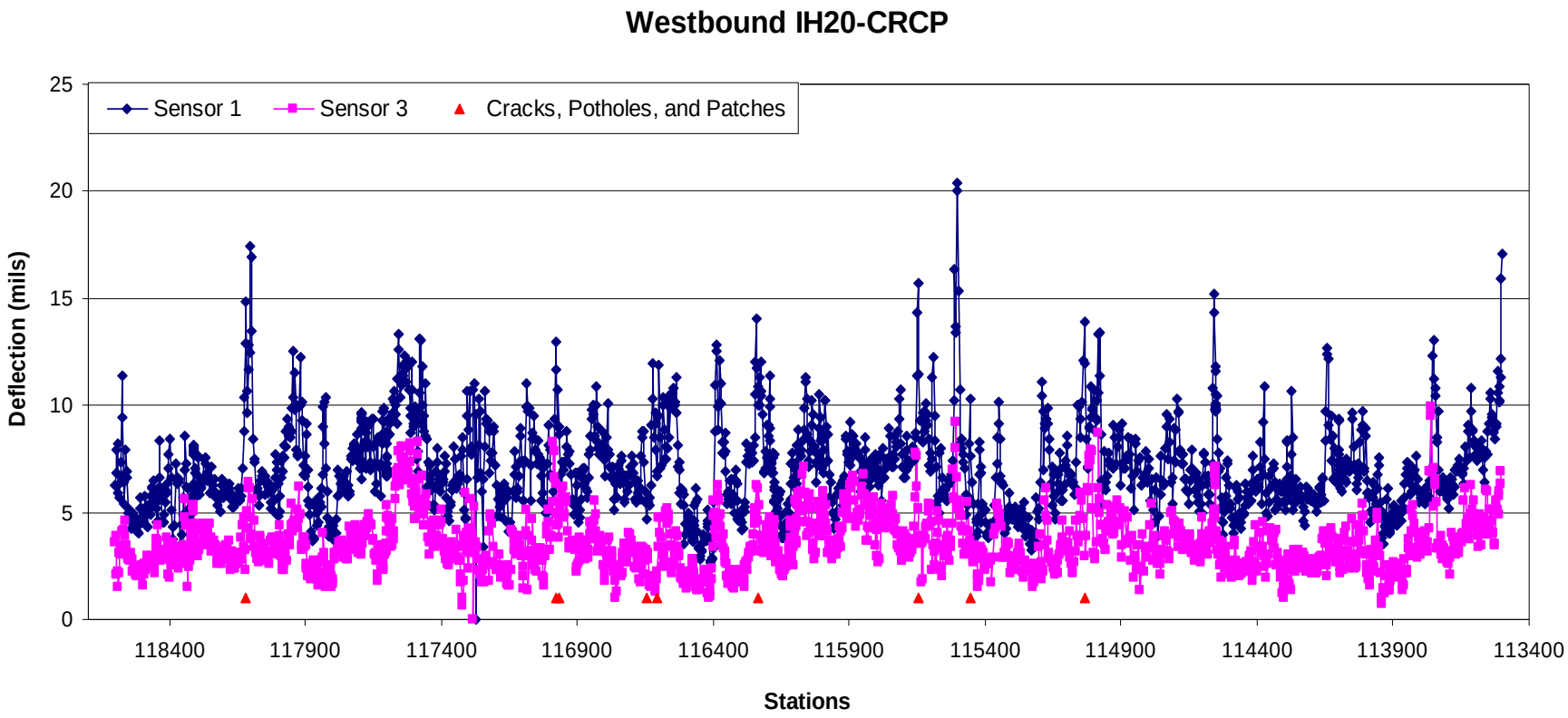

Figure B4. RDD Deflection Data and Observed Distresses on Westbound IH20 (4/4).

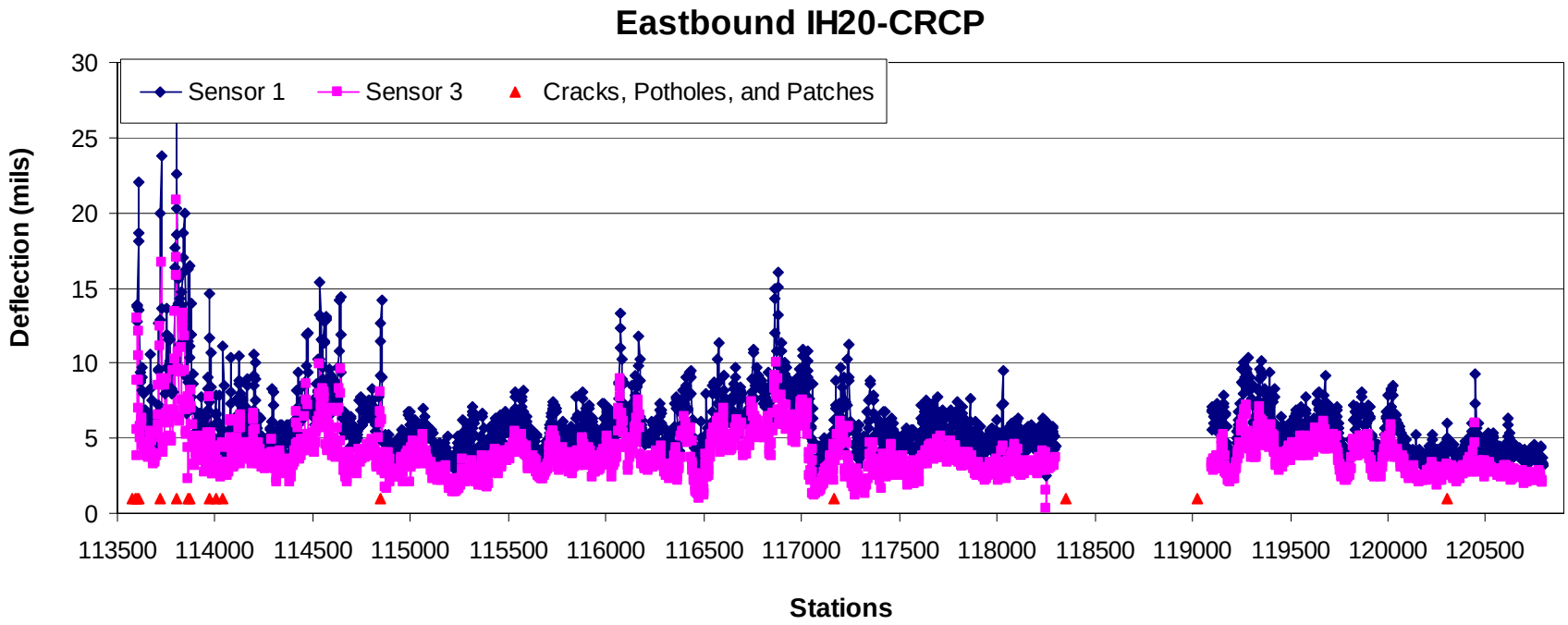

Figure B5. RDD Deflection Data and Observed Distresses on Eastbound IH20 (1/4).

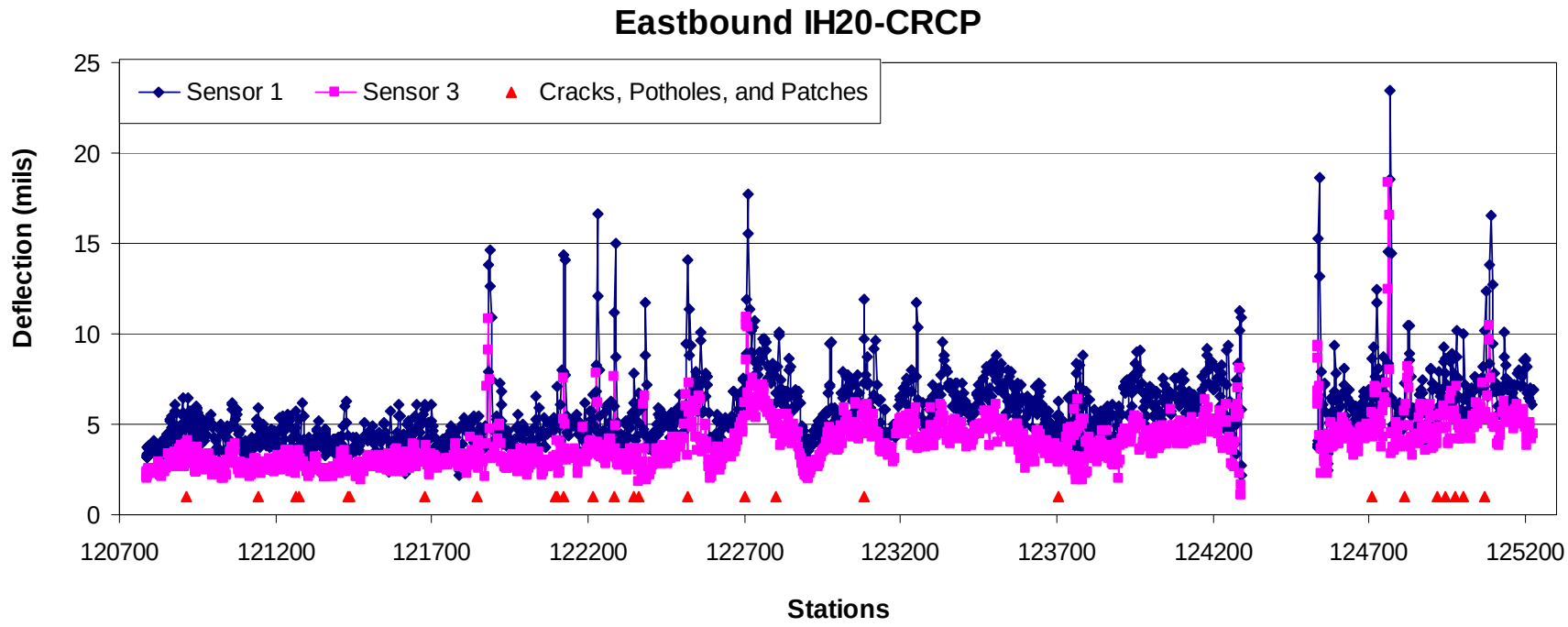

Figure B6. RDD Deflection Data and Observed Distresses on Eastbound IH20 (2/4).

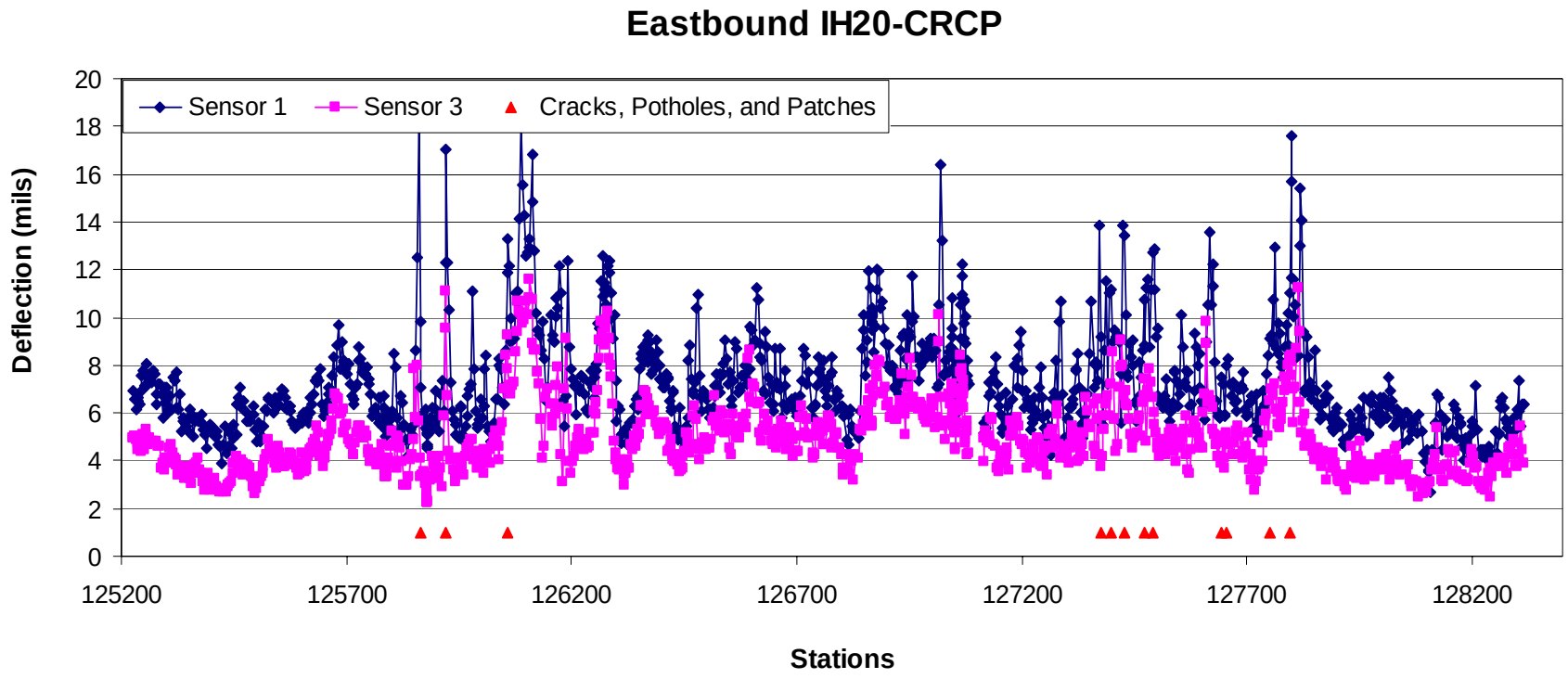

Figure B7. RDD Deflection Data and Observed Distresses on Eastbound IH20 (3/4).

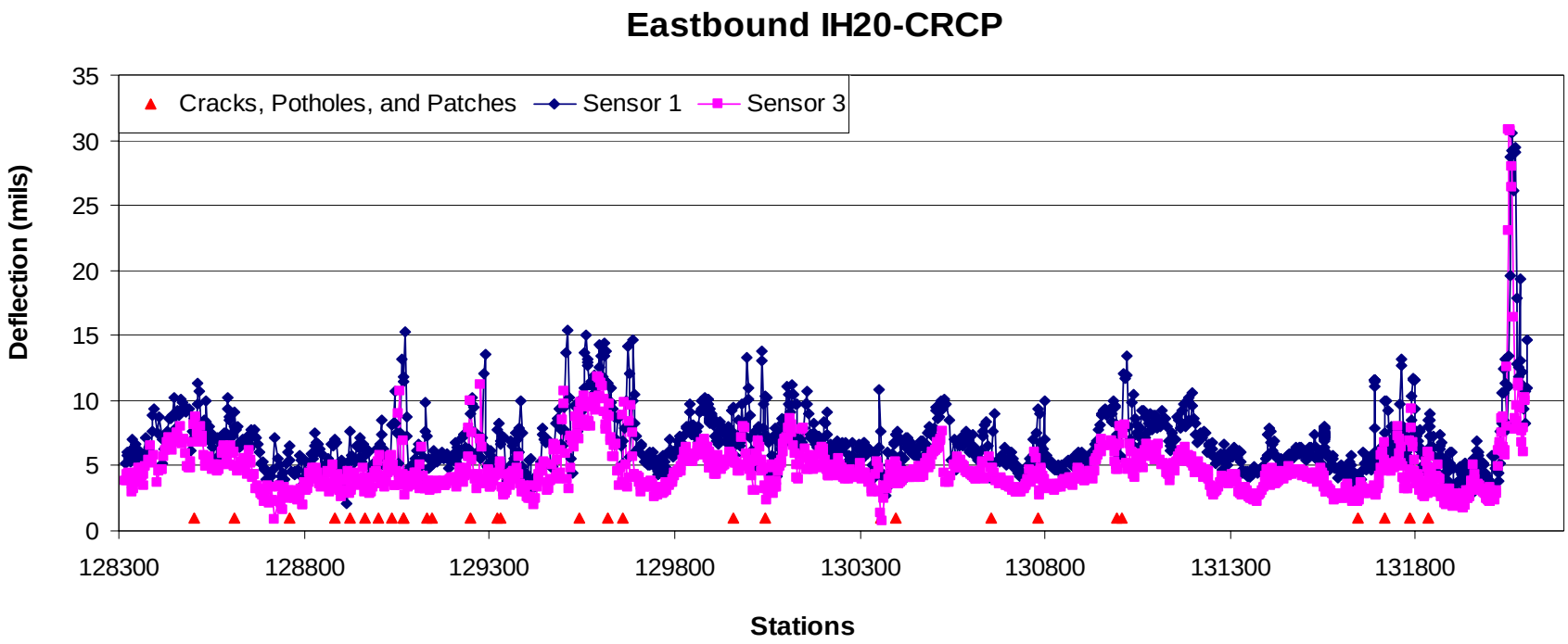

Figure B8. RDD Deflection Data and Observed Distresses on Eastbound IH20 (4/4).